



Print ISSN: 2152-4157
Online ISSN: 2152-4165

FALL/WINTER 2018
VOLUME 10, NUMBER 2

WWW.IJERI.ORG

International Journal of Engineering Research & Innovation

Editor-in-Chief: Mark Rajai, Ph.D.
California State University Northridge



Published by the
International Association of Journals & Conferences



www.ijeri.org

Print ISSN: 2152-4157
Online ISSN: 2152-4165



www.iajc.org

INTERNATIONAL JOURNAL OF ENGINEERING RESEARCH AND INNOVATION

ABOUT IJERI:

- IJERI is the second official journal of the International Association of Journals and Conferences (IAJC).
- IJERI is a high-quality, independent journal steered by a distinguished board of directors and supported by an international review board representing many well-known universities, colleges, and corporations in the U.S. and abroad.
- IJERI has an impact factor of **1.58**, placing it among an elite group of most-cited engineering journals worldwide.

OTHER IAJC JOURNALS:

- The International Journal of Modern Engineering (IJME)
For more information visit www.ijme.us
- The Technology Interface International Journal (TIIJ)
For more information visit www.tiij.org

IJERI SUBMISSIONS:

- Manuscripts should be sent electronically to the manuscript editor, Dr. Philip Weinsier, at philipw@bgsu.edu.

For submission guidelines visit
www.ijeri.org/submissions

TO JOIN THE REVIEW BOARD:

- Contact the chair of the International Review Board, Dr. Philip Weinsier, at philipw@bgsu.edu.

For more information visit
www.ijeri.org/editorial

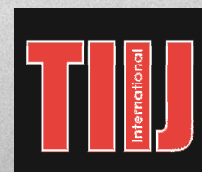
INDEXING ORGANIZATIONS:

- IJERI is indexed by numerous agencies. For a complete listing, please visit us at www.ijeri.org.

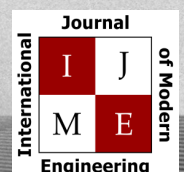
Contact us:

Mark Rajai, Ph.D.

Editor-in-Chief
California State University-Northridge
College of Engineering and Computer Science
Room: JD 4510
Northridge, CA 91330
Office: (818) 677-5003
Email: mrajai@csun.edu



www.tiij.org



www.ijme.us

INTERNATIONAL JOURNAL OF ENGINEERING RESEARCH AND INNOVATION

The INTERNATIONAL JOURNAL OF ENGINEERING RESEARCH AND INNOVATION (IJERI) is an independent and not-for-profit publication, which aims to provide the engineering community with a resource and forum for scholarly expression and reflection.

IJERI is published twice annually (fall and spring issues) and includes peer-reviewed research articles, editorials, and commentary that contribute to our understanding of the issues, problems, and research associated with engineering and related fields. The journal encourages the submission of manuscripts from private, public, and academic sectors. The views expressed are those of the authors and do not necessarily reflect the opinions of the IJERI editors.

EDITORIAL OFFICE:

Mark Rajai, Ph.D.
Editor-in-Chief
Office: (818) 677-2167
Email: ijmeeditor@iajc.org
Dept. of Manufacturing Systems
Engineering & Management
California State University-
Northridge
18111 Nordhoff Street
Northridge, CA 91330-8332

THE INTERNATIONAL JOURNAL OF ENGINEERING RESEARCH AND INNOVATION EDITORS

Editor-in-Chief:

Mark Rajai

California State University-Northridge

Associate Editors:

Paul Wilder

Vincennes University

Li Tan

Purdue University Northwest

Production Editor:

Philip Weinsier

Bowling Green State University-Firelands

Subscription Editor:

Morteza Sadat-Hossieny

Northern Kentucky University

Web Administrator:

Saeed Namyar

Advanced Information Systems

Manuscript Editor:

Philip Weinsier

Bowling Green State University-Firelands

Copy Editors:

Li Tan

Purdue University Northwest

Ahmad Sarfaraz

California State University-Northridge

Technical Editors:

Marilyn Dyrud

Oregon Institute of Technology

Publisher:

Bowling Green State University Firelands

TABLE OF CONTENTS

<i>Editor's Note (In This Issue): 3D Food Printing</i>	3
Philip Weinsier, IJERI Manuscript Editor	
<i>A Variable-Speed Turntable for Accelerometer Performance Testing</i>	5
Dale H. Litwhiler, Pennsylvania State University, Berks	
<i>Hybrid, Semi-Passive Solar Harvesting System</i>	13
Aleksandr Sergeyev, Michigan Technological University; Austin Etzel, Michigan Technological University; Joe Mayrose, Michigan Technological University	
<i>3D Food Printing Insights and Opportunities: A Capstone Design Case Study</i>	19
Joseph Piacenza, University of West Florida; Hope Weiss, California State University Fullerton; Monika Patel, California State University Fullerton; Sean Moore, California State University Fullerton; Tam Nguyen, California State University Fullerton; Nikolia Shields, University of West Florida	
<i>Countering Eavesdropping Attacks in Software-Defined Radio Networks</i> <i>Using a Moving-Target Defense</i>	29
Isaac J. Cushman, Georgia Southern University; Rami J. Haddad, Georgia Southern University; Lei Chen, Georgia Southern University	
<i>Using an Augmented Reality Tool to Improve Spatial Cognition</i>	37
Ulan Dakeev, Texas A&M University – Kingsville; Recayi Pecen, Sam Houston State University; Farzin Heidari, Texas A&M University – Kingsville; Faruk Yildiz, Sam Houston State University; Shah Alam, Texas A&M University-Kingsville	
<i>A System for Suggesting Suitable Content to the Users of Sahave</i>	43
Toqeer Israr, Eastern Illinois University; Ajay Aakula, Eastern Illinois University	
<i>Utilization of Spectral and Temporal Acoustic Features for Vehicle-Centric Emotion Recognition</i>	51
Tejal Udhan, Florida State University; Shonda Bernadin, Florida A&M University, Florida State University	
<i>Novel Use of Remote Sensing, Monitoring, and Tracking for Animals in Wild Habitats</i>	57
Ben Zoghi, Texas A&M University; Rainer Fink, Texas A&M University	
<i>Instructions for Authors: Manuscript Submission Guidelines and Requirements</i>	63

IN THIS ISSUE (P.19): 3D FOOD PRINTING

Philip Weinsier, IJERI Manuscript Editor

- Step 1: Insert extrusion material into your 3D printer.
- Step 2: From the touchscreen menu, choose what food you want to create.
- Step 3: Press the start button!

Ok, I guess that might be something of an exaggeration, but the process of printing your next meal goes something like that. When I first heard about 3D food printing, I turned up my nose at the idea and thought, “uggg, I wouldn’t eat that”! And if you take a look at the goo that is typically found in the supply tubes or hoses feeding the process, you’ll likely have the same reaction. But imagine for a second how many of our most common foods are made: breakfast cereals, cheese, cakes, cookies, pasta; pretty much all of our processed foods. They probably are in a slurry state at one point or another in the processing cycle, yet magically take shape before being packaged and sold. Or how about Star Trek—the original, with Captain James T. Kirk? Remember the replicator? Just choose what you want to eat or drink and in seconds it magically comes out. Hmm, just like my three-step process above! My point is that while we may not like seeing our formless food in a syringe, it can be made to “come out the other end” with a form, shape, and texture that we know and love.



So who does like this idea? Well, a consumer tech contributor at Forbes says that projections for The 3D food printing market are that it will reach over \$500 million by 2023. Is that a lot? And NASA, always a good gauge for cutting-edge technology, is also funding research on 3D food printing in space for long missions. Others are looking at bringing the technology to underdeveloped regions and countries. And, yes, the military is looking at it, too.

For most of us, 3D printing of food is a new phenomenon; perhaps even 3D printing of anything. Everyone, however, is familiar with 2D printing—put paper in your printer, hit print on your computer, and the machine sprays ink on the paper in a manner that makes it seem like there’s an intelligent pattern in the final product: A page full of delicate prose or a picture of your children. 3D printing is similar in that a material of some sort (instead of ink) is sprayed onto a solid platform (instead of a piece of paper). After the material has a chance to dry or solidify, another layer is sprayed on top of the first, and so on. Only now, the shape

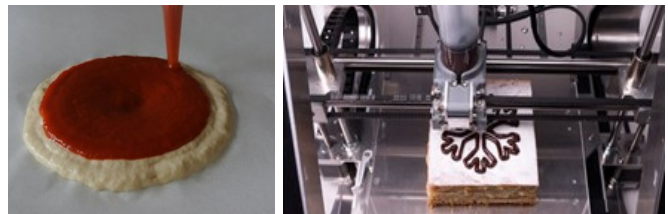
and other parameters, such as density, thickness, and color, are changed via the computer for the second and subsequent layers. After many, many layers, the final product looks like a product that we recognize as, say, a whistle, a wrench, a bolt, or other part to be connected with other parts making up a larger entity.

A couple of decades ago, 3D printing was called rapid prototyping. After the conceptual design of a product, a “blueprint” was used to build a working version of the product—a prototype—for testing. If the tests went well, the product went into mass production. Today, with the precision and repeatability that computers provide, the industrial production of products has been given the name of additive manufacturing—basically just the process of adding materials together to make something. And, yes, there is also subtractive manufacturing, where machining processes remove material in order to end with a particular shape. 3D printing, though widespread, still deals with smaller products. But as the processes and the development of industrial-size printers advance, so too will the range of products, including foods, that we’ll see.

In the article featured here (*3D Food Printing Insights and Opportunities: A Capstone Design Case Study*, p.19), preliminary research was conducted by an interdisciplinary capstone design team of mechanical and electrical engineering students at California State University Fullerton (CSUF). The team was broadly tasked with reverse engineering and manufacturing a 3D food printer.



No, neither the hamburger nor the steak actually came out of a printer. And as a vegetarian, I’m happy to wait a few more years for such foods to come hot-n-ready out of my kitchen printer. The pizza and chocolate-bedazzled layered crisp, on the other hand, I’m ready to start working on tonight!



Editorial Review Board Members

Mohammed Abdallah	State University of New York (NY)	Dale Litwhiler	Penn State University (PA)
Nasser Alaraje	Michigan Tech (MI)	Guoxiang Liu	University of North Dakota (ND)
Ali Alavizadeh	Purdue University Northwest (IN)	Louis Liu	University of New Orleans (LA)
Ammar Al-Farga	University of Jiangnan (CHINA)	Peng Liu	Washington State University (WA)
Aly Mousaad Aly	Louisiana State University (LA)	Mani Manivannan	ARUP Corporation
Paul Akangah	North Carolina A&T State University (NC)	G.H. Massiha	University of Louisiana (LA)
Lawal Anka	Zamfara AC Development (NIGERIA)	Thomas McDonald	University of Southern Indiana (IN)
Jahangir Ansari	Virginia State University (VA)	David Melton	Eastern Illinois University (IL)
Kevin Berisso	Ohio University (OH)	Shokoufeh Mirzaei	Cal State Poly Pomona (CA)
Pankaj Bhambri	Guru Nanak Dev Engineering (INDIA)	Sam Mryyan	Excelsior College (NY)
Michelle Brodke	Bowling Green State University (OH)	Jessica Murphy	Jackson State University (MS)
Shaobiao Cai	Penn State University (PA)	Wilson Naik	University of Hyderabad (INDIA)
Rajab Challoo	Texas A&M University Kingsville (TX)	Arun Nambiar	California State University Fresno (CA)
Vigyan Chandra	Eastern Kentucky University (KY)	Aurenice Oliveira	Michigan Tech (MI)
Isaac Chang	Illinois State University (IL)	Troy Ollison	University of Central Missouri (MO)
Shu-Hui (Susan) Chang	Iowa State University (IA)	Reynaldo Pablo	Indiana University-Purdue University (IN)
Hans Chapman	Morehead State University (KY)	Basile Panoutsopoulos	Community College of Rhode Island (RI)
Rigoberto Chinchilla	Eastern Illinois University (IL)	Shahera Patel	Sardar Patel University (INDIA)
Sanjeevi Chitikeshi	Murray State University (KY)	Jose Pena	Purdue University Calumet (IN)
Phil Cochran	Indiana State University (IN)	Thongchai Phairoh	Virginia State University (VA)
Curtis Cohenour	Ohio University (OH)	Huyu Qu	Honeywell Corporation
Emily Crawford	Southern Wesleyan University (SC)	John Rajadas	Arizona State University (AZ)
Brad Deken	Southeast Missouri State University (MO)	Vijaya Ramnath	Sri Sairam Engineering College (CHENNAI)
Dongyang (Sunny) Deng	North Carolina A&T State University (NC)	Desire Rasolomampionona	Warsaw University of Tech (POLAND)
Z.T. Deng	Alabama A&M University (AL)	Mohammad Razani	New York City College of Tech (NY)
Sagar Deshpande	Ferris State University (MI)	Sangram Redkar	Arizona State University-Poly (AZ)
David Domermuth	Appalachian State University (NC)	Michael Reynolds	University of Arkansas Fort Smith (AR)
Dongliang Duan	University of Wyoming (WY)	Nina Robson	California State University-Fullerton (CA)
Ryan Dupont	Utah State University (UT)	Marla Rogers	Wireless Systems Engineer
Marilyn Dyrud	Oregon Institute of Technology (OR)	Dale Rowe	Brigham Young University (UT)
Mehran Elahi	Elizabeth City State University (NC)	Karen Ruggles	DeSales University (PA)
Ahmed Elsayy	Tennessee Technological University (TN)	Anca Sala	Baker College (MI)
Rasoul Esfahani	DeVry University (OH)	Alex Sergeev	Michigan Technological University (MI)
Morteza Firouzi	University of Technology (MALAYSIA)	Balaji Sethuramasamyraja	California State University Fresno (CA)
Ignatius Fomunung	University of Tennessee Chattanooga (TN)	Mehdi Shabaninejad	Zagros Oil and Gas Company (IRAN)
Ahmed Gawad	Zagazig University (EGYPT)	Hiral Shah	St. Cloud State University (MN)
Marvin Gonzalez	College of Charleston (SC)	Ehsan Sheybani	Virginia State University (VA)
Mohsen Hamidi	Utah Valley University (UT)	Mojtaba Shivaie	Shahrood University of Technology (IRAN)
Mamoon Hammad	Abu Dhabi University (UAE)	Musibau Shofoluwe	North Carolina A&T State University (NC)
Gene Harding	Purdue Polytechnic (IN)	Siles Singh	St. Joseph University Tanzania (AFRICA)
Bernd Haupt	Penn State University (PA)	Ahmad Sleiti	University of North Carolina Charlotte (NC)
Youcef Himri	Safety Engineer in Sonelgaz (ALGERIA)	Amit Solanki	C.U. Shah University (INDIA)
Delowar Hossain	City University of New York (NY)	Jiahui Song	Wentworth Institute of Technology (MA)
Xiaobing Hou	Central Connecticut State University (CT)	Yuyang Song	Toyota Corporation
Shelton Houston	University of Louisiana Lafayette (LA)	Carl Spezia	Southern Illinois University (IL)
Kun Hua	Lawrence Technological University (MI)	Michelle Surerus	Ohio University (OH)
Ying Huang	North Dakota State University (ND)	Jalal Taheri	Bostan Abad Islamic Azad University (IRAN)
Charles Hunt	Norfolk State University (VA)	Harold Terano	Camarines Sur Polytechnic (NABUA)
Dave Hunter	Western Illinois University (IL)	Sanjay Tewari	Louisiana Tech University (LA)
Christian Bock-Hyeng	North Carolina A&T University (NC)	Li-Shiang Tsay	North Carolina A&T State University (NC)
Pete Hylton	Indiana University Purdue (IN)	Vassilios Tzouanas	University of Houston Downtown (TX)
Ghassan Ibrahim	Bloomsburg University (PA)	Jeff Ulmer	University of Central Missouri (MO)
John Irwin	Michigan Tech (MI)	Abraham Walton	Purdue University (IN)
Toqeer Israr	Eastern Illinois University (IL)	Haoyu Wang	Central Connecticut State University (CT)
Sudershan Jetley	Bowling Green State University (OH)	Jyhwen Wang	Texas A&M University (TX)
Rex Kanu	Ball State University (IN)	Liangmo Wang	Nanjing University of Science/Tech (CHINA)
Reza Karim	North Dakota State University (ND)	Boonsap Wichayangkoon	Thammasat University (THAILAND)
Satish Ketkar	Wayne State University (MI)	Alex Wong	Digilent Inc.
Manish Kewalramani	Abu Dhabi University (UAE)	Shuju Wu	Central Connecticut State University (CT)
Tae-Hoon Kim	Purdue University Northwest (IN)	Baijian "Justin" Yang	Ball State University (IN)
Chris Kluse	Bowling Green State University (OH)	Eunice Yang	University of Pittsburgh Johnstown (PA)
Doug Koch	Southeast Missouri State University (MO)	Mijia Yang	North Dakota State University (ND)
Sally Krijestorac	Daytona State College (FL)	Xiaoli (Lucy) Yang	Purdue University Northwest (IN)
Chakresh Kumar	Uttar Pradesh Tech University (INDIA)	Faruk Yildiz	Sam Houston State University (TX)
Zaki Kuruppalil	Ohio University (OH)	Yuqiu You	Morehead State University (KY)
Edward Land	Johns Hopkins Medical Institute	Pao-Chiang Yuan	Jackson State University (MS)
Shiyoung Lee	Penn State University Berks (PA)	Biao Zhang	US Corporate Research Center ABB INC.
Soo-Yen Lee	Central Michigan University (MI)	Jinwen Zhu	Missouri Western State University (MO)
Chao Li	Florida A&M University (FL)		
Jimmy Linn	Eastern Carolina University (NC)		

A VARIABLE-SPEED TURNTABLE FOR ACCELEROMETER PERFORMANCE TESTING

Dale H. Litwhiler, Pennsylvania State University, Berks

Abstract

To test the static performance of MEMS accelerometers in an academic laboratory environment, a means of producing a constant acceleration is required. One method of producing a constant acceleration is with a horizontally rotating turntable with a constant rotational speed. With the device-under-test (DUT) mounted in a fixed orientation and radius from the center of the turntable, the centripetal acceleration experienced by the DUT can be established. The acceleration can then be adjusted by controlling the turntable's speed of rotation. Wireless techniques are used to transmit the measured data from the rotating surface to a stationary data acquisition system. In this paper, the author presents the design and application of a custom variable-speed turntable for use in an academic laboratory for the testing and demonstration of various types of accelerometers. The design of a custom battery-powered wireless data acquisition system to interface with the DUT is also presented. The turntable design includes many safety features that are necessary for this type of rotating apparatus. LabVIEW software, for the formatting and display of the data received from the rotating data acquisition system, as well as accelerometer application examples and testing results are also presented and discussed.

Introduction and Motivation

Solid-state microelectromechanical system (MEMS) accelerometers are ubiquitous in modern consumer products. Among their many applications, they control the orientation of cell phone displays, monitor the vibration of home appliances, and deploy vehicle airbags in the event of a collision (Weinberg, 2009; Doebelin, 2004). In an engineering academic environment, the study of accelerometers is essential to understanding the operation of many modern systems. The concepts employed in the measurement of acceleration are well covered in engineering mechanics courses, but to demonstrate their operation, a suitable testing apparatus is required.

As part of a junior-level instrumentation and measurement course in a BSME program, accelerometers are studied. Laboratory exercises involve the use of very low-g MEMS accelerometers (typically less than 3g) as inclinometers (tilt sensors). This type of static application allows the accel-

erometers to be tested with +1g and -1g accelerations simply by changing their orientation with respect to the earth's gravitational field. This method allows for calibration of very low-g accelerometers to determine the zero-g offset and the static sensitivity of a particular device in one to three dimensions (Freescale, 2015).

To explore the static performance of higher-g accelerometers, a means for producing higher levels of constant acceleration is required. Equation 1 (Halliday & Resnick, 1981) describes a platform rotating in the horizontal plane at a constant rotational speed, ω , that can be used to produce the desired constant acceleration, a , when the DUT is located at a fixed radius, R , from the center of rotation. The acceleration produced by the rotating platform is the centripetal acceleration and is directed radially.

$$a = R\omega^2 \quad (1)$$

To transfer power and measurement signals to and from the DUT, a means of crossing the stationary to rotating parts must be used. Historically, slip rings were used for this purpose (Levy, McPherson, & Hobbs, 1948). Modern systems typically employ batteries on the rotating part to power the measurement system and DUT. Wireless methods, such as infrared/visible light and radio signals, are used to transmit the measurement data from the rotating to stationary equipment. The turntable system described here was originally constructed in a rather crude manner using a thin aluminum disc bolted to the shaft of a small 3-phase induction motor. The motor was fastened to a plywood base and driven by a variable frequency drive (VFD) unit to allow the motor's speed to be varied. The motor and VFD were part of a vendor demonstration setup that was donated to the college. Figure 1 shows a photograph of the original system.

Despite its simplistic design, the original turntable was effective for testing MEMS accelerometers in an engineering laboratory setting. A 9V battery and 5V regulator mounted near the center of the disc were used to power a PIC microcontroller and the DUT. The DUT was mounted at a carefully measured radius near the edge of the turntable. The microcontroller averaged several samples and transmitted the result via its serial port and an infrared LED. A phototransistor circuit connected to the serial port on a bench PC received the transmitted signal. LabVIEW software converted and displayed the serial data.



Figure 1. Photographs of original turntable and portable VFD.

The rotational speed of the spinning disc was controlled by the VFD and measured with a strobe light tachometer. The centripetal acceleration experienced by the DUT could be determined using the measured mounting radius and rotational speed together with Equation 1. To obtain data for negative accelerations, the disc was stopped, the DUT was rotated 180° and remounted, and the disc was spun-up again to the desired speeds. Although the crude system was effective for making measurements, it sorely lacked any kind of safety provisions that would make it useful, except for carefully controlled demonstration purposes. The thin disc was susceptible to bending if not carefully handled and stored. It was also not capable of carrying heavier DUT loads without flexing. Therefore, a safer, more robust design was needed. Figure 2 shows photographs of the redesigned turntable.

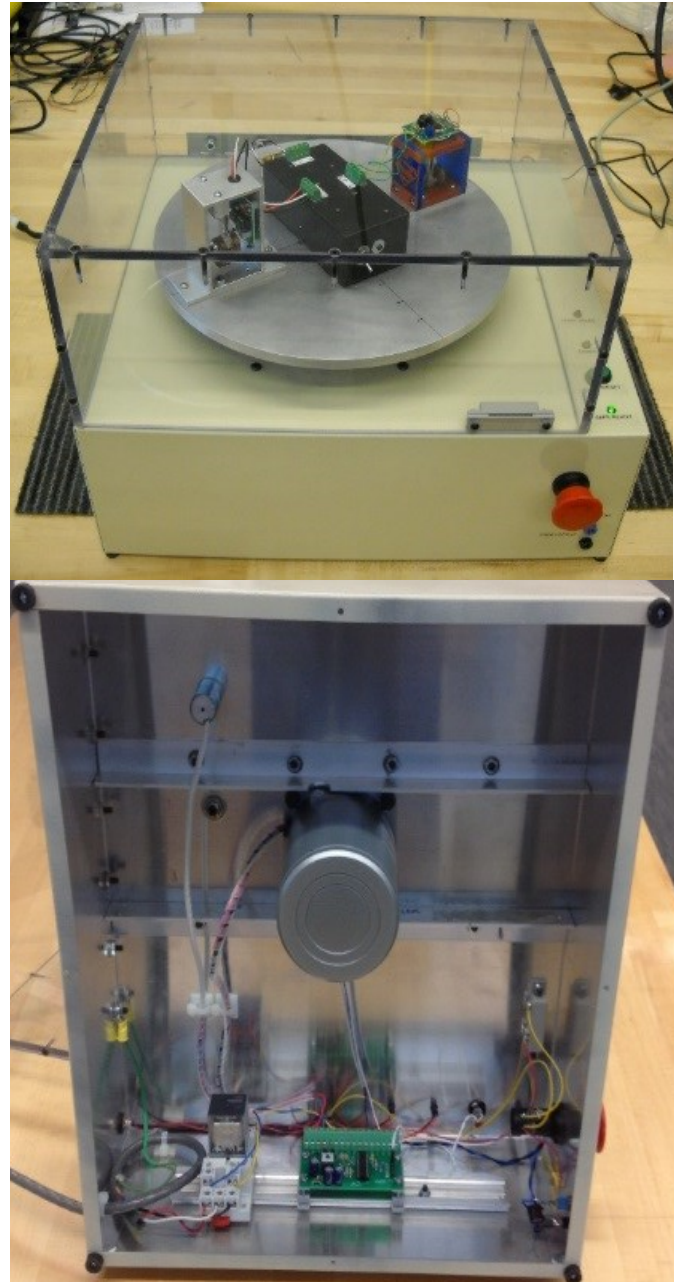


Figure 2. Photographs of redesigned turntable, top and bottom.

System Design

Turntable and Control Electronics

Figure 3 shows a block diagram of the new turntable control and drive system. Based on experience with the original design, a new turntable was designed and built with several improvements:

- A thicker aluminum platter to resist bending (a heavier disc would also serve as a better flywheel to help maintain a more constant rotational speed)
- Clear, shatter-resistant safety cover with interlocks to remove motor power when the cover is lifted
- Sturdy motor mounting enclosure
- Emergency stop button
- Braking system to quickly stop the turntable
- Battery-powered measurement system with a wireless radio data link
- Over-speed shutdown
- Optical encoder for turntable speed measurement
- Reference accelerometer for comparison measurements
- Operational status controls and indicators

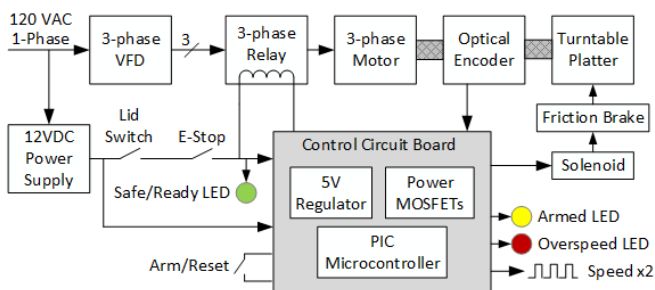


Figure 3. Turntable control and drive system block diagram.

A turntable diameter of 12 inches was chosen for this application. Small DUTs could be mounted at a radius of five inches, which allowed accelerations of 40g to be produced at about 530 RPM. This speed is easily obtained with a small 3-phase motor and VFD. The turntable was machined from 0.375"-thick aluminum in the campus machine shop. This thickness allowed tapped holes to be included for mounting the DUTs and measurement system components. A standard flange was used to mount the platter to the motor shaft. Figure 4 shows a partial assembly drawing of the turntable motor shaft apparatus.

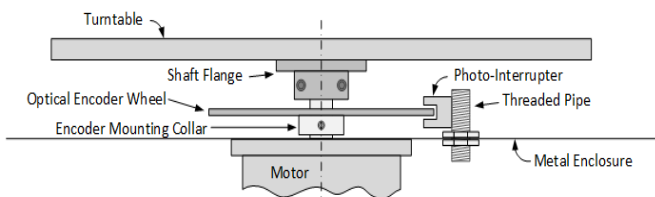


Figure 4. Assembly drawing detail showing shaft-mounted optical encoder.

Although the original turntable motor was adequate for the application, a new motor was purchased that had a slightly thicker shaft and provided mounting holes at the end rather than on the side of the motor. Figure 2 shows

how this would allow the motor to be simply mounted vertically in a sturdy 17"x 15"x 6" aluminum chassis. A 1/8 horsepower, 3-phase, 220/230 VAC induction motor manufactured by Oriental Motor was used. The original, vendor-donated, Allen-Bradley VFD was repurposed to drive the new motor. Figure 1 also shows how it was housed in a rugged tote case. A 0.25"-thick clear polycarbonate lid provided protection from any flying objects, while still allowing full visibility of the turntable area. The lid was hinged at the back edge and equipped with a magnetic reed switch at the front edge to indicate when the lid is open (open switch) or closed (closed switch). Figure 2 also shows the emergency-stop (E-stop) "mushroom" switch mounted on the front of the system enclosure. The E-stop is set (open switch) by simply pressing the mushroom and is reset (closed switch) by twisting the mushroom. The reed switch and E-stop were wired in series, such that the lid must be closed and the E-stop switch must be reset to allow power to be applied to the 3-phase contactor coil, which controls the turntable drive motor regardless of any other control signals from the system's microcontroller.

A microcontroller was used to provide additional safety functions. The 3-phase relay coil is energized via a power MOSFET device controlled by the microcontroller. Another power MOSFET is used to drive a solenoid, which applies the friction brake to quickly stop the turntable. Figure 2 further shows how the 3-phase relay and the control circuit board were mounted to a DIN rail within the chassis. The control system microcontroller software is easily updated via the programming header provided on the PCB. Figure 5 shows how the friction braking mechanism was mounted beneath the turntable. When the braking solenoid is energized, it pulls the plunger down, which pushes the brake pad up against the bottom of the platter at a radius of about three inches. The underside of the platter is kept clear with no obstructions at this radius. The braking friction can be changed by adjusting the height of the threaded fulcrum post.

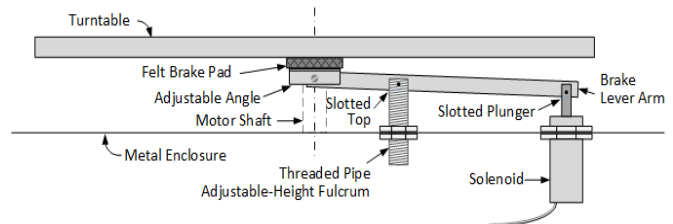


Figure 5. Assembly drawing detail showing friction brake mechanism.

Braking action is controlled by energizing the brake solenoid for a fixed time interval that is set in the microcontroller software. A braking interval of five seconds was found to work well for rotational speeds up to 531 PRM, which

produces 40g at a radius of five inches. The main purpose of the brake is to quickly stop the turntable if the lid is lifted or the E-stop button is pressed. Another benefit of the brake is to minimize the wait time until the DUTs and measurement system hardware can be accessed at the end of a test cycle.

Figure 5 also shows how the turntable speed is measured with an optical encoder wheel mounted to the motor shaft. The encoder wheel was designed and 3D printed with the help of an undergraduate mechanical engineering student. The encoder wheel was five inches in diameter, 1/16"-thick ABS plastic, and contained 120 slits near the outer edge. The wheel was mounted to the motor shaft using a standard shaft collar arrangement. With 120 slits, the frequency of output pulses of the associated photo-interrupter was numerically equal to twice the speed of the motor in revolutions per minute, as described by Equation 2:

$$\left(\frac{120 \text{ pulses}}{1 \text{ rev}} \right) \left(\frac{n \text{ rev}}{1 \text{ min}} \right) \left(\frac{1 \text{ min}}{60 \text{ sec}} \right) = 2n / \text{sec} \quad (2)$$

The embedded microcontroller's software served as a state-machine that implements the state diagram shown in Figure 6. The primary function of the microcontroller is to ensure safe operation of the turntable. As previously described, the safety lid and E-stop switches can independently de-energize the 3-phase relay. The microcontroller, however, will not allow the relay to be re-energized until both of these switches are closed and the Go/Arm button has been pressed. A timed braking interval is also applied by the microcontroller upon either opening of the safety lid or activation of the E-stop switch, and the system is returned to the starting point, STATE 0.

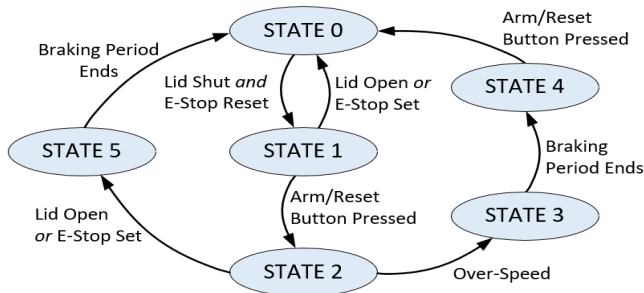


Figure 6. State diagram of embedded turntable control software.

The microcontroller continually measures the speed of the turntable by counting pulses from the optical encoder. If the number of pulses exceeds the programmed over-speed threshold, the 3-phase relay is de-energized and the braking interval is initiated. The system is then returned to the starting point, STATE 0. The over-speed threshold is set to an appropriate value based on the current application of the turntable.

Measurement System

As previously shown in Figure 2, the measurement system is battery powered and mounted at the center of the rotating turntable. The nominal 6V battery voltage is produced by four AA alkaline cells. A low-dropout (LDO) 5V regulator provides the voltage used by the PIC microcontroller, which performs the 10-bit analog-to-digital (A2D) conversions of the DUT output signal(s). The 5V LDO also powers the DUT, as needed. A separate 3.3V regulator produces the supply voltage for the XBee wireless transceiver, which is used to transmit the measured data from the turntable-mounted measurement system to the stationary computer. The XBee XB24-ACI-001 device was used in the turntable system. This device is now obsolete and has been replaced by a similar device, XB24-AWI-001 (Digi, XBee, n.d.). Figure 7 shows a block diagram of the measurement system, while Figure 8 shows a photograph of the system with the lid removed and flipped. As can also be seen in Figure 8, the bulk of the electronics are mounted on the underside of the lid.

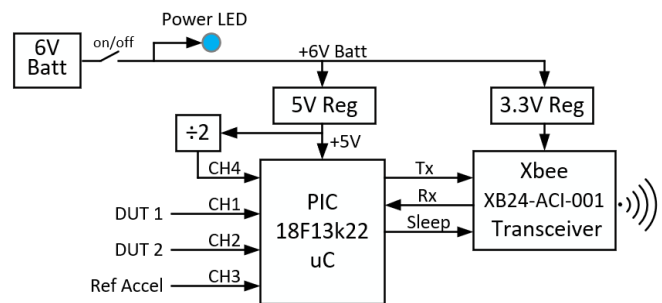


Figure 7. Turntable-mounted measurement system block diagram.

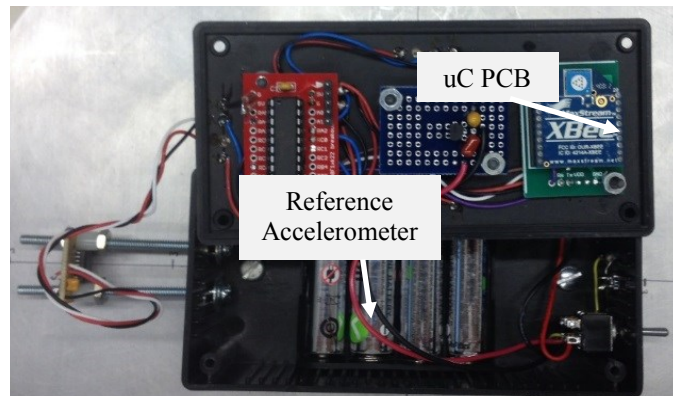


Figure 8. De-lidded turntable-mounted measurement system.

The measurement system microcontroller performs a 10-bit A2D conversion on each DUT output voltage, the reference accelerometer output voltage, and the 5V regulator output voltage (through a resistive voltage divider circuit).

cuit). Sixty-four equally spaced measurements are performed on each channel during a two-second interval. The average value for each set of 64 measurements is computed and the results are sent out the serial port at 9600 baud to the XBee transceiver. To conserve battery energy, the microcontroller awakens the XBee just long enough to transmit the measurements (about 30ms). The PIC 18F13k22 microcontroller was programmed in C using the Microchip xc8 compiler and MPLAB X IDE (Microchip, 1998-2018). The paired XBee device receives the data burst and conveys it to a PC via a USB connection. Figure 9 shows how the LabVIEW software on the PC was used to read the data bytes and reassemble them into the original measured values that are then displayed. The XBee devices were programmed using the Digi XCTU application (n.d.).

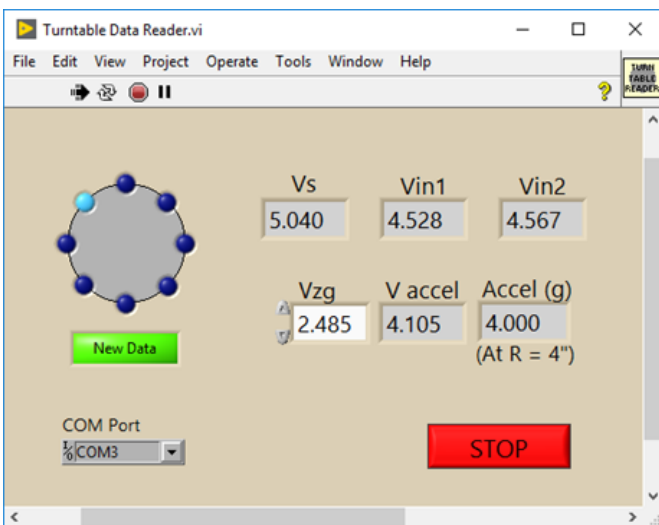


Figure 9. LabVIEW front panel for accelerometer data display.

The reference accelerometer was mounted on an adjustable, threaded mechanism such that it could be precisely placed at a given radius on the turntable. The output voltage of the reference accelerometer was used to determine the acceleration experienced by the DUTs. A Freescale MMA1250 +/-5g accelerometer was used for the reference device.

Example Applications

The initial application of the turntable was to test the performance of a student accelerometer design project. Mechanical engineering students in a third-year instrumentation and measurement course were tasked with designing and building a $\pm 4g$ accelerometer using a load cell beam as the sensing element (Litwhiler, 2018). The students could calibrate their instruments over a $\pm 1g$ range by simply changing the device orientation with respect to earth's grav-

ity. However, to test the full-scale range performance of their designs, the turntable was used to produce the required 4g acceleration. Figure 10 shows how two DUTs could be mounted and tested simultaneously. Each DUT was mounted to an aluminum footplate, which was then secured to the turntable's tapped mounting holes. This "personality" footplate mounting technique avoided the need for drilling new holes in the turntable for each new application or requiring that each application conform to the existing turntable hole pattern.

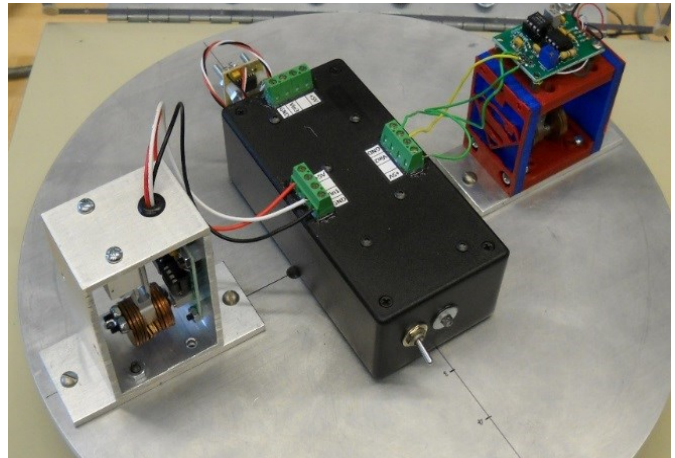


Figure 10. Two DUTs mounted to turntable and connected to a measurement system.

The turntable rotational speed needed in order to produce 4g acceleration at a radius of 4 inches is approximately 188 RPM. The student project requirements stated that their design must tolerate an acceleration of $\pm 6g$ without exceeding the limits of any component. The 6g acceleration at a radius of 4 inches was achieved with a speed of approximately 230 RPM. At this speed, the optical encoder produced 460 pulses per second. The microcontroller used an aperture time of 0.1s; therefore, 46 pulses were counted at 230 RPM. Thus, for this application, the over-speed threshold was set at 46 counts. If this threshold is exceeded, the 3-phase relay is de-energized, and the braking interval is commenced.

The DUTs were tested at rotational speeds to produce nominal accelerations of 1g, 2g, 3g, and 4g at the 4-inch radius where the DUTs were mounted. The frequency of the VFD was adjusted while monitoring the output of the calibrated reference accelerometer to determine the actual acceleration experienced by the DUTs. The turntable was then stopped to allow the DUTs to be rotated 180° about the 4-inch radius mounting point, so that acceleration in the opposite direction could be tested. Table 1 and Figure 11 show examples of data from this application.

Table 1. Turntable and reference accelerometer example data.

Nominal Accel.	VFD Frequency	Turntable Speed	Calculated Accel. at 4"	Ref. Accel. Output	Ref. Accel.
0g	0 Hz	0 RPM	0g	2.485	0.004g
1g	4.07 Hz	94 RPM	1.004g	2.885	1.001g
2g	4.90 Hz	133 RPM	2.009g	3.285	1.999g
3g	5.72 Hz	163 RPM	3.018g	3.698	3.032g
4g	6.51 Hz	188 RPM	4.014 g	4.105	4.050g

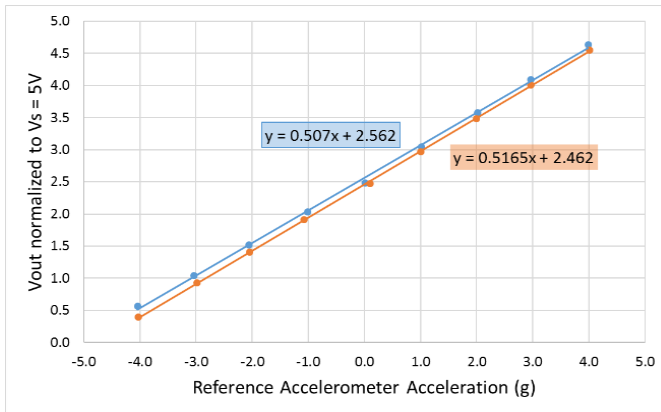


Figure 11. Plot of turntable test data for two student-built accelerometers.

Another application of the turntable was for demonstration of MEMS accelerometers for engineering and engineering technology students. To increase the visual impact of the test system and to help students appreciate the relationship between rotation and centripetal acceleration, a 40g accelerometer was used. The Freescale (now NXP) MMA2201D device mounted to a PCB was used for this demonstration. Figure 12 shows two DUTs mounted to polycarbonate personality plates on the turntable at a radius of five inches. For this application, the applied acceleration was determined by a rotational speed measurement without a reference accelerometer.

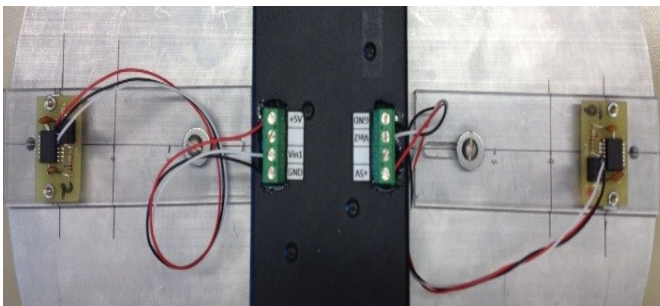


Figure 12. MMA2201D accelerometers mounted to turntable.

To produce a centripetal acceleration of 40g at a radius of 5 inches, a rotational speed of 531 RPM was needed. To allow for this speed on the turntable, the over-speed shut-down threshold was set to 550 rpm. This was done by changing the microcontroller software such that 110 counts during the 0.1s aperture time would initiate the power disconnect and braking interval. To measure the speed of rotation, a Fluke model 187 DMM was used to measure the frequency of the optical encoder output pulses. The rotational speed was adjusted via the VFD to obtain the desired acceleration. Table 2 shows sample data from this test.

Table 2. Turntable data from tests to produce up to 40g acceleration.

Nominal Acceleration	Required Nominal Speed	VFD Frequency Setting	Optical Encoder Frequency	Resulting Acceleration at 5" Radius
10g	265.4	9.04 Hz	530 Hz	9.97g
20g	375.3	12.58 Hz	750 Hz	19.96g
30g	459.7	15.29 Hz	919 Hz	29.98g
40g	530.8	17.71 Hz	1062 Hz	40.03g

Uncertainty Analysis

The uncertainty in the acceleration experienced by a DUT on the turntable can be estimated by examining Equation 1. The propagation of uncertainty from the measured quantities (radius and rotational speed) to the result (acceleration) is determined by the sensitivity of the result to each of the parameters. The sensitivity is found by taking the partial derivative of the result with respect to each measured quantity. The uncertainty in each measured quantity (u_r , u_n) is then weighted by their respective sensitivities. The overall uncertainty in the result is then found by combining the components in an RSS manner (Figliola & Beasley, 2015). Starting with Equation 1, converted to Equation 3 such that the radius is in inches, the rotational speed is in rpm, and the acceleration is in g:

$$a = (2.839 \times 10^{-5}) r n^2 \quad (3)$$

The uncertainty in the acceleration can then be found using Equation 4:

$$u_a = \pm \sqrt{\left(\frac{\partial a}{\partial r} u_r\right)^2 + \left(\frac{\partial a}{\partial n} u_n\right)^2} \quad (4a)$$

$$u_a = \pm 2.839 \times 10^{-5} \sqrt{(n^2 u_r)^2 + (2 r n u_n)^2} \quad (4b)$$

The uncertainty in the rotational speed of the turntable relates to its ability to accurately count pulses from the optical encoder during a fixed aperture time. Using a Fluke model 187 DMM to measure the frequency of the optical encoder output provided an accuracy of $\pm 0.005\%$ of the reading + 1 count (Fluke, 2002). As shown in Equation 2, the encoder output frequency is twice the value of the rotational speed in rpm. Therefore, the uncertainty in the rotational speed can be estimated to be about ± 1 rpm. The uncertainty in the measured radius relates to both the ability to accurately place the DUT on the turntable and the location of the active sensing element within the DUT (IEEE, 2009). For the purposes of this analysis, it was assumed that the DUT could be placed at a known radius to within ± 0.05 ". For small surface-mount MEMS accelerometers, the package size is on the order of 0.15" square. Therefore, the uncertainty in the location of the sensing element within the package is less than 0.075". Combining these uncertainties in an RSS manner results in ± 0.09 " uncertainty in the radius or rotation.

Larger accelerometers, such as the one designed by the engineering students, are subject to higher uncertainty in the position of the center of the seismic mass that loads the sensing element. For this analysis, the uncertainty of the center of mass was assumed to be on the order of ± 0.1 ". Once again, combining this uncertainty with that of DUT placement in an RSS manner results in an uncertainty of ± 0.11 " in the radius of rotation. Table 3 shows the overall uncertainty in the applied acceleration for some sample combinations of radius and rotational speed.

Table 3. Applied acceleration uncertainty samples.

Radius	Rotational Speed	Nominal Acceleration	Acceleration Uncertainty, u_a
4.0 ± 0.11 "	94 ± 1 RPM	1.004g	± 0.035 g
4.0 ± 0.11 "	188 ± 1 RPM	4.014g	± 0.118 g
5.0 ± 0.09 "	84 ± 1 RPM	1.002g	± 0.030 g
5.0 ± 0.09 "	531 ± 1 RPM	40.03g	± 0.736 g

Future Work and Improvements

The turntable proved to be very useful and will continue to be modified and improved to meet the needs of the engineering courses and projects. The measurement system hardware can easily be modified to allow testing of accelerometers with digital interfaces (I2C, SPI). The measurement system software can easily be modified to include two-way communication with the PC. This will allow the user

to make changes to measurement configuration while the turntable is in motion (such as changing the measurement range of a DUT with a digital communication interface). Other faculty members also expressed interest in using the turntable to test/calibrate more complex inertial measurement units.

Conclusions

The re-designed turntable centrifuge incorporates several improvements in safety, ease of use, and quality of construction. The safety features allow the system to be used more confidently by students and faculty. The turntable and measurement system controls are intuitive and easy to connect and use. The new turntable platter and metal chassis provide a very sturdy and robust platform on which to test accelerometer devices. The quality of materials and construction techniques produced a test apparatus that allows for highly repeatable measurements.

References

- Digi. (n.d.). *XCTU, next generation configuration for Xbee/RF solutions*. Retrieved from <https://www.digi.com/products/xbee-rf-solutions/xctu-software/xctu>
- Digi. (n.d.). *XBee S1 802.15.4 low-power module w/ wire antenna*. Retrieved from <https://www.digi.com/products/models/xb24-awi-001>
- Doebelin, E. (2004). *Measurement Systems, Application and Design*. (5th ed.). New York: McGraw-Hill.
- Figliola, R., & Beasley, D. (2015). *Theory and design for mechanical measurements*. (6th ed.). New York: John Wiley & Sons, Inc.
- Fluke. (2002). *Model 187 & 189 true RMS multimeter: Users manual*. Retrieved from http://assets.fluke.com/manuals/187_189_umeng0200.pdf
- Freescale Conductor. (2015). *High-precisions calibration of a three-axis accelerometer*. Retrieved from http://cache.freescale.com/files/sensors/doc/app_note/AN4399.pdf
- Halliday, D., & Resnick, R. (1981). *Fundamentals of physics*. (2nd ed.). New York: John Wiley & Sons, Inc.
- IEEE. (2009). *836-2009—IEEE recommended practice for precision centrifuge testing of linear accelerometers*. Retrieved from <https://ieeexplore.ieee.org/document/5252583/>
- Levy, S., McPherson, A., & Hobbs, E. (1948). *Calibration of accelerometers*. Retrieved from https://nvlpubs.nist.gov/nistpubs/jres/041/jresv41n5p359_A1b.pdf
- Litwhiler, D. (2018). Design, development, and testing of load cell accelerometers. *Proceedings of the 125th*

ASEE Annual Conference and Exhibition. Washington, DC: ASEE.

Microchip. (1998-2018). *MPLAB XC compilers*. Retrieved from <http://www.microchip.com/mplab/compilers>

Weinberg, H. (2009). Accelerometers – Fantasy & reality. *Analog Dialogue*, 43(2), 13-14.

Biography

DALE H. LITWHILER is an associate professor at the Penn State Berks campus. He received his BS from Penn State University, MS from Syracuse University, and PhD from Lehigh University, all in electrical engineering. Prior to beginning his academic career, he worked with IBM Federal Systems and Lockheed Martin Commercial Space Systems as a hardware and software design engineer. Dr. Litwhiler may be reached at dale.litwhiler@psu.edu

HYBRID, SEMI-PASSIVE SOLAR HARVESTING SYSTEM

Aleksandr Sergeev, Michigan Technological University; Austin Etzel, Michigan Technological University;
Joe Mayrose, Michigan Technological University

Abstract

There are a variety of solar systems installed around the globe. Some are designed to track the sun, while others are fixed-panel systems. The stationary systems lose potential power, since most of the time they are not perpendicular to the sun. The purpose of this current project was to investigate the viability, at high latitudes ($>40^\circ$), of having a solar system track the sun throughout the day. By adjusting the angle of the panels, the solar panels capture power that would typically be unattainable through a fixed-panel system. This project used a set of actively controlled solar panels and a set of stationary panels to compare power collected on any given day. The power generated from these panels was fed into a charge controller to charge a set of deep-cycle batteries. Voltage readings were taken to allow for accurate comparisons between the fixed and tracking solar panels. By comparing the data between the two sets of panels, a net power increase of up to 30% was achieved.

Introduction

Solar energy is radiant light and heat from the sun that is harnessed using a range of ever-evolving technologies, such as solar heating, photovoltaics, solar thermal energy, solar architecture, molten salt power plants, and artificial photosynthesis. To capture solar energy, a solar tracker can be used. This is a device that orients a payload toward the sun. Payloads are usually solar panels, parabolic troughs, Fresnel reflectors, lenses, or the mirrors of a heliostat. For flat-panel photovoltaic systems, trackers are used to minimize the angle of incidence between the incoming sunlight and a photovoltaic panel. This increases the amount of energy produced from a fixed amount of installed power generating capacity. In standard photovoltaic applications, it was predicted in 2008-2009 that trackers could be used in at least 85% of commercial installations.

In 2017, the U.S. Energy Information Administration announced that more than half of the utility-scale photovoltaic systems track the sun throughout the day (Today, 2017). A significant amount of research has been conducted on the feasibility of utilizing solar tracking systems and their advantages (Mousazadeh, Keyhani, Javadi, Mobli, Abrinia, & Sharifi, 2009; Chong & Wong, 2009; Abdallah & Nijmeh, 2004; Al-Mohamad, 2004; Eskiçirak, Akyol, & Karakaya, 2014). The systems that require manual adjustments of solar

panels have significant disadvantages, due to lower efficiency and manual labor involvement. The goal of this project was to establish if an open-loop, single-axis, active tracking system would be viable at high-latitude ($>40^\circ$) locations. Directly comparing the power generation from fixed and tracking panel systems can help determine the effectiveness of the system.

Project Rationale

As the efficiency of solar panels rises, it becomes more and more advantageous to implement solar tracking systems in residential and small commercial applications. These tracking systems should provide an increase in power by spending more time perpendicular to the sun. There are two main categories of tracking systems, open-loop and closed-loop. Open-loop systems rely on known coordinates for both solar azimuth and elevation. These systems operate based on solar positioning and can be accurate down to thousandths of a degree. Also, since no sensor feedback is required, the system is less complex. Closed-loop systems use different forms of light sensors to keep the array perpendicular to the sun (Safan, Shaaban, & El-Sebah, 2017; Reddy, Chakraborti, & Das, 2016). These systems are more sensitive to partial shading or covering with snow or dust, due to the high voltage levels provided by the perpendicular panels. Another type of closed-loop system uses the panels themselves as light sensors (Sharma, Vaidya, & Jamuna, 2107). This system has similar problems to other closed-loop systems, with the added disadvantage of limiting panel connections. Another disadvantage of closed-loop systems is hunting time. For a one-axis tracker, the array continues to move until the power has gone down and then moves back into the maximum power position. Dual-axis trackers frequently update the position based on the readings from light sensors; anytime this happens, the control system must take a minimum of three readings before settling on a point. In both cases, excess power is consumed by running the motors and controllers more often. This is especially true in the dual-axis tracking system (Bahrami, Okoye, & Atikol, 2016).

System Overview

This current project focused on the use of a hybrid tracking panel array. This type of system uses an open-loop system to automatically track along the solar azimuth and a

manual adjustment for the altitude of the panels. At northern latitudes, the azimuth of the sun changes much more than the altitude throughout the day. Thus, active tracking along the altitude would increase the complexity of the system with no significant gain in performance.

Since solar intensity varies from day to day, a set of stationary panels and a set of tracking panels were used simultaneously, allowing accurate daily comparisons of data. Figure 1 shows a picture of the tracking and fixed systems; the tracking system is on the right and the fixed system on the left. An Arduino MEGA R3 controls the linear actuator to track the sun across the azimuth, and it monitors the voltages of the solar panels. This system uses pre-programmed angles to move the tracking panels throughout the day, changing the solar tracker angle every half hour. Information such as location of the system and date and time information were used to calculate the required angles for adjustment of the panels (Gronbeck, 2009). The voltage from the panels is fed into a charge controller, which regulates the output to the battery array for effective charging. An inverter is connected to the battery array to allow for an AC output. Grid integration is possible with this system, provided that the inverter outputs a complete sinewave. Less expensive inverters output a modified sinewave that is not as efficient and are not compatible for grid integration.



Figure 1. Photograph of fixed and tracking system setup.

Figure 2 shows the main components as they were connected in the system. The tracking and fixed solar panels are Renogy RNG-100D 100W models (Renogy, 100W, n.d.). These were chosen for their balance of efficiency and cost. The linear actuator is from Fergelli Automations (Model FA-PO-150-12-8). It has a 150 lb. lift capacity and an 8-inch stroke with Bourne potentiometer feedback. The position feedback is crucial for obtaining accurate angle measurements. The Arduino used was a MEGA R3 with an Adafruit assembled data-logging shield (Earl, 2017). The data-logging shield was used both for voltage measurements and

for the feedback sensor on the linear actuator. The charge controller was an Outback Solar FlexMax 80A (Outback, 2017) with maximum power-point tracking. The MPPT model was chosen for its high efficiency and high mobility, due to its pre-wired configuration with a pure sinewave inverter.

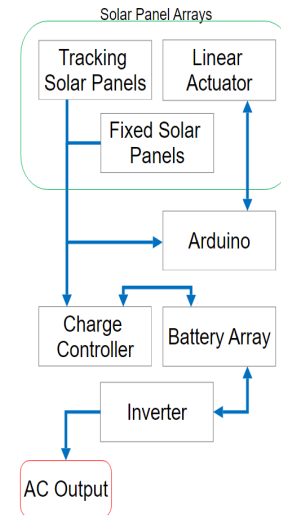


Figure 2. System component flowchart.

The battery storage bank consists of four Renogy 100Ah deep-cycle gel cells (Renogy, 100Amph, n.d.), chosen for their ability to withstand 1000 cycles to 50% depth of discharge (DOD), while a similar AGM battery would only withstand 600 cycles to 50% DOD. Figure 3 shows the full schematic of the system. The six solar panels were connected in series for most efficient power transfer. The voltage of the four fixed panels was measured as well as the full voltage of all six panels. The voltage measurements of the panels were too large for the Arduino to measure directly, so two voltage dividers were implemented to effectively reduce the voltage. The voltages were then calculated in the code using the reduced voltage from the voltage dividers and recorded on the SD card for further study. The Arduino controls a pair of 12V, 30A relays, which in turn control the linear actuator. The Arduino also outputs a 5VDC signal that was used on the linear actuator for potentiometer feedback as well as to power the motor control relays.

Programming Approach and System Operation Modes

The main approach when writing the code and deciding on operation modes was to make the code efficient, resulting in the Arduino consuming less power and improving the efficiency of the system as a whole. The code has three basic operation modes: rest, stationary data collection, and

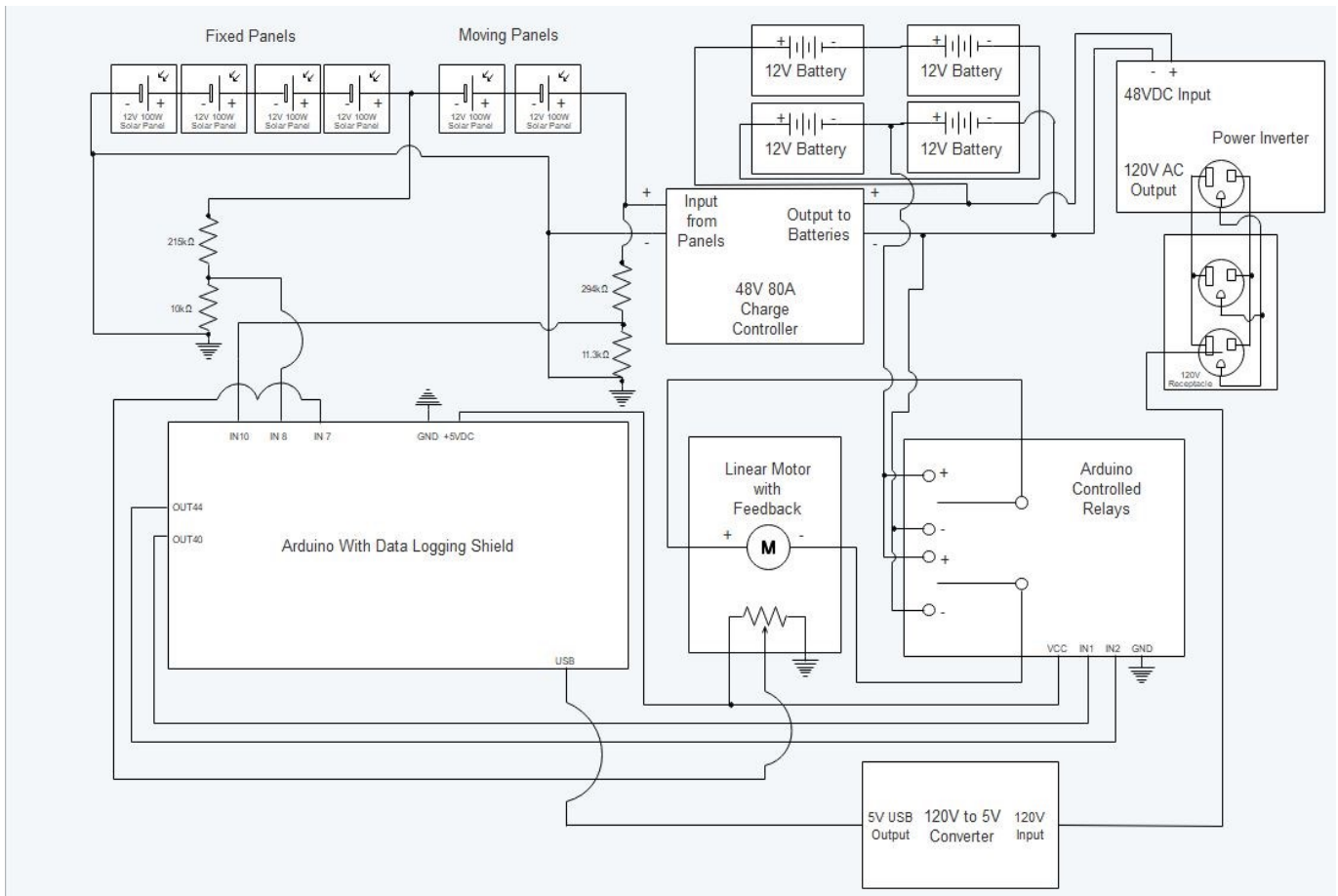


Figure 3. System schematic.

data collection with panel movement. The start and stop times of these three modes are based on the sunrise and sunset times for the current month. The rest mode is set to start at sunset and end at sunrise. These specific times are set by the user at the beginning of each month, since sunset and sunrise are not at constant times throughout the year. When the controller first enters rest mode, it moves the panels to the correct position for the morning sun and then wait until sunrise.

The stationary data collection mode occurs at two separate time periods during the day. The reason for a separate data collection mode outside of the panel movement with data collection mode is due to the mechanical limitations of the panel holder, which will be discussed later. This mode operates from sunrise until the data collection with panel movement mode begins. This mode resumes operation at the end of the data collection with panel movement mode and operates until sunset. The stationary data collection mode takes voltage readings every 10 seconds and stores them on an SD card for later analysis. Due to the mechani-

cal limitations of the panel holder, since the code keeps the panels aimed in the general direction of the sun when outside the movement range, there should still be an increased amount of power intake by the panels. This is why there are separate modes for just stationary data collection and data collection with panel movement.

Data collection with panel movement mode operates during the peak hours of solar intensity. This mode operates between three and five hours a day, depending on the time of year. The movement starts between 11:30 and 12:00 and concludes between 3:30 and 4:30; again, depending on the month. Due to the mechanical limits of the panel holder, the only azimuth angles (Bas, 2011) the system can adjust to are between -30° and 45° from due south. This means that panel adjustment occurs only 8-10 times a day. While in this mode, the panels move every half hour to a set angle, depending on the time and the month. As with the stationary data collection mode, this mode takes a data reading every 10 seconds and stores the data on the SD card for future analysis.

Figure 4 shows a flowchart of how the code and microcontroller operate throughout the day. The first part of the flowchart shows the startup procedures of the code, microcontroller, and data-logging shield. During the power-up phase of the microcontroller, the standard initializations of the microcontroller are executed. Next, the data-logging shield is powered on, and the microcontroller verifies that it is functioning properly. Finally, the code checks to verify the presence of an SD card. It then creates a new CSV file on the SD card and labels the first line of the CSV file with the appropriate labels for the data being recorded. This part of the code is only executed on startup and is then superseded by the loops shown on Figure 3.

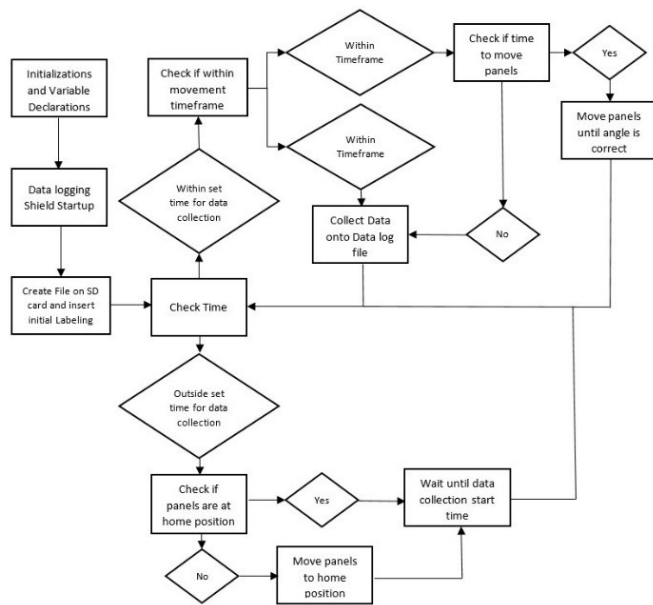


Figure 4. Microcontroller code flowchart.

Once the initializations have been completed, the code acquires the current time from the data-logging shield, which uses an onboard RTC (real time clock) chip to keep accurate time. Depending on the time of day, the code goes into one of the three modes of operation as described above. The bottom loop of Figure 3 shows the rest mode, which first verifies that the panels are in their home positions. If they are not in their home positions, the microcontroller moves them back to their home positions. The code then waits until sunrise to begin data-logging. The top loops of Figure 3 show both the stationary data collection mode as well as the data collection with panel movement mode. The microcontroller decides which mode to use, based on the time acquired from the data-logging shield (Solmetric, 2008). If the current time is within the preset timeframe for the data collection with panel movement mode, the code then checks the time against the preset times for panel angle adjustment. If the current time matches the preset times for

readjustment, the microcontroller adjusts the panels to the appropriate angle for the current time. If it is not time to move and readjust the panel's angle, the microcontroller then uses the data-logging shield to record the current data readings of the system. If the current time acquired from the data-logging shield is outside the timeframe for the data collection with panel movement mode, the microcontroller then enters the stationary data collection mode and only records data.

Cost and Parts List

Table 1 provides a list of each part and its associated cost. This table is provided to aid in the recreation of the design and to allow the data to easily be reproduced.

Data Collection and Analysis

Figure 5 shows a sample set of data acquired from the system. These data were collected using the Adafruit data-logger described above. The logger took a measurement every 10 seconds for around 5000 data points per day. The data collection started at 6:00 a.m. local time and lasted until 10:00 p.m. The average net voltage gain for Figure 5 shows that a tracking system is viable in high latitudes. Specifically, 4/27 shows a gain of 26%; 4/28 shows a gain of 21%; and, 4/29 shows a gain of 17%. Because the panels are all wired in series, the difference in voltage will be proportional to the difference in instantaneous power.

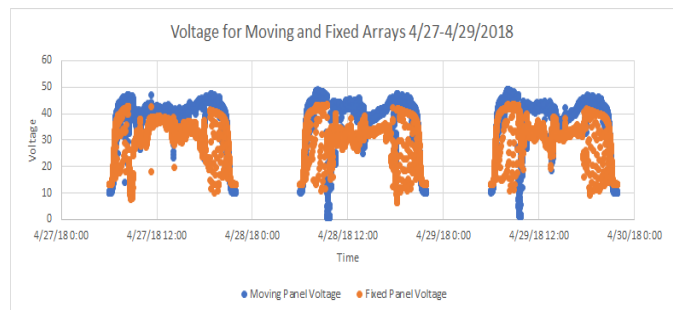


Figure 5. Voltage measurements for 4/27/2018 through 4/29/2018.

Conclusions and Future Work

Short-term data collection and analysis showed that the tracking system generates roughly 15-25% more power than a traditional fixed-panel system. Due to limited data, further experimentation and analysis are required to reach a more definitive conclusion as to the viability of a hybrid, semi-passive solar harvesting system versus a traditional fixed-panel system. However, due to the amount of additional voltage gain and the consistency of the data (see again Fig-

Table 1. Detailed parts list and associated costs.

Quantity	Item	Description	Cost per unit	Cost Total
1	Outback Power FP1 VFXR3648A solar kit	3600W 48VDC pre-wired MPPT charge controller and inverter system	\$3660.10	\$3660.10
2	Solar panel expansion	3 100W Renogy solar panels	\$377.97	\$755.94
2	Renogy battery	100Ah deep cycle battery	\$229.99	\$459.98
1	Arduino	Arduino MEGA R3 microcontroller	\$44.95	\$44.95
1	Data-logging shield	Adafruit Industries data-logging shield board	\$12.99	\$12.99
1	Relay	x2 12V 30A relay	\$8.33	\$8.33
1	Linear motor	Firgelli Automations 150lb Capacity 8in stroke with Bourmes potentiometer feedback	\$138.84	\$138.84
2	Battery boxes	Outdoor grade with ventilation	\$12.86	\$25.72
1	Stationary frame materials	Assorted lumber and hardware	\$70	\$70
1	Miscellaneous	Connectors, hardware, and wiring	\$100	\$100
4	1/8" steel tubing	38' of tubing for tracking array frame	\$150	\$150
1	Waterproof case	Container for all the circuit and delicate instruments	\$104	\$104
			Total Cost	\$5370.56

ure 5), it is evident that this system could be feasible as a power-harvesting system.

Further data collection and analysis are needed to develop a more definitive conclusion as to the viability of this system. The system is set up to collect identical sets of data throughout the coming months. To improve the accuracy of future data collection, a few upgrades will be necessary for the current system; namely, connecting the grid-tie-compatible inverter to the electrical grid. This would allow for the best data collection, as it would use all of the energy generated by the solar panels. Data collected during those months will then be used to further support or refute the claims made here.

Acknowledgments

The authors would like to thank the Michigan Technological University's School of Technology for sponsoring this project and providing the lab space for design and testing. Additional thanks to the School of Technology machine shop for their help in the construction of the aluminum and steel framing, and to Dave Camps at Blue Terra Energy for his advice and comments on traditional fixed-panel solar systems.

References

- Abdallah, S., & Nijmeh, S. (2004). Two axes sun tracking system with PLC control. *Energy Conversion and Management*, 45(11-12), 1931-1939.
- Al-Mohamad, A. (2004). Efficiency improvements of photo-voltaic panels using a Sun-tracking system. *Applied Energy*, 79(3), 345-354.
- Bas, L. (2011). *Calculating your optimal azimuth angle*. Retrieved from <https://www.civicsolar.com/support/installer/articles/effect-azimuth-angle-sun-energy-output>
- Bahrami, A., Okoye, C., & Atikol, U. (2016). The effect of latitude on the performance of different solar trackers in Europe and Africa. *Applied Energy*, 177, 896-906.
- Chong, K. K., & Wong, C. W. (2009). General formula for on-axis sun-tracking system and its application in improving tracking accuracy of solar collector. *Solar Energy*, 83(3), 298-305.
- Earl, B. (2017). *Adafruit data logger shield*. Retrieved from <https://learn.adafruit.com/adafruit-data-logger-shield/overview>
- Eskiçirak, U., Akyol, T., & Karakaya, M. B. (2014). Sun tracking system. *İstanbul Aydın Üniversitesi Dergisi*, 4(14), 1-6.

-
- Gronbeck, C. (2009). *Sustainable by design: Sun angle*. Retrieved from <http://www.susdesign.com/sunangle/>
- Mousazadeh, H., Keyhani, A., Javadi, A., Mobli, H., Abrinia, K., & Sharifi, A. (2009). A review of principle and sun-tracking methods for maximizing solar systems output. *Renewable and Sustainable Energy Reviews*, 13(8), 1800-1818.
- Outback Power FlexMax 80. (2017). Retrieved from http://www.outbackpower.com/downloads/documents/integrated_systems/flexpower_one_fxr/flexpoweronefxr_specsheet.pdf
- Reddy, J. S., Chakraborti, A., & Das, B. (2016). Implementation and practical evaluation of an automatic solar tracking system for different weather conditions. *Proceedings of the IEEE 7th Power India International Conference*. Piscatawny, NJ: IEEE.
- Renogy 100Amp batteries. (n.d.). Retrieved from <https://www.renogy.com/renogy-deep-cycle-pure-gel-battery-12-volt-100ah/>
- Renogy 100W solar panel. (n.d.). Retrieved from <https://www.renogy.com/renogy-100-watt-12-volt-monocrystalline-solar-panel/>
- Safan, Y. M., Shaaban, S., & El-Sebah, M. I. A. (2017). Hybrid control of a solar tracking system using SUI-PID controller. *Proceedings of Sensors Networks Smart and Emerging Technologies*. Piscatawny, NJ: IEEE.
- Sharma, A., Vaidya, V., & Jamuna, K. (2107). Design of an automatic solar tracking controller: Solar tracking controller. *International Conference on Power and Embedded Drive Control*. Piscatawny, NJ: IEEE.
- Solmetric. (2008). *Annual insolation as a function of panel orientation: Houghton, MI*. Retrieved from http://www1.solmetric.com/cgi/insolation_lookup/match.cgi?state=MI&city=HANCOCK%20HOUGHTON%20CO%20AP
- Today in energy. (2017). Retrieved from <https://www.eia.gov/todayinenergy/detail.php?id=30912>
- involved in promoting engineering education. Dr. Sergeev may be reached at avsergue@mtu.edu
- AUSTIN ETZEL** is pursuing an undergraduate degree in electrical engineering technology in the School of Technology at Michigan Tech. Mr. Etzel may be reached at ajetzel@mtu.edu
- JOE MAYROSE** is pursuing an undergraduate degree in electrical engineering technology in the School of Technology at Michigan Tech. Mr. Mayrose may be reached at jwmayros@mtu.edu

Biographies

ALEKSANDR SERGEYEV is a professor in the Electrical Engineering Technology program in the School of Technology at Michigan Tech. Dr. Sergeev's research interests include industrial control and automation, robotics, high-energy laser propagation through the turbulent atmosphere, developing advanced control algorithms for wave-front sensing and mitigating effects of the turbulent atmosphere, digital inline holography, digital signal processing, and laser spectroscopy. Dr. Sergeev is a member of ASEE, IEEE, SPIE, IAJC, PICMET, ATMAE, and is actively in-

3D FOOD PRINTING INSIGHTS AND OPPORTUNITIES: A CAPSTONE DESIGN CASE STUDY

Joseph Piacenza, University of West Florida; Hope Weiss, California State University Fullerton;
Monika Patel, California State University Fullerton; Sean Moore, California State University Fullerton;
Tam Nguyen, California State University Fullerton; Nikolia Shields, University of West Florida

Abstract

Additive manufacturing currently plays a key role in driving the expansion of the maker movement and has contributed to the development of 3D printers capable of unique food preparation and design. While most applications of 3D food printing concentrate on single serving and novelty food prototypes, there is an opportunity to explore design variations for a commercial, production grade 3D printer capable of creating consistently replicable food items for mid-range production facilities such as schools and hospitals. In this paper, the authors outline preliminary research conducted by an interdisciplinary capstone design team of mechanical and electrical engineering students at California State University Fullerton (CSUF) during the 2016/2017 academic year. A detailed overview of the capstone design course requirements and the team's design method are also presented. The team was broadly tasked with reverse engineering and manufacturing a 3D food printer, and identifying limitations and future research opportunities. After successfully designing and constructing a working extrusion-based Cartesian prototype, the team created a preliminary 3D food printing design database, based on a series of experiments. The database was populated with design variables (e.g., syringe pressure), quantitative results (e.g., material print height), and qualitative observations (e.g., photographs and written descriptions). A two-sided t-test was used to understand the prototype's sensitivity to changes in key variables that impacted printing performance. The 3D food printing design database provides valuable insights and baseline values for future 3D food printing research. Finally, scalability challenges were identified, and recommendations for how to meet these challenges are provided.

Introduction

Continuous improvements in additive manufacturing technologies have expanded the breadth of possible applications for 3D printing (Wegrzyn, Golding, & Archer, 2012; Wei & Cheok, 2012; Millen, Gupta, & Archer, 2012; Lipson, 2012; Leach, 2014; Petrick & Simpson, 2013). In addition to printing items from plastic and metal, opportunities now exist to print food. In 2012, Systems and Materials Research Consultancy was awarded a NASA Small Busi-

ness Innovation Research (SBIR) grant after identifying a practical need for 3D food printing in extreme environments (e.g., space), stating a need for a wide array of foods to be printed using different combinations and types of inputs (i.e., ingredients) (Systems, 2012). NASA's vision for this research was to enable astronauts to design and manufacture a variety of food options with a finite set of inputs, while having customizable control over portion size and personal taste. However, this concept has multiple challenges. Primarily, most 3D food printing is performed using extrusion-based methods that limit the food type and consistency to primarily homogenous mixtures (e.g., paste and gel), and is unable to accommodate other types of food consistencies (Sun, Zhou, Yan, Huang, & Lin, 2018; Cornell University, 2014; Cohen, Lipton, Cutler, Coulter, Vesco, & Lipson, 2007; Cohen, Lipton, Cutler, Coulter, Vesco, & Lipson, 2007; Seraph Robotics, 2015). Subsequently, an opportunity exists to examine new methods for depositing other food types (e.g., heterogeneous foods).

In this paper, the authors illustrate the efforts of undergraduate capstone design students from California State University Fullerton (CSUF), who were broadly tasked with reverse engineering and manufacturing an extrusion-based 3D food printer and identifying limitations and future research opportunities. Capstone design refers to an engineering course, often taken during the senior year, which aims to bridge the gap between engineering theory and practice (Dutson, Todd, Magleby, & Sorensen, 1997). A key objective for the team was to broaden the practical applications of existing 3D food printing technologies by specifically focusing on the creation of consistently replicable foods for mid-range production facilities, such as schools and hospitals. For example, could several (homogeneous or heterogeneous) key ingredients (e.g., sauce, dough, and cheese) be interchanged strategically to produce different food items (e.g., pizza and calzone)?

In terms of undergraduate research via capstone design, examining methods related to 3D food printing has multiple benefits. First, this work combines key elements of CSUF's mechanical and electrical engineering curriculum (e.g., CAD, system-level thinking, and additive manufacturing). Next, many capstone students, typically engineering seniors, are familiar with 3D printing through previous channels such as high school, extra-curricular hobbies, or other

courses (Irwin, Pearce, Anzalone, & Oppliger, 2014). Finally, capstone design is well studied in the literature as a mechanism for teaching engineering design, in addition to promoting creative thinking (Dutson et al., 2014; Dym, Agogino, Eris, Frey, & Leifer, 2005; Wood, Jensen, Bezdek, & Otto, 2001).

The study described here was conducted by a student capstone design team from the two-semester Mechanical Engineering 414/419 Senior Design course, during the 2016/2017 academic year. Their work focused on identifying challenges for design scalability, while considering manufacturing costs and applicable markets (e.g., retail and commercial). This project was proposed and internally funded by CSUF, based on CSUF's strategic plan for improving instructional processes that lead to increased student success. It addressed these processes directly, focusing on the implementation of high-impact practices in the classroom (Kuh, 2008; Carpenter, Morin, Sweet, & Blythe, 2017). A primary component of the senior design course is to collaborate with an industry sponsor/mentor, who will benefit from the merits of this research. Ideally, these partners/collaborators would support—both financially and technically—this project for multiple years, and the students' designs will improve iteratively. Another benefit of this study is the interdisciplinary nature that requires the mechanical engineering design team to collaborate with other disciplines. For this project, these areas include electrical engineering (e.g., electronic hardware design), computer science (e.g., programming), and business (e.g., market analysis, cost modeling, and supply chain management).

Background

3D printing is a technological process, where an object is created layer by layer from a file using CAD software. The technology of additive manufacturing has existed since the early 1980s. Until the open-source release of the 3D printer Fab@Home by researchers at Cornell University in 2006, the printers were industrial scale and expensive (Lipson & Kurman, 2013). The Fab@Home Model 1 could be used in the production of a variety of forms and materials, including, for the first time, food (Lipson & Kurman, 2013).

The basic principle for 3D printed food is solid free-form (SFF) fabrication, the ability of food material to hold and produce a solid structure without getting deformed (Lipton, Arnold, Nigl, Lopez, Cohen, Norén, & Lipson, 2010). Currently there are four types of 3D food printing techniques: extrusion-based printing, selective laser sintering, binder jetting, and inkjet printing (Godoi, Prakash, & Bhandari, 2016; Sun, Zhou, Huang, Fuh, & Hong, 2015; Liu, Zhang, Bhandari, & Wang, 2017). Extrusion-based printing is the

most commonly used technique and is typically used for hot-melt extrusion of chocolate or for the extrusion of room-temperature soft materials like frosting, processed cheese, and sugar cookies (Lipton et al., 2010; Periard, Schaal, Schaal, Malone, & Lipson, 2007). Currently, there are several extrusion-based food printing machines commercially available to print materials such as chocolate, dough, and pasta (Sun et al., 2018; Liu et al., 2017). The technique works by continuously extruding the material out of a moving nozzle and the material is able to fuse to preceding layers due to the material's properties. The second most commonly used food printing technique is selective laser sintering. This method works by fusing powder particles with high sugar content to form the solid layers. This technique has allowed for the creation of complex structures (Sun et al., 2015; Liu et al., 2017). Binderjet printing is the process of alternating between depositing layers of powder and spraying a liquid binder agent. This technique has resulted in the printing of complex structures, including structural cakes (Izdebska-Podsiad³y & ^oek-Tryznowska, 2016). Inkjet food printing works like a standard inkjet printer for paper. The ink, however, is a low-viscosity food material that is dispensed in droplet form. This technique is limited to decoration or surface filling.

3D food printing allows for food products to be designed and fabricated to meet personal and/or nutritional requirements and to create custom designs. Printing food allows for freedom of design regarding 3D shape, composition, texture, structure, and taste (Sun et al., 2015). In addition, this process is capable of creating unique goods and structures that require specialized human skills or cannot be made by humans. 3D printing of food additionally allows for the customization of the nutritional content (Wegrzyn, Golding, & Archer, 2012; Sun et al., 2015; Severini & Derossi, 2016; Severini, Derossi, Ricci, Caporizzi, & Fiore, 2018; Yang, Zhang, & Bhandari, 2017). Therefore, personalized food can be created based on a person's dietary restrictions, allergies, or health goals.

The accessibility of additive manufacturing technology has contributed to innovative advances in 3D food printing for both academic and commercial applications (Sun et al., 2015). However, current techniques need further investigation. There are many limitations, including accuracy and precision (Liu et al., 2017). Once these challenges are overcome, wider application is expected.

Methodology

For this project, the following key performance metrics were provided to the capstone design team, each applicable to their 3D printer prototype:

- **Functionality:** Does the machine perform its intended function of printing multiple and different edible foods?
- **Scalability:** Can this design scale to mid-level production applications (e.g., schools)?
- **Robustness:** Will this design produce consistently replicable and reliable food prints?
- **Cost:** Is this design financially competitive with existing 3D food printing products?

Since the majority of applications for 3D food printing are concentrated on single serving, novelty food prototypes, the team was asked to consider challenges for designing and manufacturing a commercial, production-grade 3D printer capable of creating consistently replicable food items for mid-range production facilities such as schools and hospitals. Creating a 3D printer capable of producing a variety of standardized food products for mid-level production could significantly improve food health and increase distribution efficiency, while minimizing waste and reducing costs. This work has broad-reaching applications in the domains of mechanical engineering, additive manufacturing, and food science. Another benefit of this research is its compatibility with the capstone design course series (either CSUF's or another institution's), which is formatted to allow annually recurring research projects on the same topic.

The team's method was based on Ullman's four stages of product design: project definition; product definition; conceptual design; and, product development (Wang & Shaw, 2005). Figure 1 displays an outline of the team's design method. The capstone design team worked within the constraints of the course, during CSUF's 2016/2017 academic year. This limited the team to two 15-week semesters (i.e.,

Fall 2016 and Spring 2017) to complete their prototype, and their budget could not exceed \$1000. In addition, the team was required to track all design, manufacturing, and testing activities in a cloud-based document-sharing platform (e.g., Google Drive), to pass information on to next year's team. Table 1 shows key course requirements and the justification for these requirements to help guide the students' design.

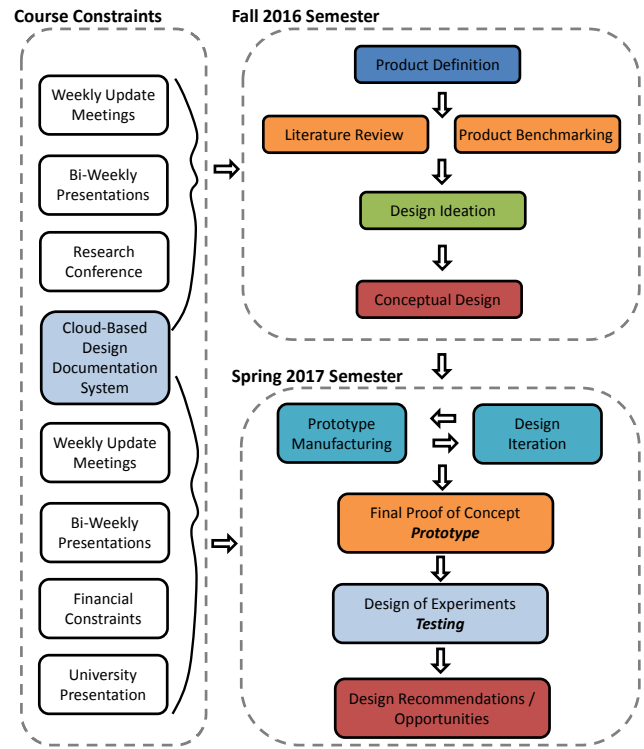


Figure 1. Student team design method.

Table 1. Key course requirements and justification.

Design Task	Justification
Create Gantt chart	Track critical deadlines and responsible individual
Perform literature review	Explore state-of-the-art research and product benchmarking
Begin cloud-based research documentation system (e.g., Google Drive)	Archive and document research to pass on to future researchers
Attend weekly update meetings with instructor	Receive feedback on design and manufacturing choices
Present bi-weekly 10-minute research update to class	Gain critical evaluation from peers
Submit project abstract to undergraduate research conference (i.e., 2016 Southern California Conference for Undergraduate Research - SCCUR)	Expose students to peer review research process
Create abstract based research poster	Understand how to concisely present work with limited time/space
Present research at undergraduate conference (e.g., SCCUR)	Opportunity to disseminate work, and receive feedback from the research community
Give 20-minute research update to class	Gain critical evaluation from peers
Display final prototype and poster at university wide event (e.g., 2017 CSUF Student Project Showcase)	Opportunity to disseminate work, and receive feedback from peers outside of department
Submit final research report	Allow students to practice technical writing

The capstone design team student selection was based on students interested in additive manufacturing but who did not necessarily have experience in this domain. As described previously, the project definition and key objectives were already outlined by the capstone design advisor. Subsequently, production definition was the first component of the team's method. An examination of the literature and existing technologies was performed, where the students found current work relating to both the fundamental science of additive manufacturing and commercial applications for 3D food printing. This review helped guide them during the design ideation phase, and identify potential 3D food printing methods that could be replicated given the temporal and financial constraints of the course. The team selected the extrusion-based food printing method, motivated by opportunities defined in the literature (Sun et al., 2018).

Conceptual Design

The conceptual design phase was guided by the project definition requirements and the course design task requirements listed in Table 1. A functional decomposition of several extrusion-based food printers was performed to help identify potential design alternatives. The most common method for depositing food to the build surface was via a syringe, activated either pneumatically or with an electro-mechanical power screw. This syringe was then coupled with a mechanism for translating three axes. Design trade-offs were examined between each of the multi-axis food printer approaches (Cartesian, Delta, Polar, Scara) identified by Sun et al. (2018).

For the syringe, the team created a functional prototype of a pneumatic extrusion system using a purchased 38.1 mm diameter syringe with a custom 3D-printed ABS plastic air input. Figure 2 illustrates the preliminary conceptual design for extrusion testing. The nozzle diameter was tested at 3 mm, based on extrusion techniques by Wang and Shaw (2005). From this design, they made several attempts to extrude different foods (e.g., corn bread mix and frosting). This initial test was performed at room temperature (i.e., ~32 degrees Celsius). Since the expanding market for 3D printing technology is driving related component costs down, the team investigated the benefits of purchasing a 3D printer to harness the multi-axis translating function, instead of designing and manufacturing one themselves. For their final conceptual design, the team chose to purchase a Prusa i3 3D (Cartesian coordinate) printing kit (Irwin et al., 2014; Prusa, 2018) and modified the printing head mechanism to accept the customized pneumatic syringe used for testing. An initial challenge was to modify the Prusa's original microcontroller and coding to activate a pneumatic valve to let pressurized air enter the syringe and start the food extrusion

process. The Prusa printer head contained a stepper motor, a heater, and a fan, all of which were removed from the unit, leaving three empty outputs on the microcontroller. The team utilized a pneumatic valve that could be activated by the original 5V stepper motor output. Figure 3 shows the pneumatic pressure inlet and pressure relief valves used. All activities leading up to the conceptual design were performed during the Fall 2016 semester.



Figure 2. Preliminary conceptual design for extrusion testing.



Figure 3. Pneumatic pressure inlet and pressure relief valves.

Product Development

After the conceptual design was finalized, the team began to finalize its design and manufacture a final product that could print different foods by pneumatically extruding the food material from the syringe onto the build platform of the printer. The product development stage occurred during the Spring 2017 semester. Figure 4 shows the Prusa 3D printer with the original filament print head removed, and a custom designed syringe mount installed. The modified syringe and 3D printed air inlet from the design phase (see again Figure 2) was replaced with a commercially available Uxcell 300 ml Luer Lock 40 mm-diameter syringe and air inlet with a 6 mm barb fitting.

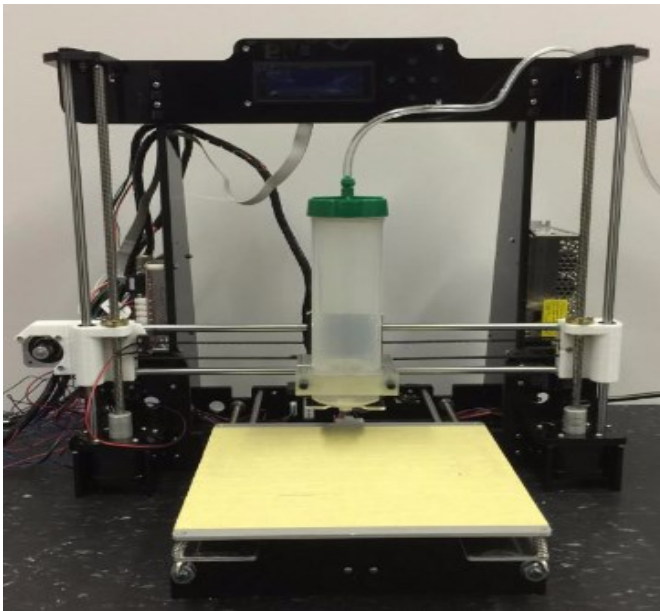


Figure 4. Initial product conceptual design.

Next, initial testing began to validate the team's conceptual design by attempting to print a 50 mm² square using frosting. The syringe pressure was set to 43.7 kPa based on the initial syringe testing results. Figure 5 illustrates the pressure release test for a 50 mm² square shape, which was successfully printed. However, the syringe continued to extrude after the pneumatic valve was closed due to remaining pressure in the cylinder. Figure 3 shows how a second valve was subsequently added in order to relieve pressure after the air inlet valve was closed. Based on initial extrusion testing, all experiments were performed at room temperature (i.e., ~32 degrees Celsius). It is also important to note that the heater was removed from the build platform for this work. After the product development phase was complete, the team selected a two-sided t-test to understand the prototype's sensitivity to changes in key variables that

impacted printing performance. Due to the temporal constraints of capstone design, the team chose to vary print geometry, material type, and syringe pressure. Table 2 summarizes the design variables and performance metrics utilized.



Figure 5. Pressure release test for a 50 mm² square shape.

Table 2. Outline of design variables and performance metrics.

Design	Quantitative	Qualitative
Material type	Material height (mm)	Geometry accuracy
Print geometry		
Syringe pressure	Material width (mm)	Ability to layer

Printer performance was measured quantitatively with material height and material width. Qualitative evaluations were also recorded and documented with photos that included geometry accuracy—did the food print in the intended shape based on input variables—and ability to layer (was solid, free-form fabrication visually apparent based on input variables). The design variables and performance metrics identified in Table 2 allowed the team to perform two-sided t-tests, once the experimental data were collected.

Results

Based on the testing configuration outline, and the team chose Betty Crocker Rich and Creamy Chocolate Frosting and Jiffy Corn Muffin Mix as their material types. A circle-and-star pattern was used for the print geometry. Discrete syringe pressure values were set at 43.7 kPa and 87.3 kPa, drawing from preliminary syringe pressure tests. Nozzle height (distance from the print bed) was initially set at 5 mm, based on initial extrusion testing. For all of the experiments presented, four layers of material were printed, with the syringe nozzle moving 5 mm upward after each layer. Material height values were recorded for each discrete layer.

To organize the experimental data, the team created a preliminary 3D food printing design database, which was populated with the design variables, the quantitative and qualitative performance metrics, and a photograph of the print from each experiment. In total, 39 individual layers were printed and analyzed. Table 3 displays a relevant subset of the design variables and performance metrics from the database. Two-sided, two-sample, unequal variance t-tests were performed to help identify which design variables (material type, print geometry, syringe pressure) had a significant impact on the quantitative design performances measured (material width, material height). Table 4 gives a summary of the number of samples (N), mean (M), standard deviation (SD), and t-test results, including the t-value (|t|), degrees of freedom (df), and significance level (p).

For material type, the t-test results showed that there was a significant difference ($p < 0.05$) in the printed material width between chocolate frosting and corn muffin mix. But there was no significant difference in printed material height between the two materials. For different printed geometries of circles and stars, there was a significant difference in printed material height but no significant difference in printed material width. As for syringe pressure, there was a significant difference in both printed material width and height between the syringe pressures of 43.7 kPa and 87.3 kPa.

From these results, it can be said that syringe pressure emerged as a critical design variable that impacts printer performance and, subsequently, should be considered as a key design parameter going forward with a new/updated design. Additionally, a more detailed study should be conducted to determine if there is a relationship between the viscosity of the material and the printed material width. Overall, these preliminary results indicate that more tests should be carried out with more material types, printed geometries, and syringe pressures for more insightful conclusions. For such future tests, quantitative measurements for

geometry accuracy and ability to layer (instead of the qualitative measures used here) should be developed and implemented.

Discussion and Future Opportunities

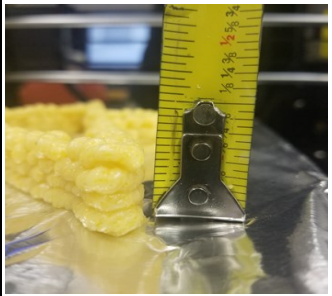
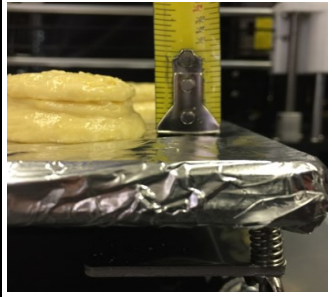
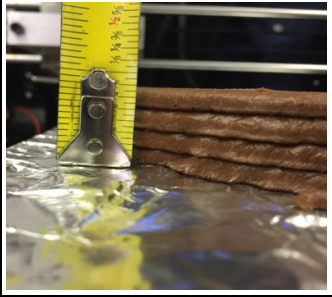
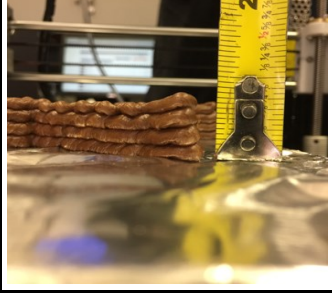
In this paper, the authors presented a case study of undergraduate research conducted by an interdisciplinary capstone design team of mechanical and electrical engineering students broadly tasked with reverse engineering and manufacturing a 3D food printer. Creating the framework for the 3D food printing design database was a significant contribution for research at the undergraduate level and provided valuable insights for future 3D food printing research. In addition, the team was able to address each of the four key performance metrics provided at the beginning of the capstone design course:

- **Functionality:** The team's conceptual design was able to successfully print two different foods.
- **Scalability:** The current conceptual design was a proof-of-concept prototype and would be difficult to scale for mid-level production applications. However, the material loading challenges discussed in the next section provide insight into design attributes that will be required for mid-level production.
- **Robustness:** Since only 39 individual layers were printed, it was difficult to conclude whether or not this design could produce consistently replicable food prints. Additional experiments need to be performed in future work in order to examine printing performance variation.
- **Cost:** Based on the proof-of-concept design presented here, this design primarily used commercially available components and very few custom parts; as such, it could be financially competitive with existing 3D food printing products.

Table 4. T-test results.

Design Variables		N	Printed Material Width (mm)					Printed Material Height (mm)				
			M	SD	t	df	p	M	SD	t	df	p
Material Type	Chocolate Frosting	22	9.1	2.9	2.36	22	0.027	5.2	0.9	0.79	27	0.434
	Corn Muffin Mix	17	12.6	5.6				4.9	1.3			
Print Geometry	Circle	17	9.2	2.8	1.90	33	0.067	4.6	0.7	2.21	34	0.034
	Star	22	11.7	5.4				5.3	1.3			
Syringe Pressure	43.7 kPa	31	9.0	1.9	3.64	7	0.004	4.7	0.8	4.39	9	0.002
	87.3 kPa	8	17.0	6.7				6.6	1.1			

Table 3. Outline of the design variables and performance metrics.

Material Geometry Pressure	Qualitative Description (from team)	Width/ Layer (mm)	Height/ Layer (mm)	Geometry Accuracy	Ability to Layer
Cornbread Star 43.7 kPa	Sinewave shape probably due to height	L1 - 11.9	L1 - 3.2		
		L2 - 10.3	L2 - 3.2		
		L3 - 11.1	L3 - 4.8		
		L4 - 11.1	L4 - 4.8		
Cornbread Star 87.3 kPa	Flattens first layer	L1 - 25.4	L1 - 7.9		
		L2 - 20.6	L2 - 4.8		
		L3 - 25.4	L3 - 6.4		
		L4 - NA	L4 - NA		
Frosting Circle 43.7 kPa	Began to print out sinewave shaped lines	L1 - 4.8	L1 - 4.8		
		L2 - 7.9	L2 - 4.8		
		L3 - 7.9	L3 - 4.8		
		L4 - 7.9	L4 - 4.0		
Frosting Circle 87.3 kPa	Print becomes smoother as the printer head prints closer to printing surface	L1 - 14.3	L1 - 8.8		
		L2 - 12.7	L2 - 9.5		
		L3 - 13.5	L3 - 7.9		
		L4 - 14.3	L4 - 7.9		
Frosting Circle 43.7 kPa	Began to print out sinewave shaped lines	L1 - 9.5	L1 - 4.8		
		L2 - 9.5	L2 - 4.8		
		L3 - 9.5	L3 - 4.8		
		L4 - 6.4	L4 - 4.0		

Another future research opportunity is exploring the impact of post processing (e.g., packaging, freezing, and baking) the final product for large-volume applications. Specifically, how does post processing impact the printed material (e.g., physically, aesthetically, etc.)? One of the unexpected challenges the team faced was the time and effort required to load the various food types into the syringe. While low-viscosity foods like corn muffin batter could be poured directly after mixing, higher-viscosity foods like frosting had to be forced in (or loaded) with a spoon or spatula. Another issue with loading the food was the formation of air pockets throughout the column of the syringe, which resulted in discontinuity during a print. Cleaning the syringe and nozzle also took more effort with high-viscosity foods.

In an effort to save time loading material, and potentially reducing the presence of air pockets and improving the syringe-cleaning process, the students experimented with the idea of prepackaging the food before it was inserted into the syringe. Prepackaging was performed by enclosing 200 ml of frosting in either wax paper (12 μm), foil (16 μm), or plastic wrap (10 μm). Each package was inserted into the syringe, and a small hole was poked through the nozzle opening. The syringe was then pressurized to 87.3 kPa until the material had been completely extruded onto the build platform, without a coordinate change. Figure 6 illustrates the three packaging types tested, with foil performing the best using qualitative observations. The foil extruded the largest volume of material, while minimizing the presence of air pockets and cleanup effort.

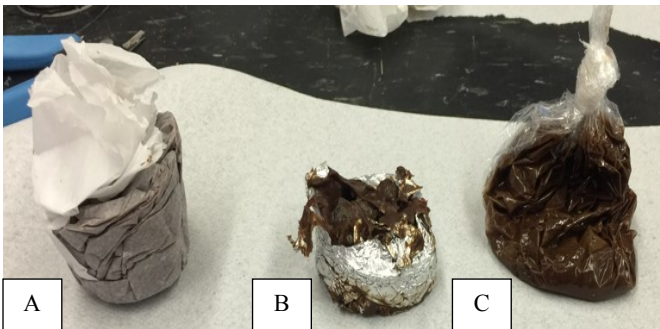


Figure 6. (a) prepackaging tests; (b) wax paper and foil; (c) plastic wrap.

This preliminary qualitative experiment highlights an additional opportunity for future research, toward the goal of creating consistently replicable food items from pre-packaged containers (similar to Keurig coffee cups), and represents a key contribution of this work. There are plans to continue this research at the University of West Florida (UWF) with another capstone design team for the 2018/2019 academic year.

Acknowledgements

The authors would like to thank California State University Fullerton for support under the Faculty Enhancement and Instructional Development (FEID) Award.

References

- Carpenter, R., Morin, C., Sweet, C., & Blythe, H. (2017). Editorial: The role of faculty development in teaching and learning through high-impact educational practices. *The Journal of Faculty Development*, 31(1), 7-12.
- Cohen, D. L., Lipton, J. I., Cutler, M., Coulter, D., Vesco, A., & Lipson, H. (2007). Hydrocolloid printing: A novel platform for customized food production. *Proceedings of the Annual International Solid Freeform Fabrication Symposium*. Pittsburg, PA: TMS.
- Cornell University. (2014). *Creative machines lab*. Retrieved from <http://creativemachines.cornell.edu/front>
- Dutson, A. J., Todd, R. H., Magleby, S. P., & Sorensen, C. D. (1997). A review of literature on teaching engineering design through project-oriented capstone courses. *Journal of Engineering Education*, 86(1), 17-28.
- Dym, C. L., Agogino, A. M., Eris, O., Frey, D. D., & Leifer, L. J. (2005). Engineering design thinking, teaching, and learning. *Journal of Engineering Education*, 94(1), 103-120.
- Godoi, F. C., Prakash, S., & Bhandari, B. R. (2016). 3D printing technologies applied for food design: Status and prospects. *Journal of Food Engineering*, 179, 44-54.
- Irwin, J. L., Pearce, J., Anzalone, G., & Oppliger, D. E. (2014). The reprop 3-D printer revolution in STEM education. *Proceedings of the 121st ASEE Annual Conference & Exposition*. Washington, DC: ASEE.
- Izdebska-Podsiad³y, J., & o³ek-Tryznowska, Z. (2016). 3D food printing: Facts and future. *Agro FOOD Industry High Tech*, 27(2), 33-37.
- Kuh, G. D. (2008). *High-impact educational practices: What they are, who has access to them, and why they matter*. Washington, DC: AAS&U.
- Leach, N. (2014). 3D printing in space. *Architectural Design*, 84(6), 108-113.
- Lipson, H. (2012). Frontiers in additive manufacturing the shape of things to come. *The Bridge*, 42(1), 5-12.
- Lipson, H., & Kurman, M. (2013). *Fabricated: The new world of 3D printing*. New York: Wiley.

- Lipton, J., Arnold, D., Nigl, F., Lopez, N., Cohen, D., Norén, N., & Lipson, H. (2010). Multi-material food printing with complex internal structure suitable for conventional post-processing. *Proceedings of the 21st Solid Freeform Fabrication Symposium*. Pittsburgh, PA: TMS.
- Liu, Z., Zhang, M., Bhandari, B., & Wang, Y. (2017). 3D printing: Printing precision and application in food sector. *Trends in Food Science & Technology*, 69, 83-94.
- Millen, C., Gupta, G. S., & Archer, R. (2012). Investigations into colour distribution for voxel deposition in 3D food formation. *Proceedings of the International Conference on Control, Automation and Information Sciences*. Piscataway, NJ: IEEE.
- Periard, D., Schaal, N., Schaal, M., Malone, E., & Lipson, H. (2007). Printing food. *Proceedings of the 18th Solid Freeform Fabrication Symposium*. Pittsburgh, PA: TMS.
- Petrick, I. J., & Simpson, T. W. (2013). 3D printing disrupts manufacturing: How economies of one create new rules of competition. *Research-Technology Management*, 56(6), 12-16.
- Prusa. (2018). *Prusa i3 3D printer*. Retrieved from <https://www.prusaprinters.org/prusa-i3/>
- Seraph Robotics. (2015). *Advanced 3D printers for researchers*. Retrieved from <http://www.seraphrobotics.com/#container>
- Severini, C., & Derossi, A. (2016). Could the 3D printing technology be a useful strategy to obtain customized nutrition? *Journal of Clinical Gastroenterology*, 50, S175-S178.
- Severini, C., Derossi, A., Ricci, I., Caporizzi, R., & Fiore, A. (2018). Printing a blend of fruit and vegetables. New advances on critical variables and shelf life of 3D edible objects. *Journal of Food Engineering*, 220, 89-100.
- Sun, J., Zhou, W., Huang, D., Fuh, J. Y. H., & Hong, G. S. (2015). An overview of 3D printing technologies for food fabrication. *Food and Bioprocess Technology*, 8(8), 1605-1615.
- Sun, J., Zhou, W., Yan, L., Huang, D., & Lin, L.-Y. (2018). Extrusion-based food printing for digitalized food design and nutrition control. *Journal of Food Engineering*, 220, 1-11.
- Systems and Materials Research Consultancy. (2012). *3D printed food system for long duration space missions*. Retrieved from https://sbir.gsfc.nasa.gov/SBIR/abstracts/12/sbir/phase1/SBIR-12-1-H12.04-9357.html?solicitationId=SBIR_12_PI
- Ullman, D. G. (2018). *The mechanical design process*. (4th ed.). New York: McGraw Hill.
- Wang, J., & Shaw, L. L. (2005). Rheological and extrusion behavior of dental porcelain slurries for rapid prototyping applications. *Materials Science and Engineering*, 397(1-2), 314-321.
- Wegrzyn, T. F., Golding, M., & Archer, R. H. (2012). Food layered manufacture: A new process for constructing solid foods. *Trends in Food Science & Technology*, 27, 66-72.
- Wei, J., & Cheok, A. D. (2012). Foodie: Play with your food promote interaction and fun with edible interface. *IEEE Transactions on Consumer Electronics*, 58(2), 178-183.
- Wood, K. L., Jensen, D., Bezdek, J., & Otto, K. N. (2001). Reverse engineering and redesign: Courses to incrementally and systematically teach design. *Journal of Engineering Education*, 90(3), 363-374.
- Yang, F., Zhang, M., & Bhandari, B. (2017). Recent development in 3D food printing. *Critical Reviews in Food Science and Nutrition*, 75(14), 3145-3153.

Biographies

JOSEPH PIACENZA is an assistant professor at the University of West Florida. Dr. Piacenza's primary research explores concept-stage robust design for complex infrastructure systems. Additional active research areas include system optimization, automotive design, sustainable building design, and additive manufacturing. Dr. Piacenza instructs the mechanical engineering Junior Design course at UWF, and is actively involved with hands-on and interdisciplinary student design projects. In addition, he is the faculty advisor for SAE Baja and SAE Aero. Dr. Piacenza may be reached at jpiacenza@uwf.edu

HOPE WEISS is an assistant professor at California State University Fullerton. Dr. Weiss' research focuses on the areas of nonlinear dynamics and chaos and engineering education. Her current research includes biomedical acoustics, active aerodynamic control systems, disease dynamics, and improving pre-requisite knowledge retention. Dr. Weiss may be reached at hweiss@fullerton.edu

MONIKA PATEL is a recent graduate of California State University Fullerton, with a BS in mechanical engineering. Ms. Patel may be reached at mail4monika@csu.fullerton.edu

SEAN MOORE is a recent graduate of California State University Fullerton, with a BS in mechanical engineering. Mr. Moore may be reached at semoore@csu.fullerton.edu

TAM NGUYEN is a recent graduate of California State University Fullerton, with a BS in mechanical engineering. Mr. Nguyen may be reached at nguyen-tam1993@csu.fullerton.edu

NIKOLIA SHIELDS is pursuing his BS in computer engineering at the University of West Florida. Mr. Shields may be reached at nas30@students.uwf.edu

COUNTERING EAVESDROPPING ATTACKS IN SOFTWARE-DEFINED RADIO NETWORKS USING A MOVING-TARGET DEFENSE

Isaac J. Cushman, Georgia Southern University; Rami J. Haddad, Georgia Southern University; Lei Chen, Georgia Southern University

Abstract

Every network system is required to maintain a certain level of security for its users. In mission-critical systems, loss or theft of data can be a severe problem for the users involved. It is possible to increase the network's level of security by confusing the attacker. The attacker will generally follow an attack process that starts with eavesdropping on the network to discover the system configuration and then, once becoming part of the network, will begin sniffing packets for either theft or destructive purposes. In this paper, the authors present a new security method that uses Moving Target Defense in an array of software-defined radio networks to split a data packet into multiple fragments and scramble the order and the frequencies used to send these fragments. The probability of an eavesdropper stealing data packets is examined for the proposed system and compared to the system without packet scrambling and fragmentation.

Introduction

Moving Target Defense (MTD) increases the difficulty for an attacker to breach a network by continuously changing security parameters. The utilization of software-defined radios (SDRs) will help the network in MTD to protect sensitive data by changing the network parameters and cause attackers to lose their trace. Wireless networks have the disadvantage of having a vast attack surface, due to the dynamically changing size of the network. In an MTD system, the attack surface is defined as the total possible ways that an attacker can breach the system (Yeung, Cho, Morrell, Marchany, & Tront, 2016). Generally, MTDs are deployed in ad-hoc type networks where many devices and IP addresses make up the network, thus having a larger attack surface. It is also important to consider the physical cost of operating an MTD, when considering the level of security a system needs for its data. For SDR networks, the most used technique is frequency hopping. This technique offers the ability to avoid malicious users from jamming or eavesdropping on the network by systematically changing the operating frequency in a given time interval. There are challenges to frequency hopping, most importantly the necessity to request access to occupy more bandwidth at any given time.

MTD has two main categories, network and host-based. The significant difference between the two is the localization of the controller. As the name implies, a network-based MTD system will have the entirety of the system controlled by a single, centralized entity, whereas a host-based MTD may have multiple host controllers, each controlling a specific group of nodes (Green, MacFarland, Smestad, & Shue, 2015). Generally, a network-based MTD system is preferred, due to the ease of synchronization; however, it may be less secure, as the attacker will have access to the entire network. A fundamental property of MTD is the mapping system. The mapping system is responsible for determining which users are considered trustworthy based on authentication or a calculated trust value. Secondary properties of network-based MTD are moving, access control, and distinguishability. This system offers potential for countering eavesdropping and intelligent jamming in a network system. However, when it is deployed in a large-scale system, it seems that packet overhead will lead to more significant losses in communication.

The moving property represents the characteristics of MTD that make it harder for an attacker to breach the system. It is broken into three sub-properties: unpredictability, vastness, and periodicity. Being unpredictable means that no one in the system should be able to determine the next step, other than the devices doing the communicating. The availability of the changing metrics determines the vastness property. This includes either changing IP addresses, ports, or frequencies; vastness also aids the unpredictability of the system. Periodicity is responsible for maintaining the synchronization between the devices within the system. This parameter provides a regularly changing time interval that should be kept a secret between transmitter and receiver.

The access control property is an enforcement policy within the system to authenticate users as they request access. Like the moving property, access control is also divided into sub-properties: uniqueness, availability, and revocability. The uniqueness property uses the mapping system to make sure that each user is guaranteed individual availability in the system dependent on the authorization. The availability property is set so that the system can fill each request; generally, this is determined by a capacity limitation within the network configuration. The revocation property is a set

of rules and standards that can remove a user from the system when a series of checks have been met. Revocation can be due to violations or simply the expiration of a time lease in the network, in which case, the user would then need to re-request for access. The last main property that makes up a network-based MTD system is the distinguishability property. This property affords the system the ability to determine trustworthy users. The ability to determine trust is typically complex, as a non-malicious user may be requesting information about the mapping system more than what is allowed and then becomes flagged as a malicious user. The typical method of distinguishing a user is to use identifiers, such as shared keys, to determine trustworthy users.

In Software Defined Networks (SDNs), denial of service (DoS) comes in the form of a signal jammer. The attack will find the frequency that the pair is on and overcrowd the medium so that the receiver cannot make sense of the retrieved data. One of the most common attacks to a network system is a distributed denial of service (DDoS) attack; in part, due to the ease of deploying this attack and to the fact of the difficulty of determining real traffic from fake traffic. Several mechanisms have been developed to counter a DDoS attack. However, most of these are reactive, meaning they happen after the attack has already occurred (Aydeger, Saputro, Akkaya, & Rahman, 2016). Using an SDN, it is possible to provide proactive defense mechanisms to seemingly random spikes in traffic on a network. The main challenge of an SDN is a crossfire attack; this attack determines where critical link connections in the network are located by observing the traceroute messages and then targeting those links. Another concern in SDNs is eavesdropping; it is the process of secretly listening to a network and copying the data as it is sent (Ma, Wang, Lei, Xu, Zhang, & Li, 2016).

To prevent theft from the network, frequency hopping is often used as a viable countermeasure. In this paper, a new security method that uses moving target defense in an array of software-defined radio networks is proposed to split the data packet into multiple fragments and scramble the order of the fragments. The effectiveness of the proposed model with fragmentation and scrambling is evaluated and compared to a basic frequency hopping system.

Related Work

The network design for moving target defense can be modeled with a varying number of available computing clusters, which the attacker will be trying to get access into. This array of computing clusters will have a common controller used to maintain synchronization during transition periods. This network is illustrated in Figure 1.

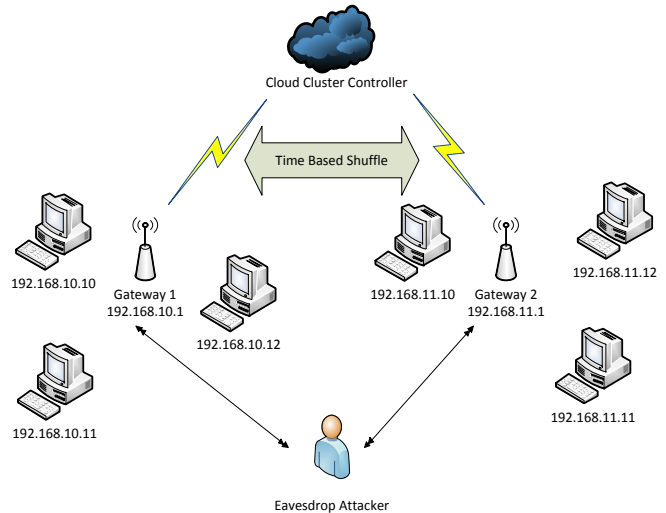


Figure 1. Moving-target defense system with attacker.

The computers connected to the gateway represent any variety of applications that can exist on a network (physical or virtual machines, software-defined radios, or mobile devices). The attacker represents any computer system that would attempt connection to any part of the network and, once in, would begin stealing or destroying information. The cloud-cluster controller is tasked with keeping a synchronized connection for the entire network by communicating the hopping time interval, the current IP, port, or frequency, and what the next hop configurations will be.

Moving Target Defense Configurations

MTD techniques can be categorized as host-based or network-based. In a network-based MTD, network properties are periodically changed to increase the difficulty for the attacker to get into the network; the more common technique is to change the IP address (Yeung et al., 2016). Utilizing IPv6 in MTD provides the network with a wide array of possible IP addresses for hopping purposes. The challenge to using IPv6, however, is the increase in overhead on the network, as hopping addresses generates network discovery protocol, NDP, and messages. IPv6 provides a substantial advantage over IPv4 in large-scale network systems and services, because IPv6 allows for a 128-bit address. An MTD network using IPv6, commonly referred to as MT6D, uses an encapsulation method to confuse the observer by generating a false sense of network activity. Using MT6D proposes a defense against an attacker by causing the attacker to spend a much higher amount of resources on reconnaissance (Yeung et al., 2016). The moving property can be handled by the DNS server with a short time-to-live assigned value so that IP addresses change frequently. The use of IPv6 is highly sought after in MTD systems and are

named MT6D, due to the fact that IPv6 offers a large array of varying IP addresses. The DNS server can also handle access control by assigning users to a unique portion of the mapped IP addresses, and then revoking them when needed. Distinguishability is the most challenging aspect to deploy in a system, because of the ability of an attacker to passively access a system (Corbett, Uher, Cook, & Dalton, 2014). Some work has been on the use of ISP DNS systems to provide trustworthiness in a system.

The mechanisms that change within an MTD system are categorized based on the mechanisms and the type of pattern they follow. Three of the mechanisms are software transformations, dynamic platform techniques, and network address shuffling (Cai, Wang, Luo, Li, & Wang, 2016). The idea of software transformations is to focus on the applications that are running on the system. In this case, the software or application will exist in different variants that will be randomly selected to be the active software version. Dynamic platform techniques involve dynamically changing properties in the operating system and hardware. Recent methods of dynamic platform techniques are to use cloud-based systems to store the operating system variants and load them accordingly.

In network address shuffling, the primary goal is to prevent reconnaissance in the system. Network address shuffling is the most common technique in MTD and involves changing the IP address or port that the network is communicating on. MTD has three fundamental patterns: hidden, variation, and assisted. In the hidden pattern, the attacker can get into the network for a varying amount of time; however, when repeating the reconnaissance stage, the network will have appeared to be no longer active. The variation pattern is comparable to hidden; however, when the attacker makes a second pass, the network will have a different set of security protocols, thereby preventing access. The assisted pattern can vary depending on the mechanisms used.

The Attack Process on a Network

The first stage of the attack process on a network is the reconnaissance stage. The focus of this stage is to determine the best angle of attack. It is because of this understanding that defenders of cyber-attacks work to make reconnaissance very difficult. Eavesdropping is one of the most significant challenges to stopping malicious acts in a network system and is the process of secretly listening to a network and copying the data as it is sent (Ma et al., 2016). Traditionally, encryption and authentication are backbone-layer defenses that are passive in the network. This means that the encryption system does not dynamically change at any giv-

en time. Moving target defense is a new method that will allow for an active defense to stop eavesdropping (Ma et al., 2016). In a traditional use of MTD, IP addresses or ports are changed to keep attackers from listening to the network; however, little is done to change network protocols, due to the complexity. Eavesdropping is categorized into two types of attacks: session attack and packet attack. In a session attack, the entirety of the communication session is grabbed by the attacker and then analyzed based on the network protocol. In a packet attack, a series of packets from the session are grabbed and analyzed for their source IP and destination IP; this could potentially give the attacker enough for a Man in the Middle or DDoS attack (Ma et al., 2016).

One proposed method is to use MTD with protocol-oblivious forwarding (POF). POF will allow the network to simply forward the packet based on the key associated with it. Otherwise, it has to parse the packet first before determining what to do with it. In this setup, the clients use dynamic message packaging and dynamic routing paths to keep the attacker confused as to what the source and destination IP addresses are. This proposed method will block both session and packet attacks by continually keeping the attacker guessing which bits of data fit the right network protocol.

Operational Costs

Operational costs of MTD can be the actual cost of the system; however, it can also affect the overall system performance, network stability, and effectiveness. The required capital investment of the physical system is first determined based on compatibility. The physical hardware requirements for the level of security needed will increase the cost of the system. The biggest challenge to an efficient MTD system is the available bandwidth of the system. To have a secure system, the total number of channels available for the system to “hide” in, directly impact the difficulty of the attacker trying to find it. To clarify this, if a system is designed so that it only has 10 available channels, then an attacker will have an easy time scanning all of the channels to find the information; whereas, if the system has 50 possible channels to pick from, the attacker will have to spend a significant amount of time trying to find the information.

Capital funding limitation is a dominant driving force behind the decision to change systems. The MTD system requires constant synchronization based on CPU cycles and memory systems in the network, which could take away from the processing power the institution may need to service its demands; this could again end up incurring severe financial losses if handled poorly. The effects on the performance metrics may also lead to a loss in availability in the

system. In a CPU system, it is possible to overclock the synchronization; however, it is not necessarily the best practice and can lead to system failures. Another operational cost of MTD is the effectiveness of the MTD system itself. Considering a dynamic MTD system with many access points, the controller has a very complex role in determining when and how requests should be handled. Deploying a large network to handle minimal security work would be wasteful and, in contrast, would be impossible to secure highly classified data in a small MTD system.

The main method of determining the right cost functions for deploying an MTD is by observing possible network parameters. First, classification and value assignment of the system should be taken care of and then experimental bandwidth consumption can be handled (Leeuwen, Stout, & Urias, 2015). The classification step determines the work factors that the system requires; these include operating expenses, capital expenses, performance in either network or host-based applications, and service impacts and scalability. Depending on the classification, a metric and unit will be assigned. The metric for operating expenses would be operator workload, and the unit would be in physical man-hours; whereas, for scalability, number of nodes and count would be the metric and unit, respectively. This classification system leads to a concise requirement and possible prediction of whether a large or small network can be handled.

Observing the physical and cyber costs of deploying a new system is crucial for defending the use of new technology. There are obvious advantages to studying these metrics and optimizing where necessary in order to provide the strongest case as to why this technology is needed, other than just for more secure data transfer.

Obfuscation of the Attack Surface

A key advantage to using software-defined networks in moving target defense is the ability to obfuscate the attack surface. By using software-defined radios, it is possible to change each of the network characteristics to protect the network. Two proposed network attacks to protect from are network reconnaissance and OS fingerprinting (Kampanakis, Perros, & Beyene, 2014). Using an SDN controller, the traffic coming through a network is monitored. If the traffic is malicious, the SDN controller will attempt to quarantine that part of the network; this is done by blocking off that group of devices. The main process of this defense is to open more ports; this causes the attacker to have to search more possible entries before finding the actual port. In the event the attacker attempts to find network configurations through an HTTP GET eavesdropping method, it is possible to change different operating system information.

The httpd service will work with the SDN controller to create a dummy service version. The network firewall is normally used to keep out attackers by preventing attacks on operating system information. However, the SDN will reassemble TCP into a spoofed version that will exist on the network; users that have access by presenting the correct key will be given the correct information from the SDN controller. In the SDN, route mutation and host randomization can also provide ideal possibilities for keeping an attacker from finding the correct path. Route mutation adds problems to the attacker in operational cost, because they would now be randomly aiming when sniffing packets. If they wanted to be more effective, they would need more robust devices and algorithms.

Many proposed algorithms make it harder for an attacker to get into the network. However, there is generally a problem for the network being defended when using high-bandwidth applications (Li, Dai, & Zhang, 2014). The focus is to make sure that the network can morph to prevent an attack, while still maintaining a time-sensitive goal for transmission set by the application. Creating a real-time traffic morphing algorithm requires three pieces that work in the algorithm. The first piece is to create an adaptive packet generation; next is maintaining deadlines in the packet generation scheduler; and, last, is to minimize redundancy. Adaptive packet generation is responsible for maintaining uniqueness in the system. The deadline schedule is responsible for not allowing the first part of the algorithm to take too long or from generating packet combinations that will cause overhead. Minimizing redundancy is a final check that the system overhead does to reduce time.

Cloud Controller Characteristics

Many common open-source cloud controllers have been used for synchronization in MTD systems. One of the most used is the OpenFlow API that can work as a load balancer, handling requests on a round-robin basis. The API works by picking from the pool and processing each request. The main method of changing network-specific characteristics is by either using an encrypted pseudorandom sequence between both the transmitter and receiver continuously or simply using a lookup table to keep track of the network changes on both ends; the latter being simpler but the table could be eventually broken into (Corbett et al., 2014). After the network controller has been set up, the next stage is to determine how packets will be sent from transmitter to receiver. Cloud-based network systems offer a potential increase in the effectiveness of software-defined radio. This is due to the cloud's ability to run more extensive applications, while the radios can perform simpler and more rapid actions (Debroy, Calyam, Nguyen, Stage, & Georgiev, 2016). Uti-

lizing a cloud-based system can amplify vulnerability detection by covering more of the attack surface; however, it does offer the ability to become a target to attack. By combining SDN and cloud, it is possible to add complexity to an attacker's attempts by splitting what can be taken away from the system. Realizing a complete network that will utilize cloud-based systems offers challenges in both total resource consumption and effective performance of the network. The operational cost of a system can significantly influence the actual utilization of a system; if the cost-to-resource usage ratio is not optimal, there is an increase to the potential of incurred financial losses for the service provider. In the presence of an attack, the controller will attempt to mark the attack path of IP addresses and block off the attack by severing the connection; the controller, then, will either be proactive or reactive, based on the advancement of the attacker in the network.

Proposed Solution

The goal of the system is to add another layer of complexity to frequency hopping using packet fragmentation, with the intention of thwarting two very popular attack types: DoS and packet sniffing. An $N \times N$ multiple-input-multiple-output (MIMO) system has the ability to transmit and receive large amounts of data at a given time. Another advantage is its ability to spread the frequency spectrum across the three pairs. Using coordinated universal time, UTC, all pairs will know precisely when to hop to another frequency or request an entirely new array of frequencies. The transmitter randomly generates the frequency lists, which are then synchronized with the receiver using a cloud-based controller. Also, the frequency of updating the lists is randomized to add a layer of security to the operation of the cloud-based controller beyond channel encryption.

Packet Fragmentation with Frequency Hopping

LabVIEW was used to initialize each universal software radio peripheral (USRP) device and transmit each fragment following the algorithm displayed in Figure 2. Each time the program loops, the packet will be split into a pseudorandom order and given to the transmitter. Simultaneously, the transmitter is prepped to send the packet by selecting its frequencies and reporting those frequencies to the cloud-based controller's database. It is also possible to have a varying number of total packets being sent from each transmitter. In this case, the attacker would need to determine what frequency the system is on, the total size of each packet and the order that it was sent in; all the while, at a designated time interval, all three of those parameters change to a new

value. Synchronization between transmitter and receiver can be achieved by using the database controller to store the current configuration set by the transmitter and synchronizing it with the receiver. It is also possible to use the cloud controller as the central source, so that both the transmitter and receiver are given all parameters. Once ready, the USRP will continuously transmit the packet until all frequencies are used. The program then selects new frequencies, scrambles the packet in a new order, and then continues.

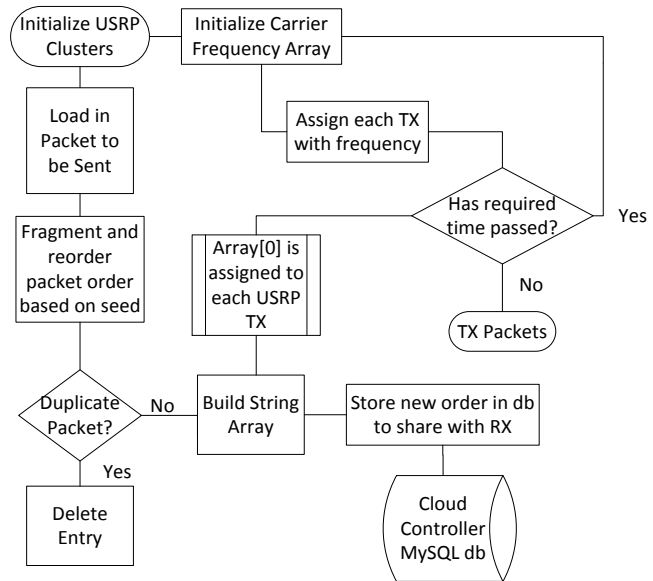


Figure 2. Flow diagram for transmission of packet.

3×3 MIMO Connection

A 3×3 MIMO system has the ability to transmit and receive large amounts of data at a given time. Another advantage of this MIMO system, when used as one-to-one SISO pairs, is its ability to spread the frequency spectrum across the pairs, while sacrificing bandwidth in order to increase data security. Using coordinated universal time, UTC, all pairs will know precisely when to hop to another frequency or request an entirely new array of frequencies. Figure 3 shows the system setup for a 3×3 USRP connection.

Experimental Results

First, a predefined number of allowed channels is given to the system (10, 25, or 50 channels) then the frequencies are pseudo-randomly shuffled, and three frequencies are assigned to be used for transmission. A hopping interval is also predetermined (10, 30, or 60 seconds) when the system begins; at the end of the hopping interval, the next frequen-

cy is selected. Once all three frequencies are used, the system will re-randomize the frequency list and select another three frequencies to be used. Figure 4 illustrates the experimental setup for the Tx/Rx pair using the NI USRP-2920 SDRs.

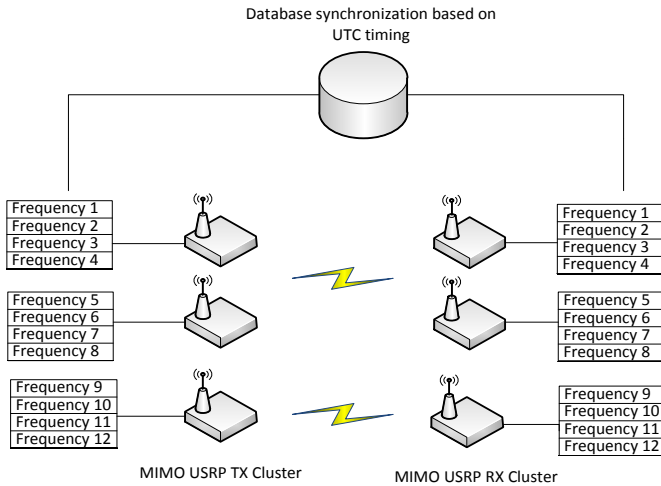


Figure 3. Structure of the 3x3 MIMO USRP network with cloud database controller.

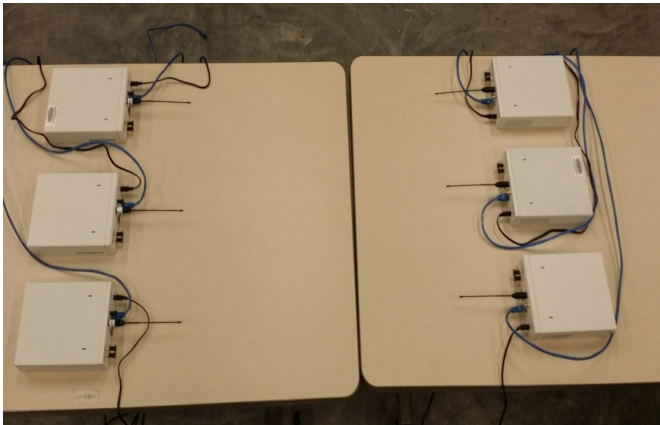


Figure 4. 3x3 MIMO USRP experimental setup.

The eavesdropper will need to know or guess the possible length of the spectrum and the packet size. The attacker will then have to scan through the entire list of frequencies from start to finish hoping to find the correct transmission frequency. As mentioned in previous sections, the packet size influences the attacker's hopping speed, too fast a speed and it may miss most of the data. In a real-world application, the packet size would be considered the right amount if the attacker knew at least how much to expect; they would simply stay connected to the network until it had collected enough data to make up the whole packet. The attacker will scan the spectrum frequencies with a hopping interval of 3 seconds in an incremental fashion.

Frequency Hopping WITHOUT Packet Fragmentation

In the first experiment, one transmitter was set up to broadcast a packet on varying frequencies to one receiver. In this case, the attacker focuses on finding the frequency that both are currently on and sniff the packet. The attacker will sweep the network as quickly as possible to steal the packet. This experiment was tested on three trials, set to the varying number of available channels. In each trial, the hopping interval of the Tx/Rx pair was set to either 10, 30, or 60 seconds. The attacker scans the entire network 100 times, checking each channel for the packet; in this case, it is a simple Hello World! message that is being sent. The relative frequency of obtaining a packet is used to model the empirical probability of successful eavesdropping using the following model. Let n_c be the number of captured packets and N the total number of packets transmitted. Then the relative frequency, f , of obtaining a packet is modeled by Equation 1:

$$f = \frac{n_c}{N} \quad (1)$$

When the total number of packets approaches infinity, the relative frequency will converge to represent the empirical probability of successful eavesdropping, p , as indicated by Equation 2:

$$p = \lim_{N \rightarrow \infty} f \quad (2)$$

This model was used to estimate the empirical probability of successful eavesdropping of the experiment and the results from each combination of channels and hopping intervals are displayed in Table 1.

Table 1. Empirical probability of successful eavesdropping using various system parameters.

Hopping Interval (sec)	10 Channels	25 Channels	50 Channels
60	$11.73 \cdot 10^{-3}$	$4 \cdot 10^{-3}$	$1.76 \cdot 10^{-3}$
30	$7.33 \cdot 10^{-3}$	$3.46 \cdot 10^{-3}$	$1.68 \cdot 10^{-3}$
10	$12 \cdot 10^{-3}$	$2.08 \cdot 10^{-3}$	$0.8533 \cdot 10^{-3}$

The experimental probabilities are determined by the total successful attempts of the attacker divided by the total number of packets that were sent during the transmission.

Frequency Hopping WITH Packet Fragmentation

The next experiment was designed to test the ability of an eavesdropper to steal the entirety of the data being transmitted when it is sent broken into multiple parts and sent across three transmitters. For this trial, the network size was chosen to be 25 channels, while the hopping time intervals stayed the same as the previous experiment. Table 2 displays the experiment results. It can be seen that when the packet is split into multiple parts, the probability of the attacker getting the entirety of the message decreases across all three of the hopping intervals.

Table 2. Empirical probability of successful eavesdropping with/without fragmentation for 25-channel system.

Hopping Interval (sec)	With Fragmentation	Without Fragmentation
60	$2.72 \cdot 10^{-3}$	$4 \cdot 10^{-3}$
30	$2.187 \cdot 10^{-3}$	$3.46 \cdot 10^{-3}$
10	$1.76 \cdot 10^{-3}$	$2.08 \cdot 10^{-3}$

Conclusions

Frequency hopping provides a level of security to a network system; however, as was shown in the results of Table 1, it alone is not a foolproof method. Packet fragmentation has been shown to be an easy and economical method for achieving a higher general level of security. This method adds another layer of confusion to the system, causing the attacker to work significantly harder to steal the information; this also showed an increase in the time and resources needed for an attacker to eavesdrop successfully. The results from experimentation showed that the difficulty of an eavesdropping attacker to recover the packet increases as the system covers more of the spectrum at random frequencies.

It is also essential to note that when there are a limited number of channels for the system to exist on, as seen from results in Table 1, the system may end up hopping too often and cross the attacker more frequently. This occurred with this system when hopping between 10 channels every 10 seconds. At the same time, having a system with a very large spectrum may incur more substantial operational costs that is considered not feasible. The proposed method can save on spectrum space by fragmenting. The results also

showed the effectiveness of the packet fragmentation method on bandwidth spectrum allocation. The probability of a successful attack when the system had 50 possible channels was significantly lower than for 25 or 10 channels; however, occupying that many channels may cause very high operational costs. Using packet fragmentation, the probability of success, when using 25 channels instead of 50, yielded a difference of $0.96 \cdot 10^{-3}$, $0.507 \cdot 10^{-3}$, and $0.9067 \cdot 10^{-3}$ for hopping intervals 60, 30, and 10, respectively. This showed the ability to be at comparable levels of security, while existing on half the bandwidth.

References

- Aydeger, A., Saputro, N., Akkaya, K., & Rahman, M. (2016). Mitigating crossfire attacks using SDN-based moving target defense. *Proceedings of the IEEE 41st Conference on Local Computer Networks*. Piscataway, NJ: IEEE.
- Cai, G., Wang, B., Luo, Y., Li, S., & Wang, X. (2016). Characterizing the running patterns of moving target defense mechanisms. *Proceedings of the 8th International Conference on Advanced Communication Technology*. Piscataway, NJ: IEEE.
- Corbett, C., Uher, J., Cook, J., & Dalton, A. (2014, March). Countering intelligent jamming with full protocol stack agility. *IEEE Security Privacy*, 12(2), 44-50.
- Debroy, S., Callyam, P., Nguyen, M., Stage, A., & Georgiev, V. (2016). Frequency-minimal moving target defense using software-defined networking. *Proceedings of the International Conference on Computing, Networking and Communications*. Piscataway, NJ: IEEE.
- Green, M., MacFarland, D., Smestad, D., & Shue, C. (2015). Characterizing network-based moving target defenses. *Proceedings of the Second ACM Workshop on Moving Target Defense*. New York: ACM.
- Kampanakis, P., Perros, H., & Beyene, T. (2014). SDN-based solutions for moving target defense network protection. *Proceeding of IEEE International Symposium on a World of Wireless, Mobile and Multimedia Networks*. Piscataway, NJ: IEEE.
- Leeuwen, B. V., Stout, W., & Urias, V. (2015). Operational cost of deploying moving target defenses defensive work factors. *Proceedings of the Military Communications Conference*. Piscataway, NJ: IEEE.
- Li, Y., Dai, R., & Zhang, J. (2014). Morphing communications of cyber physical systems towards moving-target defense. *Proceedings of the IEEE International Conference on Communications*. Piscataway, NJ: IEEE.

-
- Ma, D., Wang, L., Lei, C., Xu, Z., Zhang, H., & Li, M. (2016). Thwart eavesdropping attacks on network communication based on moving target defense. *Proceedings of the 35th International Performance Computing and Communications Conference*. Piscataway, NJ: IEEE.
- Yeung, F., Cho, P., Morrell, C., Marchany, R., & Tront, J. (2016). Modeling network based moving target defense impacts through simulation in Ns-3. *Proceedings of the Military Communications Conference*. Piscataway, NJ: IEEE.

Biographies

ISAAC CUSHMAN received his BS degree in electrical engineering from Georgia Southern University in 2016 and MS degree in applied science and engineering from Georgia Southern University in 2017. His research interests include big data, network security, and wireless communication. Mr. Cushman may be reached at ic00214@georgiasouthern.edu

RAMI HADDAD is an associate professor of electrical and computer engineering at Georgia Southern University. He received his BS degree in telecommunication and electronics engineering from the Applied Sciences University, Jordan, in 2004; MS degree in electrical and computer engineering from the University of Minnesota in 2006; and, PhD degree in electrical engineering from the University of Akron in 2011. He is the Founding Director of the Optical Networks and Smart Grid Applications (ONSmart) Laboratory, GSU. His research focuses on various aspects of optical fiber communication/networks, wireless communication, UAV ad hoc networks, multimedia communications, multimedia bandwidth forecasting, distributed power generation, smart grid applications, and engineering education. Dr. Haddad may be reached at rhaddad@georgiasouthern.edu

LEI CHEN is an associate professor of information technology at Georgia Southern University. He received his PhD degree in computer science and software engineering from Auburn University in 2007. His research interests include security, privacy and digital forensics of networks, information and the cloud, especially mobile, handheld, and wireless security. Dr. Chen may be reached at lchen@georgiasouthern.edu

USING AN AUGMENTED REALITY TOOL TO IMPROVE SPATIAL COGNITION

Ulan Dakeev, Texas A&M University – Kingsville; Recayi Pecen, Sam Houston State University; Farzin Heidari, Texas A&M University – Kingsville; Faruk Yildiz, Sam Houston State University; Shah Alam, Texas A&M University-Kingsville

Abstract

This project was developed to restructure a technical CAD course (ITEN 1311) offered in the fall, 2017, semester. The objective of the project was to develop spatial orientation skills for freshmen- and junior-level engineering students. The redesigned course introduced 3D printing of objects as well as the augmented reality (AR) tool for visual representation of two-dimensional drawing in 3D. The objective of this study was to evaluate differences between conventional classroom delivery methods (demonstration of the orthogonal views of objects) and analyzing the prototype in AR. Each of the students developed a 3D model and then 3D printed their individual projects. Moreover, groups of students collaborated to develop an assembly of their individually modeled parts within the software. Statistical t-test analyses were conducted to determine the influence of the augmented reality application in improving spatial orientation skills for the incoming freshman engineering students. This project may benefit the engineering community by restructuring introductory CAD courses for enhancement of the spatial cognition of students. The results showed that the students were able to develop the 3D model of a prototype part when they were exposed to the AR tool prior to the start of the exercise.

Introduction

Spatial cognition is the process of information and skills that could be improved via appropriate pedagogical strategies (Perez-Fabello, Campos, & Felisberti, 2018). The development of better working strategies to improve student performance in entry-level engineering CAD courses could be an effective educational tool. Through virtual reality (VR) and augmented reality (AR), users navigate and interact within three-dimensional environments (Dakeev, Pecen, Yildiz, Alam, & Heidari, ASEE, 2018). The AR provides the ability to rotate the objects as well as experience immersive interaction on a virtual overlaid environment. Since spatial skills are one of the strongest predictors of success in using the CAD software (Dakeev, Pecen, Yildiz, & Heidari, CIEC, 2018), students are also likely to draw correct structures and diagrams when they have high spatial orientation scores (Pribyl & Bodner, 1987). Additionally, Sorby and Baartmans discovered considerable improvement in spatial

cognition skills in both men and women, when augmented reality and virtual reality tools were used (2000). This current study explored how an AR tool influences the spatial cognition of first-year engineering students (men and women) in introductory CAD courses.

The students were introduced to 3D modeling software at the beginning of the academic semester with basic concepts and modeling tools of the software. The students analyzed a pre-defined part to comment on various views, such as front, right side, top, and bottom. Once the analysis was complete, the students participated in the virtual tour of the part (in an open field) to rotate the part and see the identified views. Each student developed the same part in the 3D modeling software, 3D printed the prototype, and manufactured individual group project parts on the portable CNC equipment. The final 3D-printed product was compared to the pre-defined (original) part for accuracy. Three deliverables, 3D-modeled part, 3D-printed object, and CNC-cut product, defined the successful completion of the term project. Overall project reflection summaries were captured from the students' experiences.

The spatial cognition and 3D-modeled outcomes, from orthogonal views, are required skills every engineer must possess in the automotive industry (Sorby, Casey, Veurink, & Dulaney, 2013). Applied engineering technology students may hold positions such as Quality Engineer, Manufacturing Engineer, Plant or Workshop Supervisor, Design Engineer, Continuous Improvement Coordinator, etc., all of which require explicit understanding of 3D models and blueprint readings prior to manufacturing the part. Therefore, the redesigned course may prepare students for their future professional lives and provide them with a competitive advantage.

Methodology

Researchers developed an augmented reality tool for Android devices in order to illustrate the three-dimensional representation of the model from its orthogonal (2D) views. The students downloaded the AR tool, called "Midterm_AR" (see Figure 1) from the Google play market to direct the phone's camera onto the reference blueprint provided to the student (see Figure 2). The authors collected pre- and post-test data to investigate how significantly the

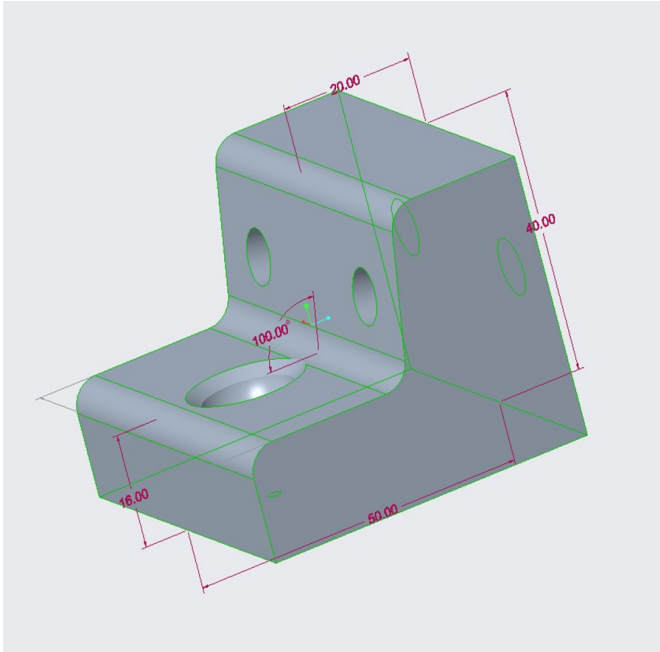


Figure 5. Three-dimensional model after four weeks of the course.

Assessment and Results

The purpose of the study was to investigate how an augmented reality tool could influence the spatial reasoning skills of freshmen- and sophomore-level engineering students. Additionally, the authors explored how prototyping exercises such as 3D printing and CNC manufacturing influenced student learning. The experimental group's outcomes were compared to those of previous CAD courses (fall, 2016, and spring, 2017), which were delivered conventionally by the same instructor. Although all 35 students completed their projects successfully, three students needed additional time and coaching to verify that their models were accurate.

Tables 1 and 2 illustrate that the pretest survey results, in SPSS, showed that the overall mean (mean pretest = 1.42) was lower than the posttest results (mean posttest = 8.58) when the augmented reality tool was introduced in the discussion. The paired sample t-test outcome revealed that the introduction of the tool significantly influenced (p value=0.001<0.05 alpha level) the spatial orientation skills of the students. Although the t-test analysis resulted in a significant difference between the pretest and posttest score means, the correlation ($r=0.418$) revealed that there was less than a 50% correlation between the two-average means. This result motivated the researchers to collect more data and investigate whether the new restructured approach would improve the correlation of scores.

Table 1. Paired sample statistics.

	Mean	N	Std. Deviation	Std. Error Mean	
Pair 1	Pretest	1.42	19.00	0.69	0.16
	Posttest	8.58	19.00	0.84	0.19

Some of the project challenges included incorrect orientation of features of the models within the software that extended the project duration for some students. For example, a developed fidget spinner's ergonomic design was reversed during the dimensioning process, which had to be reviewed for further analysis. Through class discussion and virtual inspection in augmented reality, a number of other projects were revised and updated accordingly. One-hundred percent class satisfaction and engagement suggested that the study was successful and all projects were submitted on time. The second phase of the study was to manufacture the prototype for physical inspection and 3D print it. Figure 6 illustrates two 3D-printed prototypes. The subtractive manufacturing

Table 2. Paired samples test.

		Paired Differences					t	df	Sig. (2-tailed)
		Mean	Std. Deviation	Std. Error Mean	95% Confidence Interval of the Difference				
					Lower	Upper			
Pair 1	Pretest - Posttest	-7.16	0.83	0.19	-7.56	-6.76	-37.40	18.00	0.00

of the prototype involved splitting the class into groups of 3-5 students; each group proposed a project to the instructor for final submission at the end of the semester. Figure 6 also shows how each group member modeled a 3D part independently, generated a toolpath for post processing, cut the work in a router, and provided the fully assembled result to the instructor. Figure 7 shows that some projects, such as plagues, could not be assembled; however, the individual CNC practice assignment was fulfilled.

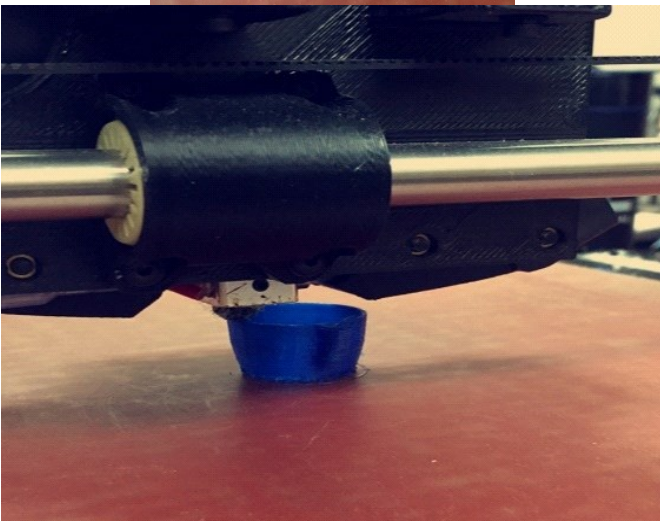


Figure 6. 3D-printed pencil holder and a cup (scaled down).



Figure 7. Group project with CNC product and final assembly.

Overall, the class was satisfied with the projects and their outcomes, some of the students expressed their class experiences as follow:

“I tried my best to put together the whole assembly but some of it did not come out the way I wanted to be because I was inexperienced with the assembly function. But I must say that I had a lot of fun towards the end because I had a better understanding of how to develop the models, especially the last project where I developed a coffee mug and printed it on a 3-D printer. Being able to 3-D print a model that I developed was very cool to do and I have never in my life been able to do such a thing. It was a very good experience to see how it worked and being able to watch the printer actually make the whole entire structure. Although my overall grade was not quite how I wanted it to be I still enjoyed being able to use this software and I can see myself doing this in the future at my future job. I really enjoy using the program and I hope to find a job working with cad.”

“Our project has been one of the most interesting things I’ve done while attending TAMUK. Even though my pencil holder is tiny, I am proud of what I have accomplished and what I learned today. I never would have thought I would be able to learn how to print from a 3D printer. Learning how the machine heats up the filament and how the tip distributed it was mesmerizing to watch. Also, I found it interesting to learn that some of the parts of the 3D printer were also

3D printed... Overall, this class has quickly become one of the most interesting classes I have taken and I feel it will be one of the most useful if I decide to go into the manufacturing industry.”

Conclusions and Continuation of Project

The authors investigated how an AR or VR tool influences the spatial cognition of first- and second-year engineering students. The objective of the project was to develop an AR tool for student use to analyze various features of a 3D model and compare it to conventional, 2D orthogonal views, as well as inspect the a 3D isometric view of the part and hunt for the dimensions from corresponding views of a CAD course delivery method. The sample image target of Figure 2 can be used as a reference source to visualize the 3D representation of the part using the AR tool (Midterm_AR). The comparative statistical analyses revealed, with 95% confidence interval, that the AR tool provided significant improvement ($p=0.01<0.05$ alpha level, and mean pretest = 1.42 < mean posttest = 8.58) in the students' spatial orientation skills. The outcomes of the project were satisfactory; therefore, the newly restructured course will continue to gather more data for further analyses and discussion. Moreover, similar activities, such as the development of an AR tool for kindergarten children to provide engaged learning, will be incorporated in other computer-aided design classes—such as Advanced Graphics and Modeling and Architectural CAD in the spring, 2018, semester. Vasilyeva & Lourenco (2012) believed that spatial cognition skills can be improved at earlier ages, 3-6 and 7-11, with high impact, as well as later in adulthood with special treatment. This project revealed that the incorporation of AR tools in introductory CAD courses may benefit both instructors in spending more time on practical aspects of the course, and the engineering community in developing similar AR tools for their areas of expertise for further explorations, as well as the students engaged in learning CAD early in their careers.

References

- Dakeev, U., Pecan, R., Yildiz, F., Alam, S., & Heidari, F. (2018). Development of virtual environment to introduce spatial reasoning to first and second year engineering students. *Proceedings of 125th ASEE Annual Conference & Exposition*. Washington, DC: ASEE.
- Dakeev, U., Pecan, R., Yildiz, F., & Heidari, F. (2018). Student spatial orientation improvement in introductory CAD courses with the integration of 3D printing and CNC technologies. *Proceedings of the Conference for Industry & Education Collaboration*. Retrieved from http://www.indiana.edu/~cieec/Proceedings_2018/Files/2018_Session_Index.htm#ETD
- Perez-Fabello, M., Campos, A., & Felisberti, M. F. (2018). Object-spatial imagery in fine arts, psychology, and engineering. *Journal of Thinking Skills and Creativity*, 27,131-138.
- Pribyl, J. R., & Bodner, G. M. (1987). Spatial ability and its role in organic chemistry: A study of four organic courses. *Journal of Research in Science Teaching*, 2(3), 229-240.
- Sorby, S., & Baartmans, B. J. (2000). The development and assessment of a course for enhancing the 3-D spatial visualization skills of first year engineering students. *Journal of Engineering Education*, 89(3), 301-307.
- Sorby, S., Casey, B., Veurink, N., & Dulaney, A. (2013). The role of spatial training in improving spatial and calculus performance in engineering students. *Journal of Learning and Individual Differences*, 26, 20-29.
- Vasilyeva, M., & Lourenco, S. F. (2012). Development of spatial cognition. *WIREs Cognitive Science*, 3, 349-362.

Biographies

ULAN DAKEEV is an assistant professor in the Industrial Technology Department in the College of Engineering at Texas A&M University-Kingsville. His areas of research include augmented and virtual reality, renewable energy (wind energy), quality in higher education, motivation, and engagement of students. Dr. Dakeev may be reached at Ulan.dakeev@tamuk.edu

REG PECEN is a Quanta Endowed Professor of Engineering Technology in the College of Science and Engineering Technology at Sam Houston State University. He holds a PhD in EE from the University of Wyoming and an MS in EE from CU Boulder. He is a former VP for Education, Go-Link Energy, a division of ALMx-Security, Inc. and former President and CEO for North American University in Houston, TX. He served as past-chair (2013-14), chair (2012-13), chair-elect (2011-12), and program chair (2010-11) of the Energy Conversion Conservation Division (ECCD) of the American Society of Engineering Education (ASEE). He also served as professor, program coordinator of electrical engineering technology (EET) and Department of Technology Graduate Degree (MS and doctoral) Programs (1998-2012) at the University of Northern Iowa. He is the recipient of the 2011 UNI C.A.R.E Sustainability Award

for the recognition of applied research of renewable energy applications at UNI and Iowa and recipient of the Diversity Matters Award to acknowledge individual contributions to the advancement of diversity-related goals at UNI. Dr. Pecen may be reached at regpecen@shsu.edu

FARZIN HEIDARI serves as associate professor of industrial management and technology at Texas A&M University, Kingsville. Dr. Heidari has 26 years' experience in manufacturing and CAD/CAM/CNC courses. He is currently serving as the Graduate Coordinator for the Industrial Management program. Dr. Farzin Heidari may be reached at farzin.heidari@tamuk.edu

FARUK YILDIZ is an associate professor of engineering technology at Sam Houston State University. His primary teaching areas are in electronics, computer-aided design (CAD), and alternative energy systems. His research interests include low-power energy harvesting systems, renewable energy technologies, and education. Dr. Yildiz may be reached at fxv001@shsu.edu

SHAH ALAM received his PhD from Louisiana State University in 2005; MS from the South Dakota School of Mines and Technology in 2002; MS and BS from the Bangladesh University of Engineering and Technology, Bangladesh, in 1998 and 1993, respectively. Dr. Alam is a registered professional engineer in Texas (TBPE No. 113655). His research interests include composite structural design and analysis, mechanical system design and analysis, solid mechanics, fatigue and fracture mechanics, computational biomedical system analysis, finite element analysis (static, dynamic, impact, cfd, thermal, etc.), renewable energy, and the structural integrity of aerospace, offshore, and subsea structures. Dr. Alam may be reached at shah.alam@tamuk.edu

A SYSTEM FOR SUGGESTING SUITABLE CONTENT TO THE USERS OF SAHAVE

Toqeer Israr, Eastern Illinois University; Ajay Aakula, Eastern Illinois University

Abstract

Sahave, a start-up company in Illinois, develops community service applications, offering three major services: blood donation, volunteering, and campaign activities. Each user is identified by a certain set of characteristics, thereby meeting certain conditions. If a Sahave user, u , subscribes to an activity then, as per traditional programming logic, that activity notification gets pushed to the rest of the users, U , who display a similar set of characteristics to user u . The problem arises when one user in the set U is not interested in that activity and still ends up receiving the notification. This spamming of the uninterested users causes discontent and dissatisfaction, and could possibly cause the user to quit. In this study, the authors analyzed user behavior and, in this paper, propose a preference system for Sahave users. In a traditional subscription model, users are notified of events for which they have subscribed, and possibly for others that similar users have opted-in for. In this paper, the authors propose machine learning algorithms to make the Sahave's system smart, by using collaborative filtering, content-based filtering, and hybrid filtering.

Collaborative filtering is based on the idea that people who agreed in their evaluation to certain items in the past are likely to agree in the future. A content-based filtering system works with data that the user provides, either explicitly (providing feedback) or implicitly (clicking on a link). A user profile is created based on user data and is used to make suggestions to the user. The system improves over time by self-training as the user provides more input or takes actions on the recommendations. A hybrid approach combines content-based filtering and collaborative filtering, utilizing the benefits of both. Depending on the problem and situation, Sahave can choose the system that will work best.

Introduction

Sahave is a startup organization in Illinois, working on community service application products. The community service application, also known as *Sahave*, deals with blood donation, volunteering, and campaign creation services (to avoid ambiguity, the company will be referred to as "*company Sahave*" and the application as just "Sahave"). Sahave has built a mobile application using technologies such as Angular JS, Ionic, Node.js, and MongoDB. This

application resides on Amazon's web service server. The application has a major feature that notifies users about related events. The current notification system in the application is not intelligent enough to understand user interest before sending a notification. This could cause some problems for users who may perceive these notifications as spam, due to the low-intelligent nature of the application.

Traditional machine learning is defined as, "A computer program is said to learn from experience E with respect to some class of tasks T and performance measure P if its performance at tasks in T , as measured by P , improves with experience E " (Mitchell, 1997). Machine learning can be very powerful with the help of more data, as illustrated in Figure 1. Because of the evolution of big data, due to social media, IoT, etc., there is a surplus of data available to train machine-learning models to perform intelligent operations.

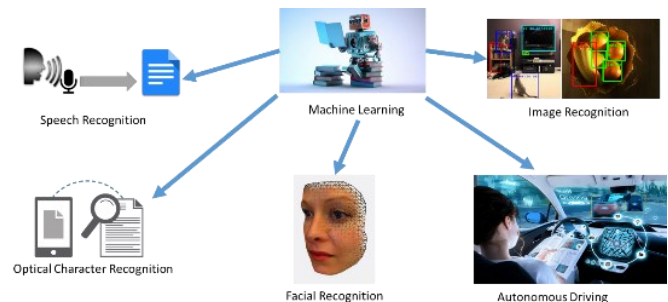


Figure 1. Machine learning application.

Take Netflix as an example. Initially, Netflix was a movie rental website, but with the help of a technology revolution, it started streaming video and on-demand services. As there is a significant number of videos and on-demand services available online, the user faces difficulty in choosing what to watch. Netflix added a recommendation feature with the help of machine-learning techniques, which suggested movies to users based on their viewing history. The Netflix recommendation system is quite intelligent for predicting which movie is best for the user, based on past action data.

Specific Problem

This paper mainly focuses on problems that Sahave users are facing, due to the notification system. The *company Sahave* offers three services: blood donation, volunteering, and campaign services. Blood donation services allow the

administrators to create a blood donation request for collecting blood from donors. Volunteer services allow administrators to create opportunity requests for social service activities for volunteers to sign up. Campaign services allow administrators to run campaign activities for specific causes to provide support for a specifically targeted cause and/or people.

Presently, *company* Sahave has a recommendation notification system, Sahave, which notifies users of interesting and related event details. However, the current system has difficulty in understanding user interests in detail. If the Sahave user has created a campaign about breast cancer and is encouraging women of certain ages to get mammography exams, then most likely male users of the system would not be interested in receiving this notification. However, the current system will push this out to all users (based on the location) who may have subscribed to health-related campaigns. Sahave depends only on broad-user preferences and location details to push such notifications. The blood donation service allows users to participate in blood donation programs. Users can also become administrators and can create their own blood donation activity. Once a user-cum-administrator has created an individual blood donation activity, it then becomes a challenge for Sahave to identify which users should be notified. Figure 2 explains the current Sahave blood donation notification system functionality.

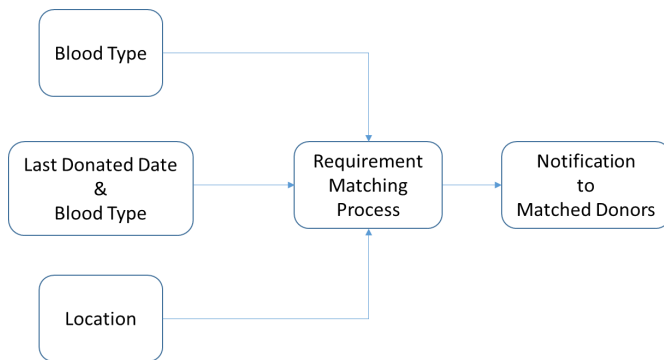


Figure 2. Blood donation service notification system.

Currently, a user-cum-administrator-created activity, Sahave, based on the details of location and blood group of that activity, sends notifications to the users, where user location and blood group details match up. However, it does not take into account the fact that the very same users have not shown prior interest in similar activities. An intelligent system is needed to analyze user profiles with past user data to make smart decisions about which users should be notified of the new event. The current system sends a notification to all matched users irrespective of users past data.

Volunteer service offers a platform to the users to create volunteer activities. In this service, every user has the ability to create events for different service-oriented purposes. Suppose a Sahave user created a spoken English development program activity to help people improve conversational English skills. Figure 3 explains the current Sahave volunteer service notification system functionality.

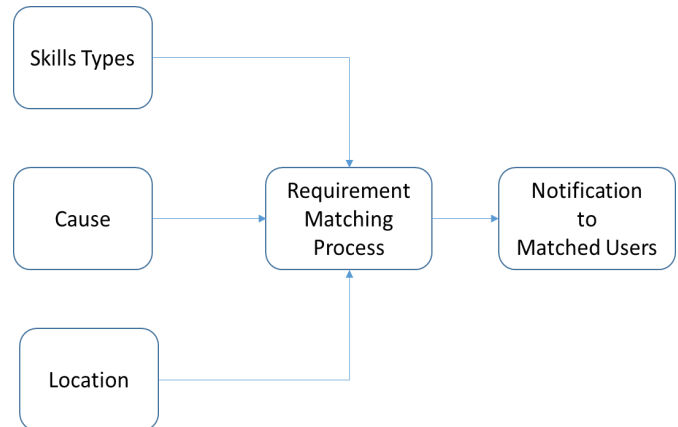


Figure 3. Volunteer service notification system.

The event will be conducted in a particular place at a specific time. After the user has created the event, the current Sahave recommendation system will push the notifications to all of the users located in that particular area with the matched skillset, using some predefined conditions. However, this is not useful for a user already proficient in English. If a similar activity is created again and the same user is spammed again with a notification for an English class event, the user may be extremely unhappy and will most likely either block or unsubscribe from the notification list. A user always expects to receive recommendations that match his or her interests. If the system sends unrelated notifications at regular intervals, then the user will not be happy. The main problem in the current system is that it is too difficult to understand varying user interests. The trouble with the current system is that it is not able to correlate user personal criteria with past activities. If 100 Sahave users create a volunteer event at the same place with the same criteria, then it pushes notifications to all users who meet these criteria 100 times. However, this will cause quite an unpleasant experience for users, especially when they might not be interested in such activities.

Research

The research problem needs to take into account details using different contexts and note that solving this problem using traditional programming languages would be difficult. The recent technology evolution in big data offers support

to intelligently deal with user problems. Machine learning can deal with problems that are difficult to resolve using traditional programming languages.

A machine-learning model was developed using different algorithm functions. Many algorithms can help in developing a machine-learning model to understand user preferences in different dimensions for effective recommendations to the users. But every model requires user “training” data to predict values in a real-time scenario based on such data. The current system can be replaced with the new machine-learning-based recommendation system, which is broadly divided into three approaches, based on user data: collaborative filtering, content-based filtering, and hybrid filtering (Aggarwal, Tomar, & Kathuria, 2017).

Collaborative Filtering

Assumption. Users having a similar interest in the past are most likely to have a similar interest in future.

Collaborative filtering is defined as the system trying to send a notification to the user based on the popularity of the item. Collaborative filtering is classified into two types, based on items and users (Aggarwal, Tomar, & Kathuria, 2017). Figure 4 shows user-based filtering and is based on user reviews such as ratings on specific items. Now suppose that user X is attending three events—a dance class, an English language verbal event, and an English language writing skills event—and user Y is attending two of those three events. In this case, user-based filtering suggests that user Y attend the remaining third event. Here, there is a correlation between user X and user Y, so an algorithm identifies unmatched events that can be recommend to each user. A user-based collaborative filtering system makes the recommendations to users based on user data.



Figure 4. User-based collaborative filtering (UB-CF).

Figure 5 shows item-based collaborative filtering, which mainly explores the relationship between items. If a user attends a particular volunteer event, then he/she may attend other, closely related events. Or, if user X is attending an English language verbal event and many users in the past also attended an English language writing skills event along with the verbal event, then there is a high probability that user X would also like to attend an English language writing skills event (Collaborative, 2012). An item-based collaborative filtering system makes the recommendations based on item data.

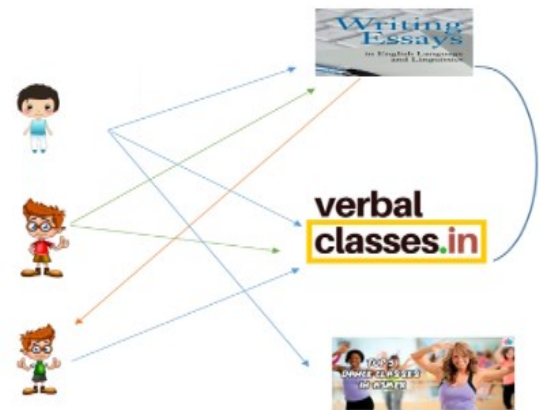


Figure 5. Item-based collaborative filtering (IB-CF).

Here is another example to illustrate how a collaborative filtering system makes recommendations. Table 1 presents five opportunity creation events and five people. A “+” indicates that the person participated in the event, and a “-” indicates that the person did not participate in the event. To predict if Ken would like to attend an event for résumé building, his previously attended events are compared to the events of the other users. In this case, the events of Ken and Mike are identical, and Mike liked résumé building, so everyone can predict that Ken likes the résumé building opportunity as well.

Table 1. User event attendance.

	Amy	Jeff	Mike	Chris	Ken
Cricket	-	-	+		+
Teaching Skills	-	+	+	-	+
Acting	+		-	+	-
Business Skills	-	-	+	-	+
Resume building	-	+	+	-	?

However, the system cannot depend on similar-person criteria every time. Instead of relying on the most similar person, a prediction is usually based on the weighted average of several users' recommendations. How can the system calculate a weight coefficient to assign to user attendance values? The weight given to a person's attendance is determined by the correlation between that person and the person who will make a prediction.

As a measure of correlation, the Pearson correlation coefficient can be used. The Pearson correlation coefficient helps to determine the relationship between two variables; the relationship unit varies from -1 to +1, -1, when there is a perfect negative linear relationship and +1, when there is a perfect positive linear relationship (Sari, Dal'Col Lúcio, Santana, Krysczun, Tischler, & Drebes, 2017). The relationship between two persons/events can be calculated using this coefficient. The attendance of persons X and Y of event k is written as X_k and Y_k , while $X!$ and $Y!$ are the mean values of all their event attendance in the past. The correlation between X and Y is then given by Equation 1 (Collaborative, 2012):

$$r(X, Y) = \frac{\sum_k (X_k - X!) (Y_k - Y!)}{\sqrt{\sum_k (X_k - X!)^2 \sum_k (Y_k - Y!)^2}} \quad (1)$$

In Equation 1, k is an element of all of the events that both X and Y have attended in the past. A prediction for the event attendance of person X of the event item i , based on the attendance of people who have attended event item i , can be computed using Equation 2 (Collaborative, 2012):

$$P(X_i) = \frac{\sum_k (Y_i) r(X, Y)}{n} \quad (2)$$

where, k consists of all of the people, n , who have attended event item i .

Note that a negative correlation can also be used as a weight. For example, Amy and Jeff have a negative correlation and Amy did not like résumé building, which could be used as an indication that Jeff will enjoy résumé building. If no one has attended event item i , the prediction is equal to the average of all of the events that person X attended. The constrained Pearson measure is similar to the normal Pearson measure but uses the mean value of possible attended events instead of the mean values of the attended events of persons X and Y. The system can make accurate predictions to Sahave users based on a collaborative filtering mechanism.

Content-Based Filtering

Assumption. The key parameters in the content of an item are more closely related to the user experience data than the generic metadata. Hence, this will separate relevant items from non-relevant items.

A content-based recommendation system works with user-provided data. Based on those data, a user profile is generated, which is then used to make suggestions to the user. As the user provides more input or takes action on recommendations, the engine becomes more and more accurate (Aggarwal, Tomar, & Kathuria, 2017). Term frequency (TF) and inverse document frequency (IDF) are used in information retrieval systems as well as content-based filtering mechanisms. They are used to find the comparative importance of a document, article, news item, movie, etc. TF is known as the frequency of a word in a document. IDF is defined as the inverse of the document frequency among the whole corpus of documents (Aggarwal, Tomar, & Kathuria, 2017).

Figure 6 shows the content-based filtering mechanism. As per the content-based filtering approach, this new system creates profiles for each user, based on the user's previous action data. If a user-cum-administrator created two volunteer activities, say, training on Web development and training on writing development, the new system will find which activity is notified based on the word terms in the activity data and user profile data. It is certain that "the" will occur more frequently than "development," but the relative importance of "development" is higher than the more frequent word "the." A TF-IDF weighting technique will negate the effect of high-frequency words in determining the importance of an activity to the user.

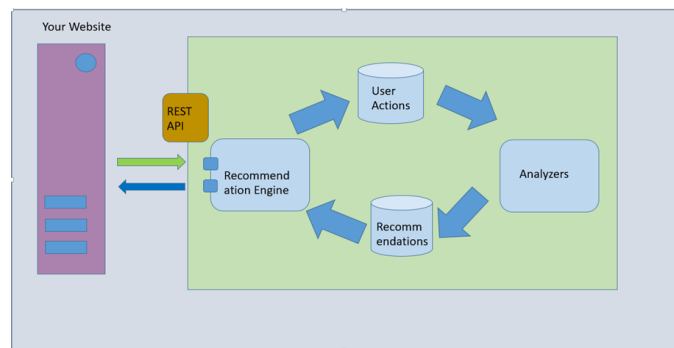


Figure 6. Content-based filtering mechanism.

While calculating a TF-IDF, many unimportant high-frequency words, such as "the," "and," "more," etc. can be identified. The log is then used to dampen the effect of high

-frequency words, as indicated by Equation 3. For example, TF = 3 vs TF = 4 is vastly different from TF = 10 vs TF = 1000. The importance of a word cannot be calculated using simple word count in an item (Aggarwal, Tomar, & Kathuria, 2017). Table 2 indicates that the effect of high-frequency words is dampened, and new values are more comparable to each other, as opposed to the original raw-term frequency.

$$\begin{cases} 1 + \log_{10} tf_{i,d}, & \text{if } tf_{i,d} > 10 \\ 0, & \text{otherwise} \end{cases} \quad (3)$$

Table 2. Term frequency and weighted term frequency values.

Term Frequency	Weighted Term Frequency
0	0
10	2
1000	4

The TF-IDF Method

Eliminate stop words—Example: “in,” “the,” “so,” “but,” etc. Find the importance of a word’s measure by calculating the TF.IDF score (term frequency multiplied by inverse document frequency).

Term frequency—Word count in the content:

$TF(t) = (\text{Number of times the term } t \text{ appears in the document}) / (\text{Total number of terms in the document})$

$IDF(t) = \log_e(\text{Total number of documents} / \text{Number of documents with the term } t \text{ in it})$

Assume that two events and a user profile contain the words listed in Table 3, then calculate term frequency and inverse document frequency.

How the Vector Space Model Works

$TF(\text{training}, v1) = 3/6 = 0.5$

$TF(\text{training}, v2) = 1/4 = 0.25$

$TF(\text{user}, u) = 1/6 = 0.16$

$IDF(\text{training}) = \log(3/3) = 0$

$TF.IDF(\text{training}, v1) = 0 * 0.5 = 0$

$TF.IDF(\text{training}, v2) = 0 * 0.25 = 0$

$TF.IDF(\text{user}, u) = 0 * 0.16 = 0$

$TF(\text{Web}, v1) = 2/6 = 0.33$

$TF(\text{Web}, v2) = 0/4 = 0$

$TF(\text{user}, u) = 2/6 = 0.66$

$IDF(\text{Web}) = \log(3/2) = 0.17$

$TF.IDF(\text{Web}, v1) = 0.33 * 0.17 = 0.22$

$TF.IDF(\text{Web}, v2) = 0.17 * 0 = 0$

$TF.IDF(\text{user}, u) = 0.17 * 0.66 = 0.11$

$TF(\text{writing}, v1) = 0/6 = 0$

$TF(\text{writing}, v2) = 1/4 = 0.25$

$TF(\text{user}, u) = 1/6 = 0.16$

$IDF(\text{writing}) = \log(3/2) = 0.17$

$TF.IDF(\text{writing}, v1) = 0.17 * 0 = 0$

$TF.IDF(\text{writing}, v2) = 0.17 * 0.25 = 0.04$

$TF.IDF(\text{writing}, u) = 0.17 * 0.16 = 0.02$

$TF(\text{Development}, v1) = 1/6 = 0.16$

$TF(\text{Development}, v2) = 2/4 = 0.5$

$TF(\text{Development}, u) = 2/6 = 0.66$

$IDF(\text{Development}, V) = \log(3/3) = 0$

$TF.IDF(\text{Development}, v1) = 0.16 * 0 = 0$

$TF.IDF(\text{Development}, v2) = 0.5 * 0 = 0$

$TF.IDF(\text{Development}, v2) = 0.66 * 0 = 0$

Table 3. User profile, volunteer events 1 and 2, and word count.

Volunteer event 1(v1)	Word	Count
	Training	3
	Web	2
	Development	1
Volunteer event 2(v2)	Word	Count
	Training	1
	Writing	1
	Development	2
User profile(u)	Word	Count
	Training	1
	Writing	1
	Development	2
	Web	2

After calculating TF-IDF scores for the user profile, and volunteer events as shown in Table 4, the system can determine which event is closer to the user profile. This is accomplished using the vector space model, which computes the nearness, based on the angle between the vectors. A vector space model is algebraic, which helps in filtering information and relevancy ranking (Arguello, 2013). A vector is a point in the vector space; thus, calculating the similarity between two items is required. The items need to be stored as vectors of attributes in n -dimensional space.

Table 4. User profile and volunteer events 1 and 2.

S.no	Web	Training	Development
Volunteer event 1	0.66	0	0
Volunteer event 2	0	0	0.33
User profile	0.11	0	0

Figure 7 represents the three-dimensional vector space for simplicity, which is defined as a basis vector with “training web development” attributes. Figure 7 is a 3D representation of three attributes: development, Web, and training. The vector space model ranks the event based on vector space similarity between volunteer activity events and user profiles. The system performs a cosine similarity between the user profile vector and volunteer activity vector then calculates the angle between the vectors. From Equation 4, the ultimate reason for using cosine is that the value of cosine will increase with a decreasing value of the angle, which signifies more similarity. The angle between the user profile vector and volunteer activity 1 is 0, and the angle between the user profile vector and volunteer activity 2 is 90. Hence, volunteer activity 1 is closer to the user profile.

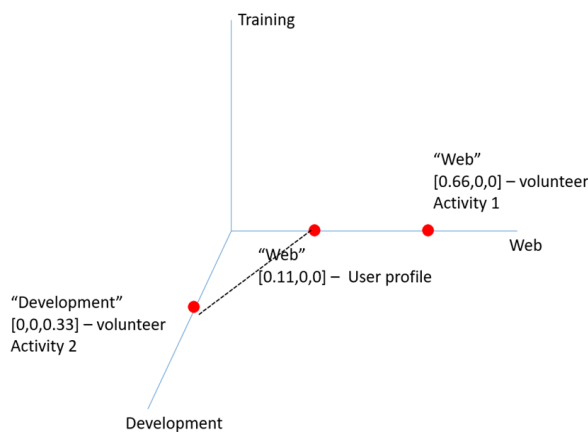


Figure 7. Vector space model.

$$\cos \theta = \frac{\text{volunteer activity1} \cdot \text{user profile}}{\text{volunteer activity1} \text{user profile}} \quad (4)$$

Hybrid Filtering

Many times, there will be scenarios for which either content-based filtering or collaborative filtering may not apply completely, or both of them can be used. For these scenarios,

the recommendation system uses hybrid filtering. Both content-based filtering and collaborative filtering have their advantages and disadvantages. The following specific problems can be distinguished for content-based filtering.

- Content description: It is difficult to generate a meaningful content description in every area of business (Hybrid, 2012).
- Over-specialization: A content-based filtering system could not recommend items if the last user’s behavior does not provide evidence for this. Additional techniques must be added to allow the system the capability to make a recommendation that is not within the scope of what the user has already shown interest in (Hybrid, 2012).

A collaborative filtering system does not have these weaknesses, because it does not require content in order to recommend an item to a user. The system can handle any kind of information. Furthermore, the system can recommend items to a user that may have very different content from what the user has previously indicated interest in. Finally, because recommendations are based on the opinions of others, it is well suited for subjective domains like art. However, collaborative filtering does introduce certain problems of its own:

- Early-rater problem: Collaborative filtering systems are not able to recommend new items to users, since they do not have user ratings on which to make predictions. Even if users start participating in events, it will take some time before the events have received enough of a participation count to make accurate recommendations. Similarly, recommendations will also be inaccurate for new users only having attended a few events (Hybrid, 2012).
- Sparsity problem: In many information domains, the items have more data for a person that they can discover. This makes it hard to find events that are attended by enough people on which to base predictions (Hybrid, 2012).
- Gray sheep: In general, user groups with overlapping characteristics are needed. Even if such groups exist, individuals may not be able to agree or disagree with any group of people and will receive incorrect recommendations (Hybrid, 2012).

A hybrid filtering system is a combination of content-based filtering and collaborative filtering. This system could take advantage of both the representation of the content as well as the similarities among users. In a hybrid approach, two types of information need to be combined for the recommendation, and it is possible to use the recommendations of the two filtering techniques independently (Hybrid, 2012).

Collaborative filtering is based on the correlation between users to make predictions. Such a correlation is most meaningful and accurate when users have attended many events in common. Furthermore, the lack of access to the content of the items prevents similar users from being matched, unless they have attended the exact same event. For example, if one user liked the event “listening skills” and another liked the event “writing skills,” they would not necessarily be matched together. A hybrid approach called collaboration via content deals with these issues by incorporating both the information used by content-based filtering and collaborative filtering. In collaboration via content, both the attendance at events and the content of the events are used to construct a user profile. The selection of terms that describe the content of the events is done using content-based techniques. The weight of terms indicates their importance for the user. Table 5 shows an example of the kind of information available for making a prediction about the event résumé building for Ken with collaboration via content.

Table 5. User attendance and event content scores.

	Experienced	Software Engineer	Fresher	Host	Hyderabad	Résumé Building
Amy	1	0	1.2	0.2	0.2	–
Jeff	2.1	0	0.5	3	2.2	+
Mike	1.3	1.5	0.2	3.2	1.9	+
Chris	1.1	2	2.8	0.8	0	–
Ken	0.8	1.1	0	2	1.2	?

Just as with collaborative filtering, the Pearson correlation coefficient can be used to compute the correlation between users. Instead of determining the correlation with a user who attended the events, however, term weights are used. Because this method has a greater number of items from which to determine similarity than collaborative filtering, the problem of users not having enough common events attended is no longer an issue. Furthermore, unlike content-based filtering, predictions are based on the impressions of other users, which could lead to recommendations outside the normal environment of a user. However, to make recommendations about events, it is still necessary that enough users attend the event. Just as with collaborative filtering, new events cannot be recommended if no user has attended the events.

Another approach to combining collaborative and content-based filtering is to make predictions based on a weighted average of the content-based recommendation and the collaborative recommendation. The rank of each item being recommended could be a measure of the weight. In this

way, the highest recommendation receives the highest weights.

Discussion

This study shares the most useful techniques for utilization in the Sahave application for the effective recommendation engine. Both collaborative and content-based filtering approaches have their own ways of resolving the issue, but using a combination of both approaches can address the issue in a different context. Applications cannot blindly rely on these systems, because both have limitations. If the application does not have sufficient data, users cannot expect accurate recommendations. If the application has fewer users, then it would be good to have a traditional recommendation system engine instead of developing one that is based on machine learning. Users can expect good recommendations from the system recommended from this study, if and only if the user and item counts are relatively high. If user access is minimal, then there might be a chance of inaccurate recommendations getting pushed to the users, due to inconsistent user data.

Conclusions and Future Work

Sahave is an application for community work such as blood donation, volunteer activities, and managing campaigns. It currently faces problems when it tries to notify its users of new events, sometimes resulting in unwanted/unneeded notifications. Overall, these problems can be considerably decreased by using the methods discussed in this paper. Sometimes it is difficult to recommend exact user interests every time. If the system does not have a good amount of user data, then it is difficult to predict user interest accurately. In this paper, the authors discussed three models for resolving user problems. Many organizations prefer to implement a hybrid filtering approach, as it combines both content-based and collaborative filtering approaches. Sahave has not yet implemented a recommendation system using machine-learning techniques. They have just recently launched the Sahave application. Once a relatively large amount of data is generated, then they make use of the system recommended in this study.

References

- Aggarwal, P., Tomar, V., & Kathuria, A. (2017). Comparing content based and collaborative filtering in recommender systems. *International Journal of New Technology and Research*, 3(4), 65-67. Retrieved from https://www.ijnr.org/download_data/IJNTR03040022.pdf

-
- Arguello, J. (2013, February 13). *Vector space model*. [PowerPoint slides]. Retrieved from https://ils.unc.edu/courses/2013_spring/inls509_001/lectures/06-VectorSpaceModel.pdf
- Collaborative filtering*. (2012, January 23). Retrieved from <http://recommender-systems.org/collaborative-filtering/>
- Hybrid recommender systems*. (2012, January 22). Retrieved from <http://recommender-systems.org/hybrid-recommender-systems/>
- Mitchell, T. M. (1997). *Machine learning*. New York: McGraw-Hill.
- Sari, B. G., Dal'Col Lúcio, A., Santana, C. S., Krysczun, D. K., Tischler, A. L., & Drebes, L. (2017). Sample size for estimation of the Pearson correlation coefficient in cherry tomato tests. *Ciência Rural*, 47(10), 1–6. doi: <http://dx.doi.org/10.1590/0103-8478cr20170116>

Biographies

TOQEER ISRAR is a Professional Engineer and an assistant professor at Eastern Illinois University. He earned his PhD in electrical and computer engineering, 2014, from the University of Ottawa, Ontario, Canada, and his BEng and MASc in electrical engineering degrees from Carleton University, Ontario, Canada. He is an internationally recognized expert in the areas of performance and software engineering, and has several years' of experience in industry. Dr. Israr may be reached at taisrar@eiu.edu

AJAY AAKULA is a student at Eastern Illinois University. He holds a Bachelor of Technology degree in Electronics and Communication Engineering from Jawaharlal Nehru Technological University, Hyderabad, India. Currently, he is pursuing a master's program in computer technology at Eastern Illinois University. He has over three years' of experience as an application developer, and he has worked in banking and healthcare. Mr. Aakula may be reached at aakula@eiu.edu

UTILIZATION OF SPECTRAL AND TEMPORAL ACOUSTIC FEATURES FOR VEHICLE-CENTRIC EMOTION RECOGNITION

Tejal Udhan, Florida State University; Shonda Bernadin, Florida A&M University, Florida State University

Abstract

It is an established fact that the emotional state of human drivers influences their driving performance. Negative emotions while driving may have serious consequences, such as road-rage incidents and fatal crashes. If, however, a vehicle is “smart” enough to respond to a driver’s undesirable emotional state, it may be able to thwart negative outcomes of these accidents. Positive and negative emotions are expressed differently by humans through their speech and facial expressions. Since speech-based systems are less distracting than visual interactive systems for in-car applications, the authors present here an acoustic system for analyzing four different human emotions: anger, happiness, sadness, and neutrality (no emotion). However, speech emotion recognition is an emerging field and presents many challenges. The set of most powerful features that can differentiate between emotions is not defined; hence, the selection of features is a critical task. Since spectral features are primary indicators of human emotions and temporal features better model transitions in emotions, the authors analyzed these two types of acoustic features for emotion recognition. Frequency formants are used as spectral and zero-crossing rate as temporal features. A new algorithm based on a decision tree was designed to utilize these features for speaker-dependent emotion recognition.

Introduction

Speech is a method of communication or expression of thoughts in spoken words. It is the most common and fastest means of communication between humans. This fact compelled researchers to study acoustic signals as a fast and efficient means of interaction between humans and machines. For authentic human-machine interaction, the machines should exhibit sufficient intelligence to distinguish different human voices and their emotional states. It is well known that the emotional state of human drivers highly influences their driving performance. Road-rage incidents occur when drivers become emotionally enraged due to the actions of another driver. This anger may lead to a high-speed chase, tailgating, and sometimes even death due to a traffic crash or physical contact. If a car is “intelligent”

enough to respond to a driver’s emotional state, it may be able to thwart negative outcomes of road-rage incidents.

Speech emotion recognition, extracting the emotional state of speakers from acoustic data, plays an important role in enabling machines to be intelligent. Most current research in this field focuses on using facial recognition techniques to characterize emotion (Tarnowski, Kołodziej, Majkowski, & Rak, 2017). However, for vehicle-centric applications, audio and speech processing may provide better noninvasive and less distracting solutions than other interactive in-vehicle infotainment systems (Lo & Green, 2013). Hence, utilization of acoustic features is preferred for emotion recognition in human drivers. In this paper, the authors present a new algorithm based on low-level acoustic features for emotion recognition of four common emotions: anger, happiness, sadness, and neutrality.

Speech is a complex signal containing information about messages contained in speech, speaker, language, and emotions. It contains linguistic (encoded in speech) and paralinguistic (related to speaker) information. The primary objective of speech is to convey information, encoded as linguistic content. Paralinguistic information includes a speaker’s age, sex, emotional state, and cognitive capacities. Due to their cognitive abilities, humans are capable of both conveying and understanding linguistic and paralinguistic parts of speech with minimal effort. Speech processing can be defined as the field to determine speech features, understand how the features characterize the information contained in speech, and implement this knowledge to design machines capable of understanding human speech. Although speech processing deals only with the physiological nature of the speech signal, the speaker’s emotional state also imparts some of the features to human speech. Additionally, different human emotions affect speech features distinctively and, hence, to have optimized speech recognition systems, the human emotions in speech also must be considered. Acoustic emotion recognition finds many applications in the modern world, ranging from interactive entertainment systems, medical therapies, and monitoring from various human safety devices (Cavazza, Charles, & Mead, 2002; Yang & Chen, 2012; Kessous, Castellano, & Caridakis, 2009; Ververidis & Kotropoulos, 2006).

Background

Emotions are specific and consistent collections of physiological responses triggered by internal or external stimuli as a representation of certain objects or situations. The internal stimuli consist of changes in a person's body that produces pain, or an external stimulus such as the sight of another person; or the representation, from memory, of a person, or object, or situation in the human thought process. The research also suggests that the basics of most emotional responses are preset in the genome (Damasio, 2000). In a general sense, emotions are a part of the bio-regulatory mechanism that humans have evolved to maintain life and survive. Emotions form an intermediary layer between stimulus and behavioral reaction, which replaces rigid reflex-like response patterns, allowing for greater flexibility in behavior (Scherer, 1982; Tomkins & Karon, 2008).

It has also been suggested that one of the major functions of emotion is the constant evaluation of stimuli in terms of relevance and the preparation of behavioral responses that may be required by these stimuli (Scherer, 1982; Arnold, 1963). Emotional reactions are essential in acquiring new behavior patterns and are a prerequisite for learning (Bower, 1981; Mowrer, 1973). The precise composition and dynamics of emotions are specific to an individual and are based on environmental and individual development. However, basic traits are consistent across all humans.

Speech is an informative source for the perception of emotions; for example, talking in a loud voice when feeling very happy, speaking in an uncharacteristically high-pitched voice when greeting a desirable person, or the presence of vocal tremor when something fearful or sad has been experienced. This mental recognition of emotions indicates that listeners are able to infer the speaker's emotional state reasonably accurately, even when the visual information about a speaker, such as the speaker's photo or video, is unavailable. This theory of cognitive emotion inference forms the basis for speech emotion recognition (Udhan & Bernadin, 2018).

Based on the definition of emotions as including a physiological component, both voluntary and involuntary effects on the human speech production apparatus can be expected, and the characteristics of vocal expression are the net result of these effects (Sethu, Epps, & Ambikairajah, 2014). Researchers have noted that characteristics affecting human movement also affect the voice production mechanism and, consequently, the voice. This theory is substantiated by the fact that vocal expressions of all basic emotions are similar in different languages (Udhan & Bernadin, 2018; Sethu, Epps, & Ambikairajah, 2014). Another research finding

suggests that various aspects of a speaker's physical and emotional state, including age, sex, and personality, can be identified by voice alone (Kramer, 1963). This presence of low-level information even in short utterances can influence the interpretation of the words being uttered; moreover, the emotions can be recognized from segments of speech as short as 60 ms (Pollack, Rubenstein, & Horowitz, 1960). Consequently, Scherer, Banse, & Wallbott have demonstrated that emotion can still be recognized even if the linguistic content of the message contained in speech is not interpreted; this serves as evidence for the existence of vocal (acoustic) characteristics specific to emotions (2001).

Experimental listening studies with human subjects demonstrate a strong relationship between qualitative acoustic features and perceived emotions (Gobl, 2003); many researchers studying the auditory aspects of emotions have been trying to define this relation (Cowie, Douglas-Cowie, Tsapatsoulis, Votsis, Kollias, Fellenz, & Taylor, 2001; Murray & Arnott, 1993). Different speech features, such as pitch, energy, frequency band ratios, jitter, shimmer, and frequency formants, are researched for the purpose of acoustic emotion recognition. However, feature selection for acoustic emotion recognition is in the early stages of research, since no set of ideal features is available to be readily used for optimal emotion recognition techniques.

Challenges of Acoustic Emotion Recognition

The development of machines capable of demonstrating human conversational skills is one of the long-sought goals of speech recognition. However, understanding linguistic and paralinguistic parts of speech using a machine has not yet been achieved. Specifically, extraction of paralinguistic parts of speech involving emotions is a challenging task, since machines do not have the cognitive capabilities that humans do. The importance of emotion recognition systems has increased with the need to improve naturalness and efficiency of speech-based human-machine interfaces (Cowie et al., 2001). The aim of an emotion recognition system is to extract features that are representative of the speech patterns characterizing only the emotional state of the speaker, while simultaneously masking the patterns that are characteristic of all other information (Udhan & Bernadin, 2018). Such features can then be utilized for automatically determining the emotional state of the speaker. However, no ideal features are identified, and the search for the best features that maximize emotion-specific information, while minimizing dependence on other aspects, is one of the central challenges in emotion recognition.

Since ideal features do not exist, pattern recognition techniques are used to make a decision about an emotional state based on chosen features. Depending on which aspect of the speech signal they describe, features are broadly categorized into low-level or high-level descriptors. Low-level features describe the acoustic, prosodic, or spectral properties of the speech signal, without considering the linguistic content of the speaker’s message (Udhan & Bernadin, 2018). High-level features, on the other hand, are based explicitly on linguistic content without taking into account any variations in the acoustic features of the speech signal. Even though evidence suggests that both contain emotion-specific information (Chul & Narayanan, 2005), to limit the complexity of the emotion recognition system, most acoustic emotion recognition systems rely on low-level acoustic, prosodic, and spectral features (Ververidis & Kotropoulos, 2006; Kwon, Chan, Hao, & Lee, 2003).

The lack of agreement about a theory of emotions complicates this process of data collection. Human languages exhibit many “emotion denoting” adjectives. A “Semantic Atlas of Emotion Concepts” lists 558 words with emotional connotations (Sethu, Epps, & Ambikairajah, 2014; Averill, 1975). It is very challenging to represent these high numbers in both collecting emotion data and constructing automatic recognizers that are capable of distinguishing such a large number of classes (Cowie & Cornelius, 2003). However, it may be that not all of these terms are equally important and, given the specific research aims, it could be possible to select a subset of these terms for fulfilling certain requirements.

While the aim of these approaches is to reduce the number of emotion-related terms, it has also been argued that emotions are a continuum and these terms, even a very large number of them, do not capture every shade of emotion a person can distinguish. The dimensional approach to emotion categorization is also related to this line of argument (i.e., it describes shades of emotions as points in a continuous two- or three-dimensional space). Emotional states are described in terms of a two-dimensional circular space, with its axes labelled “activation” or “arousal” (going from passive to active) and “evaluation” or “valence” (going from negative to positive) (Cowie et al., 2001). Figure 1 shows a two-dimensional emotion states model depicting different emotional states. An important question with the dimensional approach is then if these emotion dimensions capture all relevant properties of the emotion concepts or if they are simplified and reduced descriptions. For the analysis and from a recognition point of view of acoustic emotion recognition, a continuum of emotions is an intractable problem, and a finite and relatively small number of emotional categories are a necessity.

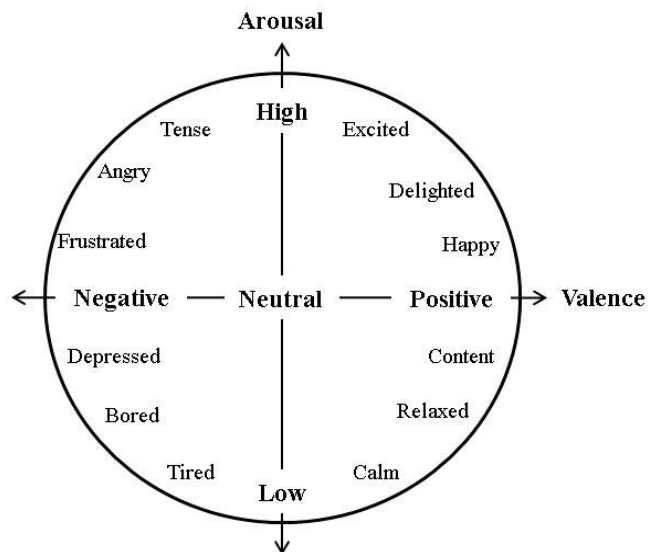


Figure 1. Two-dimensional emotion state model.

Another challenge in emotion recognition is the lack of a common database to compare recognition rates. Scherer (2003) stated that a review of about 30 studies yielded an average recognition rate of about 60%. However, direct comparisons of recognition rates are futile, since different datasets analyze different emotions. The datasets collected from acted and elicited emotional speech are also one of the challenging factors. There is no clear consensus, since the acted speech data may not reflect what emotions people would produce spontaneously. However, research shows that even elicited emotions are acted, although for different reasons (Cowie & Cornelius, 2003). Using speech based on acted emotions has numerous advantages; namely, control over the verbal and phonetic content (different emotional states can be produced using the same emotionally neutral utterance) and ease of producing full-blown emotions. The high level of control over the linguistic content could also potentially allow direct comparisons of prosodic and voice quality parameters for different emotional states.

Data Description

The emotional speech database used in these current experiments was the LDC Emotional Speech and Transcripts Corpus. This database was mainly chosen on the basis of language and variety of emotions. The dataset is in English and contains 14 emotions along with the neutral state. It contains data from three male and four female speakers, including audio recordings and the corresponding transcripts. The audio was recorded at a sampling rate of 22,050 Hz. Professional actors were used as subjects for recording the data. The emotion categories were neutral, hot anger,

cold anger, panic, anxiety, despair, sadness, elation, happiness, interest, boredom, shame, pride, contempt, and disgust (Liberman, Davis, Grossman, Martey, & Bell, 2002). This research analyzed data from one male and one female speaker. Data samples for only four emotions were considered for emotion recognition, since these four emotions are the most frequently occurring emotions in everyday life: anger, happiness, sadness, and neutrality (no emotion), and the impact of negative emotions like anger and sadness are more harmful in driving applications than the other emotions (James & Nahl, 2000).

Methodology

In this study, the authors evaluated two acoustic features, zero crossing rate and frequency formants, temporal and spectral features, respectively, to recognize the four different emotions for an acted speech dataset. The choice of features was based on readily available tools for calculation of these features. Since these were one-dimensional features, they could be easily analyzed for vehicle-centric applications. Values for total zero crossings and frequency formants were acquired using PRAAT software. Mean zero crossing rate and first four frequency formants were used for emotion recognition. Zero crossing rate (ZCR) is a feature that characterizes only a part of the spectrum. It provides a rough estimate of the dominant frequency in the speech signal encapsulated in a single-dimensional frame-based feature. ZCR has previously been used as a feature for emotion recognition (Huang & Ma, 2006; Lugger, Janoir, & Yang, 2009). For discrete time, it can be calculated using Equation 1:

$$ZCR = \frac{1}{N} \sum_{i=0}^{N-1} \left| \text{sign}(x[i]) - \text{sign}(x_{-1}(i-1)) \right| \quad (1)$$

where, $x[i]$ is the speech signal; $x_{-1}(N)$ is a temporary array created to store previous frame values; and, N is the total number of samples in a frame (Lugger, Janoir, & Yang, 2009).

A zero crossing occurs if the successive samples have different algebraic signs, where the values of sign are a function of Equation 2:

$$\begin{aligned} \text{If } x(i) > 0, \text{ then } \text{sign}(x[i]) &= 1 \\ \text{If } x(i) = 0, \text{ then } \text{sign}(x[i]) &= 0 \\ \text{If } x(i) < 0, \text{ then } \text{sign}(x[i]) &= -1 \end{aligned} \quad (2)$$

For this study, mean zero crossing rates were evaluated for each utterance of a single emotion and used as a feature

for emotion recognition. Frequency formants can be defined as resonances of vocal tract and estimation of their location and frequencies at that location, which is significant for emotion recognition (Khulage & Pathak, 2012). In this study, the first four frequency formants corresponding to the maximum pitch were used for emotion recognition. Figure 2 shows the block diagram of emotion recognition. The features acquired from PRAAT were evaluated using a decision-tree-based algorithm designed in MATLAB. While analyzing emotion data, 80% was used for training and 20% for testing the accuracy of the emotion recognition algorithm. A total of 20 test signals were used for each speaker.

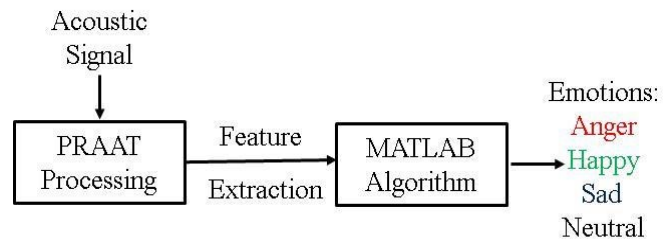


Figure 2. Block diagram of acoustic emotion recognition.

Results and Discussion

The frequency formants for male speakers do not have many variations across the same emotion category and, hence, provide a reliable feature for emotion recognition. Although mean ZCR is a good criterion for speech recognition, it does not establish any concrete pattern for emotion recognition and gives similar values for all of the emotions. As a result, emotion recognition in male speakers has an accuracy rate of 85% for acoustic test signals. The first two frequency formants have distinct values for each emotion, which result in higher emotion recognition accuracy. For female speakers, the frequency formants have a very wide range for three emotions: happiness, sadness, and anger. Hence, the mean ZCR becomes a critical criterion for emotion recognition. The mean ZCR, however, is almost similar for happiness and anger, since both emotions represent high arousal. The formants for emotions sadness and neutrality have quite similar values, which resulted in the lowest accuracy for sad emotion in the female speaker of about 60%. The overall accuracy of emotion recognition for the female speaker using this method was 71%.

Table 1 shows the confusion matrix for overall accuracy of the emotion recognition system for both male and female speakers using this method. The low accuracy in emotions sadness and neutrality was specifically attributed to the female speaker. An increased number of sample errors in emotions anger and happiness were due to both being high-

arousal emotions resulting in high formant frequencies. Figure 3 shows the comparison of individual accuracies in male and female speakers for each emotion.

Table 1. Confusion matrix for overall accuracy of emotion recognition.

Emotions	Happy	Anger	Sadness	Neutral
Happy	32	4	1	3
Anger	3	33	0	4
Sadness	2	0	29	9
Neutral	3	0	6	31

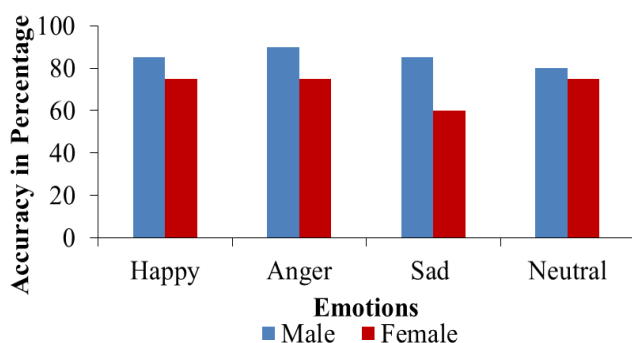


Figure 3. Emotion recognition accuracy comparison.

Conclusions

The algorithm presented here successfully recognized emotions in the male speaker. Out of four frequency formants, the first two were distinctive for each emotion, which resulted in better accuracy of emotion recognition. However, for sad and neutral emotions in male speakers, the accuracy dropped slightly, due to their similarity in frequency formants. Qualitative voice features should be explored for these emotions. For female acoustic data, the selected features were insufficient to describe the selected emotions. Hence, other features that are dependent on voice quality, such as pitch, intensity, and mean signal energy, should be evaluated.

References

Arnold, M. (1963). *Emotion and personality*. New York: Columbia University Press.

Averill, J. R. (1975). A semantic atlas of emotional concepts. *JSAS Catalog of Selected Documents in Psychology*, 5, 330.

Bower, G. H. (1981). Mood and memory. *American Psychologist*, 36, 129-148.

Cavazza, M., Charles, F., & Mead, S. (2002). Character-based interactive storytelling. *IEEE Intelligent Systems*, 17(4), 17-24.

Chul, M. L., & Narayanan, S. (2005). Toward detecting emotions in spoken dialogs. *IEEE Transactions on Speech and Audio Processing*, 13(2), 293-303.

Cowie, R., & Cornelius, R. (2003). Describing the emotional states that are expressed in speech. *Speech Communication*, 40(1-2), 5-32.

Cowie, R., Douglas-Cowie, E., Tsapatsoulis, N., Votsis, G., Kollias, S., Fellenz, W., & Taylor, J. (2001). Emotion recognition in human-computer interaction. *IEEE Signal Processing Magazine*, 18(1), 32-80.

Damasio, A. R. (2000). A second chance for emotion. In R. D. Lane & L. Nadel (Eds.). *Cognitive neuroscience of emotion* (pp. 12-23). New York: Oxford University Press.

Gobl, C. (2003). The role of voice quality in communicating emotion, mood and attitude. *Speech Communication*, 40, 189-212.

Huang, R., & Ma, C. (2006). Toward a speaker-independent real-time affect detection system. *Proceedings of the 18th International Conference on Pattern Recognition*. Los Alamitos, CA: IEEE.

Liberman, M., Davis, K., Grossman, M., Martey, N., & Bell, J. (2002). *Emotional prosody speech and transcripts*. Retrieved from <https://catalog ldc.upenn.edu/LDC2002S28>

James, L., & Nahl, D. (2000). *Road rage and aggressive driving*. Amherst, N.Y.: Prometheus Books.

Kessous, L., Castellano, G., & Caridakis, G. (2009). Multi-modal emotion recognition in speech-based interaction using facial expression, body gesture and acoustic analysis. *Journal on Multimodal User Interfaces*, 3(1-2), 33-48.

Khulage, A. A., & Pathak, B. V. (2012). Analysis of speech under stress using linear techniques and non-linear techniques for emotion recognition system. *Computer Science & Information Technology*, 6, 285-294.

Kramer, E. (1963). Judgment of personal characteristics and emotions from nonverbal properties of speech. *Psychological Bulletin*, 60(4), 408-420.

Kwon, O., Chan, K., Hao, J., & Lee, T. (2003). Emotion recognition by speech signals, Proceedings of the 8th European Conference on Speech Communication and Technology. Baixas, France: ISCA.

Liberman, M., Davis, K., Grossman, M., Martey, N., & Bell, J. (2002). *Emotional prosody speech and transcripts*. Retrieved from <https://catalog ldc.upenn.edu/LDC2002S28>

-
- Lugger, M., Janoir, M.-E., & Yang, B. (2009, January). Combining classifiers with diverse feature sets for robust speaker independent emotion recognition. *Proceedings of the 17th European Signal Processing Conferenc.* Glasgow, Scotland: EUSIPCO.
- Mowrer, O. (1973). *Learning theory and behavior.* Huntington, New York: Krieger.
- Murray, I., & Arnott, J. (1993). Toward the simulation of emotion in synthetic speech: A review of the literature on human vocal emotion. *The Journal of the Acoustical Society of America*, 93(2), 1097-1108.
- Pollack, I., Rubenstein, H., & Horowitz, A. (1960). Communication of verbal modes of expression. *Language and Speech*, 3, 121-130.
- Scherer, K. (1982). The nature and function of emotion. *Social Science Information*, 21(4-5), 507-509.
- Scherer, K. (2003). Vocal communication of emotion: A review of research paradigms. *Speech Communication*, 40(1-2), 227-256.
- Scherer, K., Banse, R., & Wallbott, H. (2001). Emotion inferences from vocal expression correlate across languages and cultures. *Journal of Cross-Cultural Psychology*, 32, 76-92.
- Sethu, V., Epps, J., & Ambikairajah, E. (2014). Speech based emotion recognition. In T. Ogunfunmi, R. Togneri, & M. S. Narasimha (Eds.). *Speech and audio processing for coding, enhancement and recognition* (pp. 197-228). New York: Springer.
- Tomkins, S., & Karon, B. (2008). *Affect imagery consciousness.* New York: Springer.
- Udhan, T., & Bernadin, S. (2018). Speaker-dependent low-level acoustic feature extraction for emotion recognition. *The Journal of the Acoustical Society of America*, 143(3), 1747-1747.
- Ververidis, D., & Kotropoulos, C. (2006). Emotional speech recognition: Resources, features, and methods. *Speech Communication*, 48(9), 1162-1181.
- Yang, Y., & Chen, H. (2012). Machine recognition of music emotion. *ACM Transactions on Intelligent Systems and Technology*, 3(3), 1-30.

feature utilization, which will help in speech pattern recognition. Her expertise includes PRAAT, MATLAB, and fuzzy clustering analysis techniques. Ms. Udhan may be reached at tu13b@my.fsu.edu

SHONDA BERNADIN is an associate professor in the Electrical and Computer Engineering Department the Florida A&M University-Florida State University College of Engineering. Dr. Bernadin received her BS degree in electrical engineering from Florida A&M University in 1997, her MS degree in electrical and computer engineering from the University of Florida in 1999, and her PhD degree in electrical engineering from Florida State University in 2003. She is currently the director of the Speech Processing and Data Analysis Laboratory. Her research interests include speech analysis and pattern recognition, feature extraction, data mining, instructional design, and engineering education. Dr. Bernadin may be reached at bernadin@eng.fsu.edu

Biographies

TEJAL UDHAN is a PhD candidate in the Department of Electrical and Computer Engineering, Florida State University. She is a research assistant in the Speech Processing and Data Analysis Laboratory. Her research interests include speech processing systems, data mining, and pattern recognition techniques. She graduated from Marathawada Institute of Technology (Aurangabad, India) with a BE in Electronics and Communication. Currently, she is working with Dr. Shonda Bernadin in the Department of Electrical and Computer Engineering on low-level acoustic

NOVEL USE OF REMOTE SENSING, MONITORING, AND TRACKING FOR ANIMALS IN WILD HABITATS

Ben Zoghi, Texas A&M University; Rainer Fink, Texas A&M University

Abstract

Parks and wildlife management require a discrete system that can automatically and continuously monitor animal patterns and behaviors in remote environments in an efficient manner that does not disturb the animals. In this study, the authors developed a stand-alone monitoring system that can inconspicuously monitor and track animals in their natural habitat and transmit data/footage to an off-site viewing module. The genesis of the Argus Vision name is in ancient Greek Mythology. Argus Pantoptes was an all-seeing giant with 100 eyes, who stood watch for the Goddess Hera. Upon his death, and as a tribute to her trusted watchman, Hera took the eyes of Argus and placed them on the tail of her favorite bird, the peacock. The Argus Vision logo is the tail of the peacock with the eyes of Argus. Monitoring is accomplished using wireless outdoor cameras set up onsite. The cameras are connected via a telemetry network to a central control unit that takes all of the feeds and broadcasts them, in real time, to an Android application on a personal tablet. The end user is then able to control the cameras remotely and monitor their location without being onsite, thereby eliminating the need for researchers to do the cumbersome job of going out into the habitat to retrieve footage and risk disrupting the animals. The Argus Vision is a unique system and the project aimed to develop power supply, wireless communication, data storage, and control capabilities for the system.

Introduction

Biologists currently use camera traps to monitor and track wildlife in their habitats (Swann, Hass, & Wolf, 2004; Garcia-Sanchez, Garcia-Sanchez, Losilla, Kulakowski, Garcia-Haro, Rodriguez, López-Bao, & Palomares, 2010). These camera traps work well for collecting images of shy animals, but present two primary issues: disturbance and inefficiency. This problem can be overcome by use of remote vision technology that allows the user to monitor animals in their wild habitats wirelessly and without disturbing or startling the animals (Paek, Hicks, Coe, Govindan, 2014). Similar to other recently published systems that use still camera footage to monitor bird nesting in the wilderness (Baratchi, Meratnia, Havinga, & Skidmore, 2013; Neumann, Martinuzzi, Estes, Pidgeon, Dettki, Ericsson, & Radeloff, 2015; Locke, Cline, Wetzels, Pittman, Brewer, &

Harveson, 2005), the aim of the Argus Vision project was to design and implement a live video monitoring system to track water fowl patterns and habits in a remote location.

Argus Vision is a system that allows the customer to monitor remote locations without having to be onsite. It was designed to be used in rough, rugged, remote environments to monitor animal-landscape interaction, vegetation, reproduction cycles, expansion, and safety. Argus Vision has a wide range of applications and would be an ideal system to use for facility security. The system could also be extended to use in habitats where poaching might occur, for border patrol, homeland security, and hunting. The functional requirements for Argus Vision are wireless capability, long-range access point, Wi-Fi enabled, battery powered, ability to operate for an extended time, low-battery (state-of-charge) notification, solar panels to charge batteries, controllable cameras, pan, tilt, and zoom functionality, infrared night vision, ability to interface with Android tablet, Android user application, ability to interact with a server, recording and video storage, GPS locator, and a durable and weatherproof enclosure.

Design Overview

Figure 1 shows the conceptual block diagram, which depicts the high-level concept of the system.

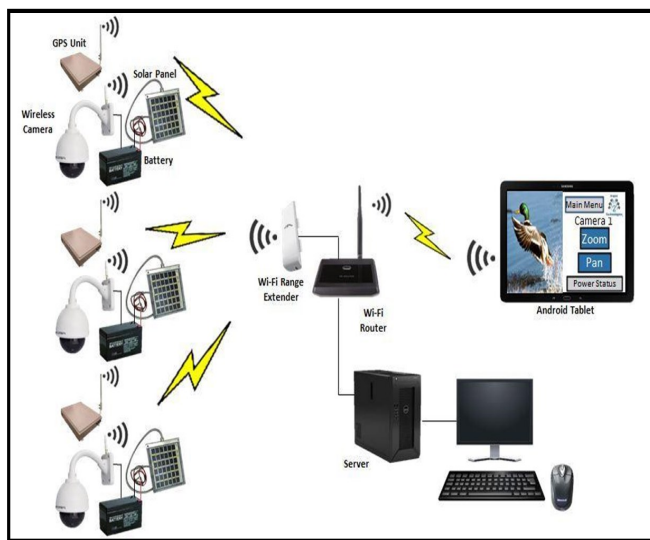


Figure 1. Conceptual block diagram.

The actual design integrated all of the components depicted in Figure 1 into one system. Cameras were set up inconspicuously at the various remote locations. Circuits were designed to power the cameras and GPS units from a solar-charged battery. The batteries and GPS units were housed in weatherproof enclosures. A server was located onsite and able to store the video and transmit it to an Android tablet. The end user was able to control the multiple cameras remotely, including panning and zooming, via the Android tablet, essentially offering a real-time view of the location without being onsite. Based on the conceptual block diagram and research conducted on how the different modules and devices needed to connect, the functional block diagram in Figure 2 was developed. The heart of the Argus Vision system was the MSP430 microcontroller. The peripheral modules, Wi-Fi and GPS, were selected based on their embedded communication protocol and the corresponding number of communication ports available on the microcontroller. Table 1 shows the performance specifications for Argus Vision.

Hardware Design

The Argus Vision PCB schematic was designed in Eagle CAD and consisted of four subsections: power, microcontroller, Wi-Fi, and GPS.

1. The power section inputs a 12V battery voltage source that then goes directly into the 3.3V regulator to supply a steady voltage to the rest of the circuits. The power section also contains a voltage divider to determine the battery voltage level for display to the user.
2. Circuitry in the microcontroller section includes decoupling capacitors and a JTAG connector.
3. The XBee S6B module is the Wi-Fi module for the Argus Vision. It can use RPSMA-connected antennas, which are readily available. The module is connected over UART to the MSP430 microcontroller to send the data for transmission to the Wi-Fi module. The device is also connected to two DIO ports on the MSP430 to turn the module on and off.

Figure 2. Functional block diagram.

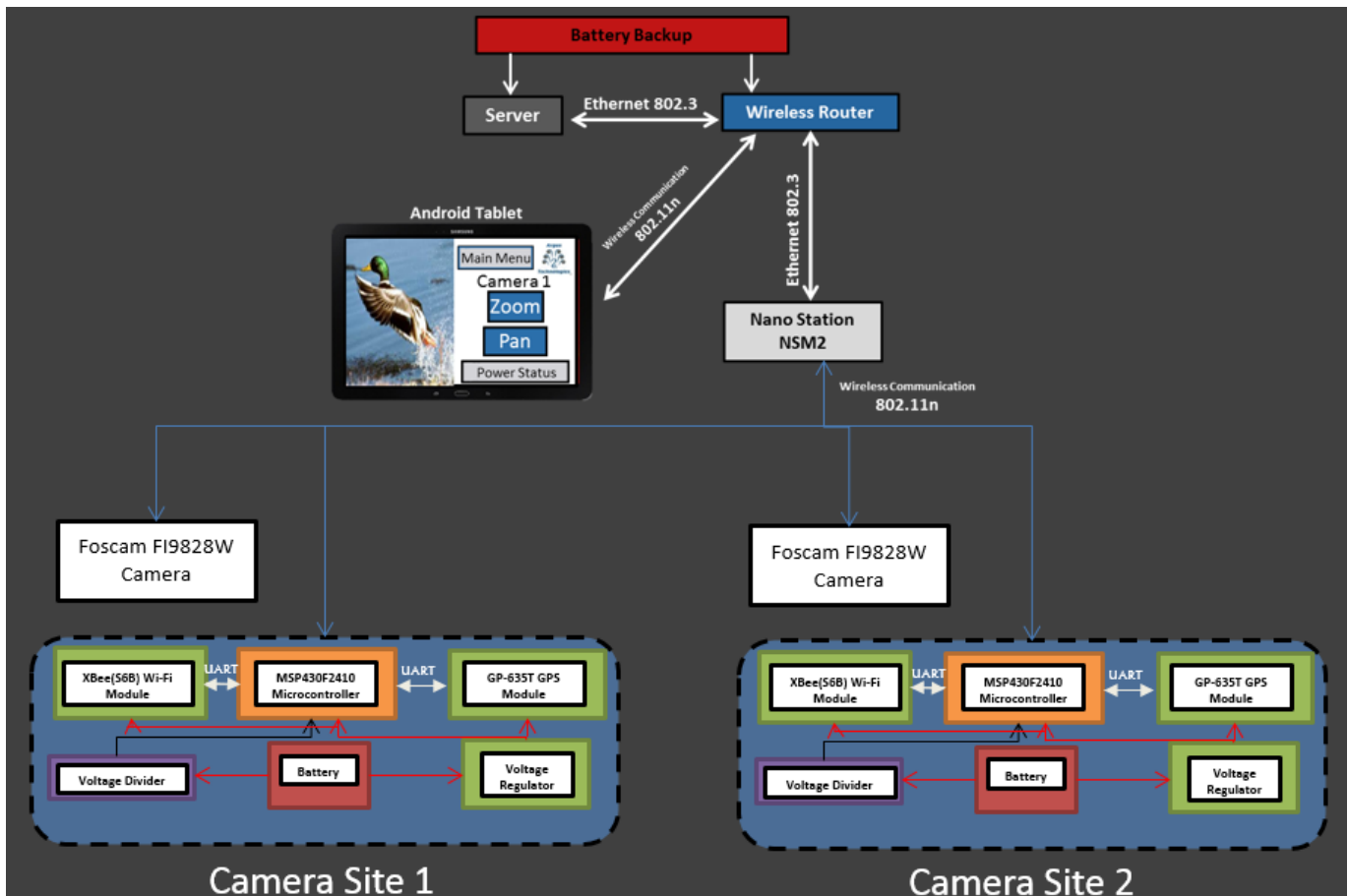


Table 1. Performance specifications.

Function	Specification	Details
Wireless Capability	Long range access point	>1km wireless communication
	Wi-Fi enabled	2.4 GHz IEEE Standard 802.11n
Battery	Operates for and extended time period	Battery life of ≥ 24 hours
	Low battery (state of charge) notification	Notification sent when battery is $< 10V$
	Solar panels to charge batteries	Rechargeable to 12V DC via solar panels
Controllable Cameras	Pan, tilt, and zoom functionality	<ul style="list-style-type: none"> • 355° pan • 90° tilt • 3x optical zoom
	Infrared night vision	≤ 20 meters
Interfaces with Android tablet	Android user application	<ul style="list-style-type: none"> • Real-time video footage from multiple cameras • Display GPS location of cameras • View battery state of charge • Control camera functions
Interacts with server	Records and stores video	<ul style="list-style-type: none"> • Server will store video for up to 30 days • Server will have at least 1TB of storage available to accommodate data storage • Allows user application to access stored video
GPS Locator	Wi-Fi enabled	<ul style="list-style-type: none"> • Unassisted acquisition • Accuracy within 10 meters
Enclosure	Weatherproof	<ul style="list-style-type: none"> • Withstand rain and heavy water flow
	Mountable	<ul style="list-style-type: none"> • Capable of being mounted to a pole or tree without defect to functionality • Small size

4. The GP-635T GPS module is connected to the PCB via a 6-pin female JST connector. UART is used to communicate with the MSP430 to send the GPS data from the module to the microcontroller. The device also connects to a DIO port on the MSP430 to power the module on and off.

Android Software Design

When the Argus Vision Android app is opened, the home or main screen appears. All subsequent screens and functions are inherent to the main activity. From within the main screen, the user should first click the “Setup Menu” button in order to set up all of the cameras in the system. Once the user inputs the number of cameras and clicks the “Connect” and “Save” buttons, the system will be automatically set up. Clicking the Save button will direct the user back to the home screen for a choice of whether to view the live feed or archived footage of any camera in the system. Users also have the option of viewing a map of all of the

cameras in the system and to then either view live or archived footage of any camera, based on its location. If the user chooses the “View Live Feed” button, the Foscam Android app will open, and the user will then be able to view the live footage as well as control the camera. If the user selects the “View Archived Footage” button, the ES File Explorer Android app will open, and the user will have to log into the server to view the archived footage, organized by date, of any camera. Figure 3 shows the hierarchy chart for the application.

Embedded Code Design

Argus Vision’s embedded software uses a timer to determine when all other tasks should occur. The battery percentage level is transmitted to the tablet every four hours and the GPS coordinates every 24 hours. To implement this, the timer is used to count by seconds. When the timer count reaches 60 seconds, two other counts are incremented by one, creating two separate 1-minute counters, one for

GPS timing and the other for battery percentage timing. Development began using a development board specified for the MSP430. The first task was to successfully read and parse GPS data from the GPS module on the development board. Once this was complete, the next task was to successfully implement the on-board ADC on the development board to read the correct voltage value from a voltage divider connected to an external battery. The existing code modules were tested on the actual boards, and they were successful. The next task was to implement the Wi-Fi module. UART was used for the Wi-Fi module communication. The next task was to implement the timer in the microcontroller and, once that was complete, some minor tweaking was necessary to make all of the pieces of code work together.

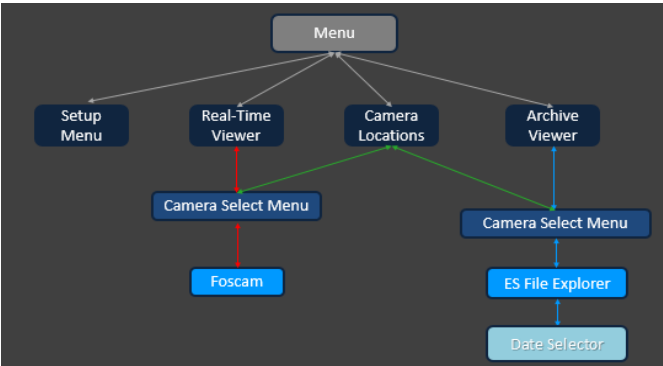


Figure 3. Android app hierarchy chart.

Testing

To ensure that Argus Vision worked as expected and met all functional requirements, the test matrix of Table 2 was developed.

1. **Wi-Fi Connection:** This test verified that the cameras could connect to the wireless access point at distances greater than 300 ft. and receive at a signal of at least 70 dBm. With the system being remote, it was verified that the connection was working correctly in a far-field communication setup. This test also estimated the distance at which the cameras and access point could be separated and maintain reliable communications. The results indicated a strong, usable wireless connection at 301 ft.
2. **Battery Life:** To confirm that the battery could operate at least 72 hours, the PCB and camera were fully powered and allowed to transmit video and GPS data until the battery failed. This test was timed to verify that the battery capacity was sufficient to handle the full operational load. The results indicated that the battery lasted over 72 hours without powering off the camera.
3. **GPS Coordinates:** This test confirmed that the GPS coordinates from the microcontroller corresponded to the location that the GPS module was within 10m when the data were read. This was done by compar-

Table 2. Test matrix.

	Battery Powered	GPS Locator	Real-time view	Video Archiving	Android App	Camera Control	Enclosure	Wireless Communication
Wi-Fi Connection at >300ft								X
Battery Life	X							
GPS coordinates		X			X			X
Real-Time Monitoring			X		X			X
Camera controllability via android app			X		X	X		X
View Archived data on app				X	X			X
Weatherproof enclosure							X	
Battery status displays in android app	X				X			X
Field test	X	X	X	X	X	X	X	X

ing the actual camera location to the coordinates displayed in the Argus Vision app using Google Earth. The test indicated that correct GPS coordinates were broadcast to the tablet and being populated on the map in the Argus Vision Android application.

4. Real-Time Monitoring: To ensure that the camera properly transmitted real-time video, it was set up at a location with Person 1. Person 2 then viewed the video feed from another location while communicating with Person 1 in order to ensure that the video did not have a noticeable delay. Results indicated that Person 2 could immediately identify all of the movements of Person 1.
5. Camera Control via Android App: This test ensured that the camera could be controlled from the app. If the user was able to pan, tilt, and zoom the camera, this verified that the app functioned correctly, the user had control over the cameras, and wireless communications were working. The test showed that the camera settings were controllable from within the Argus Vision Android application.
6. View Archived Data on Android App: This test verified that the server was set up properly and had the ability to store video footage from the cameras for at least 30 days, as well as verify the ability to transmit the stored data to the Argus Vision Android app via Wi-Fi. The test was successful; the user could access and view stored video from 30 days prior via the Argus Vision Android app.
7. Weatherproof Enclosure: In this test, the operation of the Argus Vision system was verified under various weather conditions. The enclosure was designed to be weatherproof and to protect the system's hardware from hazardous outdoor weather conditions. Neither the PCB nor battery were damaged by simulated inclement weather.
8. Battery Status Display in App: Argus Vision needs to display battery life in order to prevent the PCB and camera from dropping below operating voltage levels. If the 12V DC battery drops below 10V DC, a notification appears in the Argus Vision Android app. This test was successful.
9. Field Test: As a final test, the Argus Vision system was installed on a ranch, which was a real-world environment as close as possible to actual operation. The PCB, cameras, and tablet were powered on and the Android app launched. The functioning of the user interface and the data display on the app were verified. All parts of the Argus Vision system functioned as specified in the performance requirements.

Conclusions

The Argus Vision System is a unique video surveillance system that was designed for use in remote locations. It was proven to be useful in providing facility security and the designers plan to expand it for use as game cameras for hunting as well as research purposes. The system addressed all of the specified needs and requirements to allow for system scaling to almost any use. The small-form factor allows the system to be discrete and non-invasive to the environment and animals living in the area.

Acknowledgments

The research team appreciates the effort and contributions of the following ESET senior students to this project: Michael Sanders, Michael Crowley, Kevin Erskine, and Danisha Stern.

References

- Baratchi, M., Meratnia, N., Havinga, P. M., Skidmore, A. K. (2013). Sensing solutions for collecting spatio-temporal data for wildlife monitoring applications: A review. *Sensors (Basel)*, 13(5), 6054-6088.
- Garcia-Sanchez, A.-J., Garcia-Sanchez, F., Losilla, F., Kulakowski, P., Garcia-Haro, J., Rodriguez, A., López-Bao, J.-V., & Palomares, F. (2010). Wireless sensor network deployed for monitoring wildlife passages. *Sensors (Basel)*, 10(8), 7236-7262.
- Locke, S. L., Cline, M. D., Wetzel, D. L., Pittman, M. T., Brewer, C. E., & Harveson, L. A. (2005). A web-based digital camera for monitoring remote wildlife. *Wildlife Society Bulletin*, 33(2), 761-765.
- Neumann, W., Martinuzzi S., Estes, A. B., Pidgeon, A. M., Dettki, H., Ericsson, G., & Radeloff, V., (2015). Opportunities for the application of advanced remotely-sensed data in ecological studies of terrestrial animal movement. *Movement Ecology*, 3(1), 8.
- Paek, J., Hicks, J., Coe, S., & Govindan, R. (2014). Image-based environmental monitoring sensor application using embedded wireless sensor network. *Sensors (Basel)*, 14(9), 15981-16002.
- Swann, D. E., Hass, C. C., & Wolf, S. A. (2004). Infrared-triggered cameras for detecting wildlife: An evaluation and review. *Wildlife Society Bulletin*, 32, 357-365.

Biographies

BEN ZOGHI is the Victor H. Thompson Chair Professor of Electronics System Engineering Technology at Texas A&M. He directs the RFID/Sensor Lab and the new online professional Master of Engineering in Technical Management degree. A member of the Texas A&M University faculty for 30 years, he has distinguished himself as a teacher, writer, and researcher and has been honored for his teaching excellence by the college and Texas A&M University's Association of Former Students. Ben's academic and professional degrees are from Texas A&M (PhD), The Ohio State University (MSEE), and Seattle University (BSEE). Dr. Zoghi may be reached at zoghi@tamu.edu

RAINER FINK is an associate professor with a joint appointment in engineering technology and industrial distribution as well as biomedical engineering. He is the director of the Texas Instruments Mixed-Signal Test Laboratory, a state-of-the-art semiconductor production test and validation facility at Texas A&M University. His areas of expertise include semiconductor testing and validation as well as medical device design and testing. Dr. Fink has been teaching mixed-signal test methods at A&M as well as in industry since 1998. Dr. Fink may be reached at fink@tamu.edu

INSTRUCTIONS FOR AUTHORS: MANUSCRIPT FORMATTING REQUIREMENTS

The INTERNATIONAL JOURNAL OF ENGINEERING RESEARCH AND INNOVATION is an online/print publication designed for Engineering, Engineering Technology, and Industrial Technology professionals. All submissions to this journal, submission of manuscripts, peer-reviews of submitted documents, requested editing changes, notification of acceptance or rejection, and final publication of accepted manuscripts will be handled electronically. The only exception is the submission of separate high-quality image files that are too large to send electronically.

All manuscript submissions must be prepared in Microsoft Word (.doc or .docx) and contain all figures, images and/or pictures embedded where you want them and appropriately captioned. Also included here is a summary of the formatting instructions. You should, however, review the [sample Word document](http://ijeri.org/formatting-guidelines) on our website (<http://ijeri.org/formatting-guidelines>) for details on how to correctly format your manuscript. The editorial staff reserves the right to edit and reformat any submitted document in order to meet publication standards of the journal.

The references included in the References section of your manuscript must follow APA-formatting guidelines. In order to help you, the sample Word document also includes numerous examples of how to format a variety of scenarios. Keep in mind that an incorrectly formatted manuscript will be returned to you, a delay that may cause it (if accepted) to be moved to a subsequent issue of the journal.

1. **Word Document Page Setup:** Two columns with ¼" spacing between columns; top of page = ¾"; bottom of page = 1" (from the top of the footer to bottom of page); left margin = ¾"; right margin = ¾".
2. **Paper Title:** Centered at the top of the first page with a 22-point Times New Roman (Bold), small-caps font.
3. **Page Breaks:** Do not use page breaks.
4. **Figures, Tables, and Equations:** All figures, tables, and equations must be placed immediately after the first paragraph in which they are introduced. And, each must be introduced. For example: "Figure 1 shows the operation of supercapacitors." "The speed of light can be determined using Equation 4:"

5. **More on Tables and Figures:** Center table captions above each table; center figure captions below each figure. Use 9-point Times New Roman (TNR) font. Italicize the words for table and figure, as well as their respective numbers; the remaining information in the caption is not italicized and followed by a period—e.g., "*Table 1.* Number of research universities in the state." or "*Figure 5.* Cross-sectional aerial map of the forested area."
6. **Figures with Multiple Images:** If any given figure includes multiple images, do NOT group them; they must be placed individually and have individual minor captions using, "(a)" "(b)" etc. Again, use 9-point TNR.
7. **Equations:** Each equation must be numbered, placed in numerical order within the document, and introduced—as noted in item #4.
8. **Tables, Graphs, and Flowcharts:** All tables, graphs, and flowcharts must be created directly in Word; tables must be enclosed on all sides. The use of color and/or highlighting is acceptable and encouraged, if it provides clarity for the reader.
9. **Textboxes:** Do not use text boxes anywhere in the document. For example, table/figure captions must be regular text and not attached in any way to their tables or images.
10. **Body Fonts:** Use 10-point TNR for body text throughout (1/8" paragraph indentation); indent all new paragraphs as per the images shown below; do not use tabs anywhere in the document; 9-point TNR for author names/affiliations under the paper title; 16-point TNR for major section titles; 14-point TNR for minor section titles.

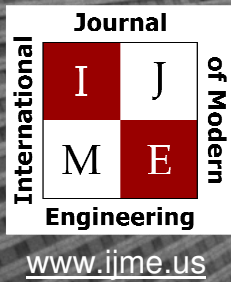
11. **Personal Pronouns:** Do not use personal pronouns (e.g., "we" "our" etc.).
12. **Section Numbering:** Do not use section numbering of any kind.
13. **Headers and Footers:** Do not use either.

14. **References in the Abstract:** Do NOT include any references in the Abstract.
15. **In-text Referencing:** For the first occurrence of a given reference, list all authors—last names only—up to seven (7); if more than seven, use “et al.” after the seventh author. For a second citation of the same reference—assuming that it has three or more authors—add “et al.” after the third author. Again, see the sample Word document for specifics.
16. **More on In-Text References:** If you include a reference on any table, figure, or equation that was not created or originally published by one or more authors on your manuscript, you may not republish it without the expressed, written consent of the publishing author(s). The same holds true for name-brand products.
17. **End-of-Document References Section:** List all references in alphabetical order using the last name of the first author—last name first, followed by a comma and the author’s initials. Do not use retrieval dates for websites.
18. **Author Biographies:** Include biographies and current email addresses for each author at the end of the document.
19. **Page Limit:** Manuscripts should not be more than 15 pages (single-spaced, 2-column format, 10-point TNR font).
20. **Page Numbering:** Do not use page numbers.
21. **Publication Charges:** Manuscripts accepted for publication are subject to mandatory publication charges.
22. **Copyright Agreement:** A copyright transfer agreement form must be signed by all authors on a given paper and submitted by the corresponding author before that paper will be published. Two versions of the form will be sent with your manuscript’s acceptance email.
23. **Submissions:** All manuscripts and required files and forms must be submitted electronically to Dr. Philip D. Weinsier, manuscript editor, at philipw@bgsu.edu.
24. **Published Deadlines:** Manuscripts may be submitted at any time during the year, irrespective of published deadlines, and the editor will automatically have your manuscript reviewed for the next-available issue of the journal. Published deadlines are intended as “target” dates for submitting new manuscripts as well as revised documents. Assuming that all other submission conditions have been met, and that there is space available in the associated issue, your manuscript will be published in that issue if the submission process—including payment of publication fees—has been completed by the posted deadline for that issue.

Missing a deadline generally only means that your manuscript may be held for a subsequent issue of the journal. However, conditions exist under which a given manuscript may be rejected. Always check with the editor to be sure. Also, if you do not complete the submission process (including all required revisions) within 12 months of the original submission of your manuscript, your manuscript may be rejected or it may have to begin the entire review process anew.

Only one form is required. Do not submit both forms!

The form named “paper” must be hand-signed by each author. The other form, “electronic,” does not require hand signatures and may be filled out by the corresponding author, as long as he/she receives written permission from all authors to have him/her sign on their behalf.



Print ISSN: 2157-8052
Online ISSN: 1930-6628



INTERNATIONAL JOURNAL OF MODERN ENGINEERING

ABOUT IJME:

- IJME was established in 2000 and is the first and official flagship journal of the International Association of Journal and Conferences (IAJC).
- IJME is a high-quality, independent journal steered by a distinguished board of directors and supported by an international review board representing many well-known universities, colleges and corporations in the U.S. and abroad.
- IJME has an impact factor of **3.00**, placing it among the top 100 engineering journals worldwide, and is the #1 visited engineering journal website (according to the National Science Digital Library).

OTHER IAJC JOURNALS:

- The International Journal of Engineering Research and Innovation (IJERI)
For more information visit www.ijeri.org
- The Technology Interface International Journal (TIIJ).
For more information visit www.tiij.org

IJME SUBMISSIONS:

- Manuscripts should be sent electronically to the manuscript editor, Dr. Philip Weinsier, at philipw@bgsu.edu.

For submission guidelines visit
www.ijme.us/submissions

TO JOIN THE REVIEW BOARD:

- Contact the chair of the International Review Board, Dr. Philip Weinsier, at philipw@bgsu.edu.

For more information visit
www.ijme.us/ijme_editorial.htm

INDEXING ORGANIZATIONS:

- IJME is indexed by numerous agencies.
For a complete listing, please visit us at www.ijme.us.

Contact us:

Mark Rajai, Ph.D.

Editor-in-Chief
California State University-Northridge
College of Engineering and Computer Science
Room: JD 4510
Northridge, CA 91330
Office: (818) 677-5003
Email: mrajai@csun.edu



www.tiij.org



www.ijeri.org

The International Journal of Engineering Research & Innovation (IJERI) is the second official journal of the International Association of Journals and Conferences (IAJC). IJERI is a highly-selective, peer-reviewed print journal which publishes top-level work from all areas of engineering research, innovation and entrepreneurship.



IJERI Contact Information

General questions or inquiries about sponsorship of the journal should be directed to:

Mark Rajai, Ph.D.

Founder and Editor-In-Chief

Office: (818) 677-5003

Email: editor@ijeri.org

Department of Manufacturing Systems Engineering & Management

California State University-Northridge

18111 Nordhoff St.

Room: JD3317

Northridge, CA 91330